Politecnico di Milano
Dipartimento di Scienze e Tecnologie Aerospaziali
Corso di Laurea Magistrale in Ingegneria Aeronautica

Probability of Ballistic Impact Penetration via Stochastic Multiscale Modeling of PMC Composite

Relatore: Prof. Marco ANGHILERI

Tesi di Laurea di:
Tommaso RANDOLFI
Matricola: 834145

Anno Accademico 2020-2021

Abstract

The parameters of any mechanical or structural system possess a random variation as a function of space and time. The randomness in fracture parameters are related to uncertainties involved at the design and manufacturing stages, as well as the uncertain nature of the operating conditions. At the design stage, randomness is present in the test data regarding material strength values, elastic constants, engineering constants, damage parameters and the material properties pertinent to the service life. The randomness of material properties significantly affects the functioning of the mechanical component and is unavoidable even with the best quality control measurements. In structures like impact resistant components, where failure initiation is a locally driven event, the influence of randomness in material properties is no more negligible when the goal is to obtain the most accurate results possible. In order to account for this statistical variations in microscale material properties, a new numerical approach, different from the actual deterministic one, is required. In the first part of this work is developed a computational framework based on the combination between Monte Carlo method and the Generalized Method of Cells implemented in NASA MAC/GMC code to estimate composite properties distributions starting from constituents characteristics variation using carbon-epoxy T800/F3900 unidirectional tissue as example material. Output of this first step of the multiscale modeling are then used as input for ballistic impact simulations to estimate the probability velocity response (PVR) of a multi-layer composite plate and to analyze, through sensitivity analysis, the correlation between macroscale impact simulation results and stochastic microscale input.

Sommario

I parametri di ogni sistema meccanico o strutturale variano casualmente in fuzione dello spazio e del tempo. La casualità dei valori di rottura è correlata ad incertezze legate alle fasi di design e produzione come anche ad incertezze legate alle condizioni operative. Nella fase di design, questa variabilità è presente nei risultati dei test riguardanti i valori delle proprietà di resistenza del materiale, costanti elastiche, costanti ingegneristiche, parametri di danneggiamento e parametri del materiale pernitenti alla vita operativa. La casualità delle proprietà del materiale influenza in maniera significativa il funzionamento del componente meccanico ed è inevitabile anche con il più rigorso sistema di controllo qualità. In strutture come assorbitori di impatto, dove l'iniziazione della rottura è un fenomeno strettamente locale, l'influenza della variabilità delle proprietà del matieriale non è più trascurabile quando è necessario ottenere dei risultati con elevata accuratezza. Allo scopo di includere questa variabilità statistica delle caratteristiche microstrutturali del materiale, un nuovo approccio, differente dall'attuale approccio deterinistico, è richiesto. Nella prima parte di questo studio, viene sviluppato un framework computazionale basato sulla combinazione del metodo Monte Carlo ed il "Generalized Method of Cells" implementato nel codice NASA MAC/GMC per stimare la distribuzione delle proprietà in materiali compositi partendo dalle variazioni delle caratteristiche dei materiali costituenti utilizzando come esempio un tessuto unidirezionale carbonio-epossidico T800/F3900. I risultati di questa prima parte della modellazione multiscala vengono poi utilizzati come input per le simulazioni di impatto balistico per stimare la curva prbabilistica di risposta di una piastra in composito multistrato e per analizzare, attraverso un'analisi di sensitività, la correlazione tra i risultati delle simulationi di impatto a livello macrostrutturale e gli input stocastici di natura microstrutturale.

Contents

List of Figures

List of Tables

Chapter 1

Introduction

In today's aerospace industry, both for military and civil use, composite material are becoming more and more widely used. Their diffusion started to mitigate weight increases and both aircraft and aeroengine manufactures started replacing metal with composite. Through the 1980s and 1990s the application of composites in aircraft engines was relatively limited. More than half of the total composite volume was directly associated with nacelle components such as thrust reversers acoustic lines, cascades, blocker doors, radial drive fairings and cowlings. On some models, aramid fibers (often in the form of dry fibers belt) were used to reinforce aluminum fan cases. Composite nose cones, a variety of air ducts and engine air-oil seals were fairly common as well. Pushed by weight savings reasons, very soon, thanks also to their high stiffness, strength and energy absorption capabilities, these advanced materials started to be used in many more components. When it entered service in 1995, GE's GE90 engine applied many advanced materials and resin transfer molding processing to introduce a number of new composite components; most notably, large fan blades made from hundreds of plies of intermediate-modulus carbon fiber prepreg. Since then, composite blades, fan containment cases, bypass ducts, stator vanes and a host of less glamorous detail components and brackets have become common not only in commercial jets but also in business and military aircraft.

Among all these components, it's possible to find structures such as the engine containment systems that shows to how composites started to be increasingly employed also in impact susceptible location where structural reliability is a critical issue and a damage event could compromise the entire structure and lead to a catastrophic event. Materials that possess high strength, high modulus and strength to weight ratio, such composites, represents the ideal candidates for protective structures and for these reasons the current and next generation fan casings are being manufactured not from traditional metals but from composite

materials.

Figure 1.1: engine containment structure

Due to safety reasons and the increasing use of advanced multi-phase materials it's easy to understand how also a development of the design techniques is necessary. this complex multi-phase material requires new approaches for a more accurate design to guarantee both the structural efficiency and reducing the cost dedicated to experimental tests. In impact test or even more in engine fan-blade out tests the set up of the experiment is particularly complex and expensive. This fact represent an issue since in many tests can be observed that the impact response of composite structures is characterized by a probabilistic velocity response (PVR) curve. Obtaining this curve requires a large number of tests resulting in a huge expense of time and money. Understanding the reasons for this non deterministic behavior is the first step for the development of more accurate computational methods that can help having safer, more efficient and cheaper structures.

Historically since metals and the most part of engineering materials were homogeneous, efforts were made in defining precise unique values such as minimum guaranteed limit load or ultimate load. This kind of approach has then been applied also to composite materials identifying an average value for all those parameters used in structural design. In the specific case of impact resistant composite structures this design process cannot be considered the most efficient and may be compared to a worst case scenario since the maximum of loading and the minimum of strength are treated not only as representative of design situations but also as simultaneous occurrence.
When analyzing fatigue or impact event it must be understood that, as the failure of the material is a locally driven event, the influence of the stochastic distribution of parameters such as fiber strength, fiber volume fraction, fiber angle and arrangement and presence of voids should be investigated and eventually

considered.

The parameters of any mechanical or structural system possess a random variation as a function of space and time. The randomness in fracture parameters are related to uncertainties involved at the design and manufacturing stages, as well as the uncertain nature of the operating conditions. At the design stage, randomness is present in the test data regarding material strength values, elastic constants, engineering constants, damage parameters and the material properties pertinent to the service life. The randomness of material properties significantly affects the functioning of the mechanical component and is unavoidable even with the best quality control measurements.

Test on a single material specimen or structure yield a define value for each material parameter such as the elastic constant, engineering constant and damage parameters but when a number of specimen are tested, the parameter values randomly fluctuate from specimen to specimen. Within the same structure itself the values of any parameter display an uncertain spatial variation and environmental degradation can increase the uncertain fluctuations. The sample to sample variation, spatial variation within the structure and variations due to environmental effects in strength, deterioration, deformation and damage parameters of most of the present day engineering materials is random. This is particularly the case with fiber reinforced composite materials. Variations in fiber size, fiber volume fraction, fiber orientation, void content, matrix properties, interfaces and thickness of lamina are always present and unavoidable. As a result, the elastic constants, engineering constant and deformation parameters of fiber reinforced composite material possess a random variation.

The intrinsic probabilistic nature of composite material characteristics is the reason why experimental impact tests are characterized, as said previously, by a PVR and parameters such as the V_0 and V_{50} velocities are used to describe the probabilistic penetration behavior of composite systems. Here the V_x velocity is defined as the projectile impact velocity V that has an $x\%$ probability of penetrating through the fabric system. Precisely estimating velocity parameters such as the V_0, $V_{0.1}$, and V_1 velocities is important to prevent overestimating the type and thickness of the fabric structure which directly relates to the cost and weight savings, as well as to ensure that the impacting projectile is always defeated by the fabric target in order to safeguard human life. The most common method to estimate the probabilistic fabric impact behavior is through destructive experimental impact testing namely: shooting multiple fabric targets over a range of impact velocities. Shot selection techniques are used to guide the

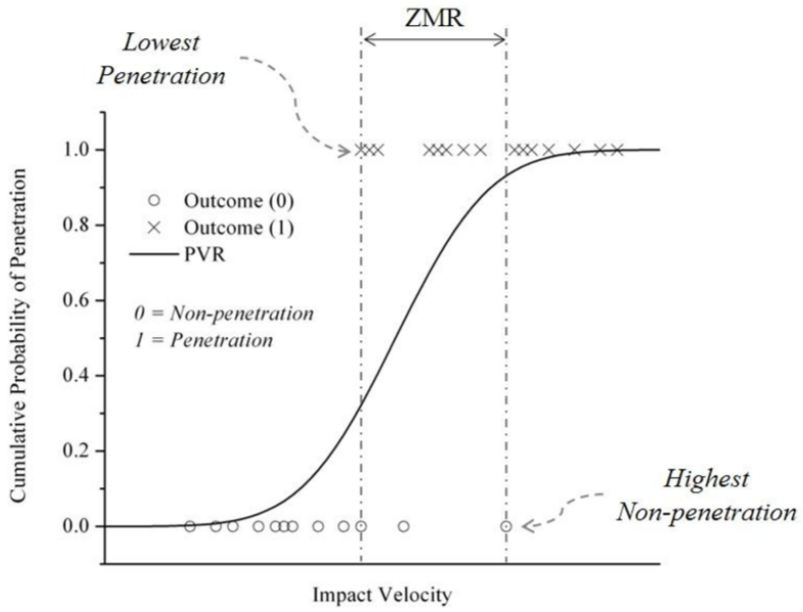

Figure 1.2: Example of PVR curve

choice of impact velocities while statistical analyses techniques are used to estimate the probabilistic penetration response based on the outcome of each test. The existence of the zone of multiple response (ZMR in figure 1.2) and the probabilistic fabric penetration response is a consequence of the source of variability, categorized by intrinsic and extrinsic influences. The sources respectively refer to those certain material properties or factors that stochastically vary from one sample to another and from one experimental test to another. Then, depending on whether the projectile engages a set of stronger or weaker material area at the impact site, the outcome could alter respectively between a non penetration or a penetration during successive impact tests.

There are many sources of variability, with each source having a different extent of effect on the probabilistic impact response depending on the degree of coupling between the sources of variability as well as the particular impact scenario. It is thus critical to understand both the isolated and coupled effect of these sources on the PVR curve to ensure that the structure perform at the required level of protection. In composite materials there are many properties that shows randomness and to determine the PVR curve for each combination of design inputs a huge number of tests has to be performed. It quickly becomes clear that only relying on destructive experimental testing would result impractical for the required time, cost, material, labor and infrastructure. Ex-

perimental impact testing can be considered a good approach in the sense that it constitutes real data that simultaneously incorporates all potential form of variability. However this also happen to be a drawback since it's extremely difficult to isolate the source of variability and understand which is the effect of the single source and witch are predominant.

An alternative to destructive experimental impact testing is to use computational techniques such as the finite element method (FEM). As a result of recent increases in computational capabilities, numerous models have been developed to simulate material behavior across multiple length scales [24]. While most material models are deterministic in character, real materials exhibit statistical variations in properties and features over a range of different length scales. The obvious advantage of using numerical simulations to study the impact response of composite is the complete control over the source of variability incorporated into the study. Thus the effect of each probabilistic property can be studied and conceptual composite architectures with parametric varied material properties can be easily and rapidly simulated. Traditional FE analyses are still based on deterministic techniques that do not account for the sources of variability and therefore cannot predict the probabilistic impact response (i.e. PVR curve).

The development of a stochastic computational framework represent an important opportunity to raise a new level in structure modeling and design, especially for components that are influenced by probabilistic sources of variability. Between the possible approaches that can be used the theory of multiscale modeling has shown a good grade of success combined with a good computational efficiency. Multiscale modeling allows the analyst to design the material including parameters like fiber arrangement and packing, fiber strength and defects, matrix characteristic and void presence. Once the architecture and the microscale level parameters are defined it's possible to obtain the usual engineering FEM input values. This bridging between microscale and macroscale allows to implement probabilistic distributions on material constituents properties and study their single or combined effect on the engineering constant used to perform the final FE analysis.

1.1 Motivation of the study

With the increase of the use of composite material in impact susceptible structures and the increase attention of the aeronautical industry to efficiency and cost the creation of a new mathematical procedure could improve the power and reliability of numerical simulations used in ballistic impacts reducing the necessity of expensive and often very hard to set up, experimental testing.

For this reasons inside the NASA Advanced Composite Project a collaboration between Livermore Software Technology Corp (LSTC), George Mason University, Ohio State University, Arizona State University and NASA Glenn Research Center started to work on the creation of a new LS-Dyna Material Model, MAT 213, which will incorporate the results of the final sensitivity simulations of this work to introduce inbuilt stochastic parameters.

This will help to produce more accurate and non-deterministic simulations without the necessity of extensive experimental campaigns.

1.2 Organization of the work

The primary research object is to develop a computational procedure able to predict the probabilistic ballistic impact performances of a composite structure. After introducing the basic theory of composite materials (Chapter 2) to create the actual framework using the technique of multiscale modeling the three principal steps followed are:

- Identification of the main software and their combinations (Chapter 3);
- Development of the stochastic microscale analysis (Chapter 4);
- Sensitivity analysis is implemented to comprehend the influence of the stochastic microscale parameters in the material rupture (Chapter 5);
- Creation of a set of macroscale impact simulations to obtain the PVR (Chapter 6) ;

The material chosen to test this analytical procedure is strengthened epoxy carbon-fiber orthotropic reinforced polymer T800-F3900 which has been used to calibrate the MAT213 material model in LS-DYNA for the creation of the numerical model ballistic experiment which will be used for the final PVR curve generation. [28]

Chapter 2

Fundamentals of composite materials

A composite material can be defined as a combination of two or more materials that results in better properties than those of the individual components used alone. In contrast to metallic alloys, each material retains its separate chemical, physical, and mechanical properties. The two constituents are a reinforcement and a matrix. The main advantages of composite materials are their high strength and stiffness, combined with low density, when compared with bulk materials, allowing for a weight reduction in the finished part. The reinforcing phase provides the strength and stiffness. In most cases, the reinforcement is harder, stronger, and stiffer than the matrix. The reinforcement is usually a fiber or a particulate. Particulate composites have dimensions that are approximately equal in all directions. They may be spherical, platelets, or any other regular or irregular geometry. Particulate composites tend to be much weaker and less stiff than continuous fiber composites, but they are usually much less expensive. Particulate reinforced composites usually contain less reinforcement (up to 40 to 50 volume percent) due to processing difficulties and brittleness. A fiber has a length that is much greater than its diameter. The length-to-diameter (l/d) ratio is known as the aspect ratio and can vary greatly. Continuous fibers have long aspect ratios, while discontinuous fibers have short aspect ratios. Continuous-fiber composites normally have a preferred orientation, while discontinuous fibers generally have a random orientation. Examples of reinforcement arrangements is shown if figure 2.1.

Continuous-fiber composites are often made into laminates by stacking single sheets of continuous fibers in different orientations to obtain the desired strength and stiffness properties with fiber volumes as high as 60 to 70 percent. Fibers produce high-strength composites because of their small diameter; they contain

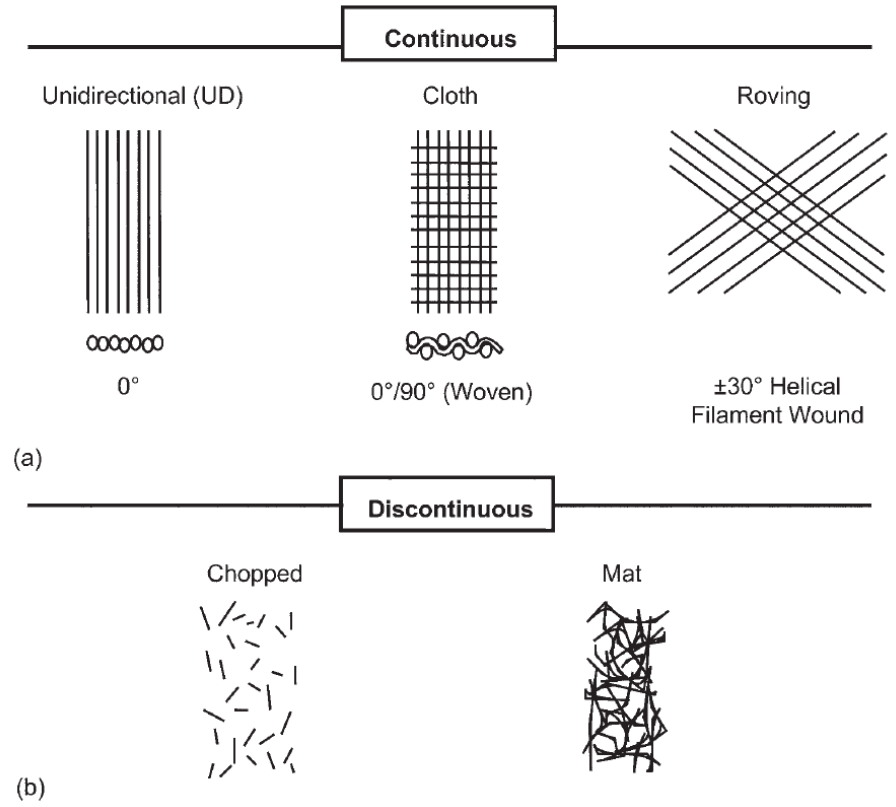

Figure 2.1: Reinforcements typology

far fewer defects (normally surface defects) compared to the material produced in bulk. As a general rule, the smaller the diameter of the fiber, the higher its strength, but often the cost increases as the diameter becomes smaller. In addition, smaller-diameter high-strength fibers have greater flexibility and are more amenable to fabrication processes such as weaving or forming. Typical fibers include glass, aramid, and carbon, which may be continuous or discontinuous. The continuous phase is the matrix, which is a polymer, metal, or ceramic. Polymers have low strength and stiffness, metals have intermediate strength and stiffness but high ductility, and ceramics have high strength and stiffness but are brittle. The matrix (continuous phase) performs several critical functions, including maintaining the fibers in the proper orientation and spacing and protecting them from abrasion and the environment. In polymer and metal matrix composites that form a strong bond between the fiber and the matrix, the matrix transmits loads from the matrix to the fibers through shear loading at the interface. The type and quantity of the reinforcement determine the final properties. The highest strength and modulus are obtained with continuous-fiber

composites. There is a practical limit of about 70 percent of volume reinforcement that can be added to form a composite. At higher percentages, there is too little matrix to support the fibers effectively. Continuous-fiber composites are used where high strength and stiffness are required (but at a higher cost), and discontinuous-fiber composites are used where cost is the main driver and strength and stiffness are less important.

2.1 Laminates

Continuous-fiber composites are normally laminated materials (Fig. 2.2) in which the individual layers, plies, or laminae are oriented in directions that will enhance the strength in the primary load direction. Unidirectional (0°) laminae are extremely strong and stiff in the 0° direction. However, they are very weak in the 90° direction because the load must be carried by the much weaker polymeric matrix. While a high-strength fiber can have a tensile strength of 3500 MPa or more, a typical polymeric matrix normally has a tensile strength of only 35 to 70 MPa (Fig. 2.3). The longitudinal tension and compression loads are carried by the fibers, while the matrix distributes the loads between the fibers in tension and stabilizes the fibers and prevents them from buckling in compression. The matrix is also the primary load carrier for interlaminar shear (i.e., shear between the layers) and transverse (90°) tension. Because the fiber orientation directly impacts mechanical properties, it seems logical to orient as many of the layers as possible in the main load-carrying direction. While this approach may work for some structures, it is usually necessary to balance the load-carrying capability in a number of different directions, such as the 0°, +45°, -45°, and 90° directions. A balanced laminate having equal numbers of plies in the 0°, +45°, –45°, and 90° degrees directions is called a quasi-isotropic laminate, because it carries equal loads in all four directions.

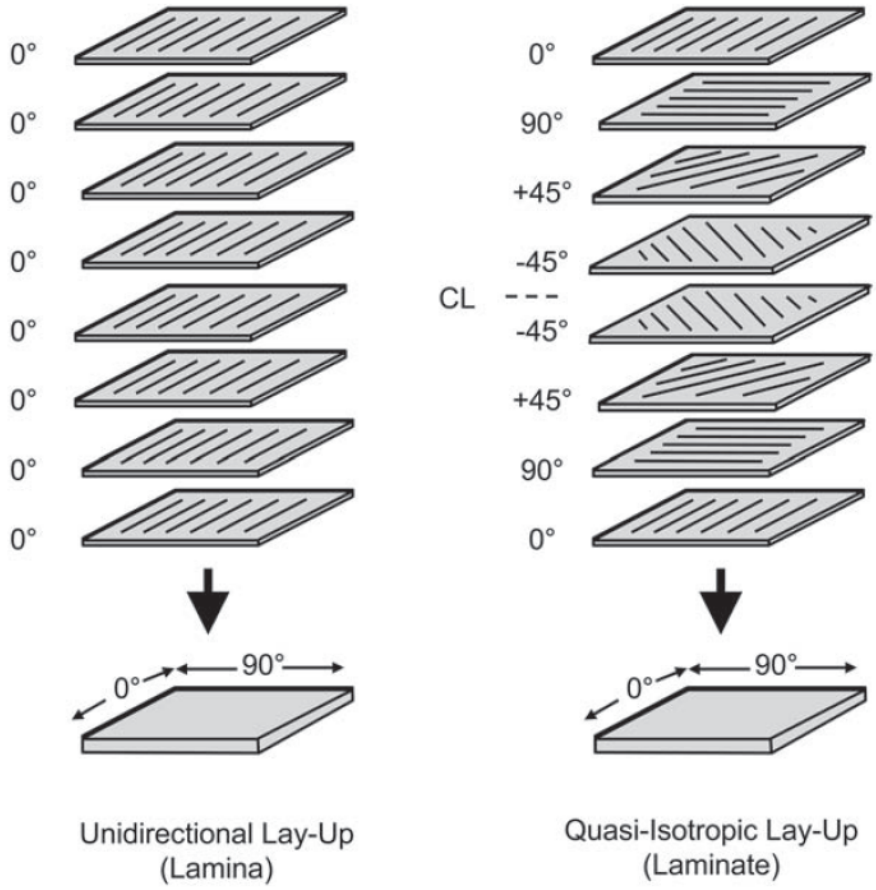

Figure 2.2: Lamina and Laminate lay-ups

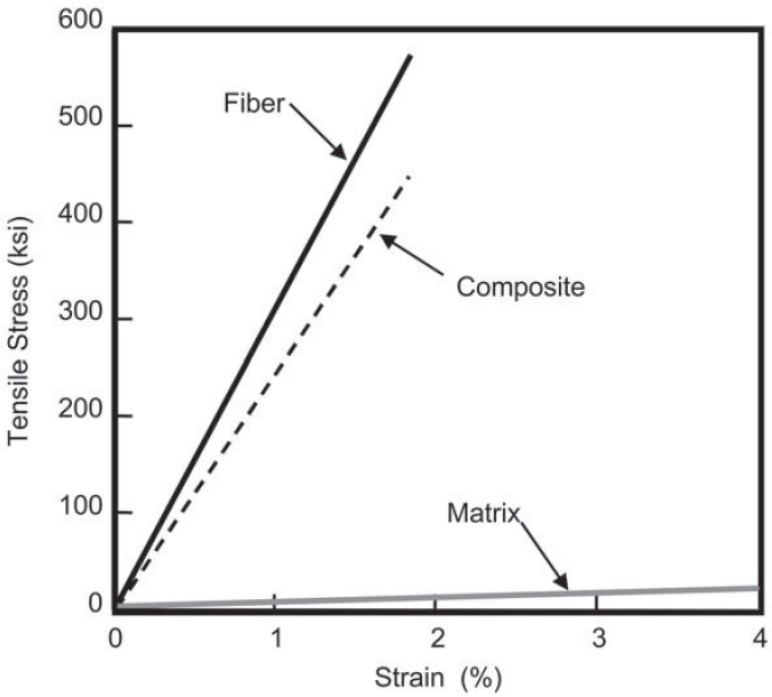

Figure 2.3: Vf distribution

Fundamental Property Relationship

When a unidirectional continuous-fiber lamina or laminate is loaded in a direction parallel to its fibers (0^o or 11-direction) the longitudinal modulus E_{11} can be estimated from its constituents properties by using what is known as the rule of mixtures:

$$E_{11} = E_f V_f + E_m V_m \tag{2.1}$$

where E_f is the fiber modulus, V_f is the fiber volume percentage, E_m is the matrix modulus, and V_m is the matrix volume percentage. The longitudinal tensile strength σ_{11} also can be estimated by the rule of mixtures:

$$\sigma_{11} = \sigma_f V_f + \sigma_m V_m \tag{2.2}$$

where σ_f and σ_m are the ultimate fiber and matrix strengths, respectively. Because the properties of the fiber dominate for all practical volume percentages, the values of the matrix can often be ignored; therefore:

$$E_{11} = E_f V_f \tag{2.3}$$

$$\sigma_{11} = \sigma_f V_f \tag{2.4}$$

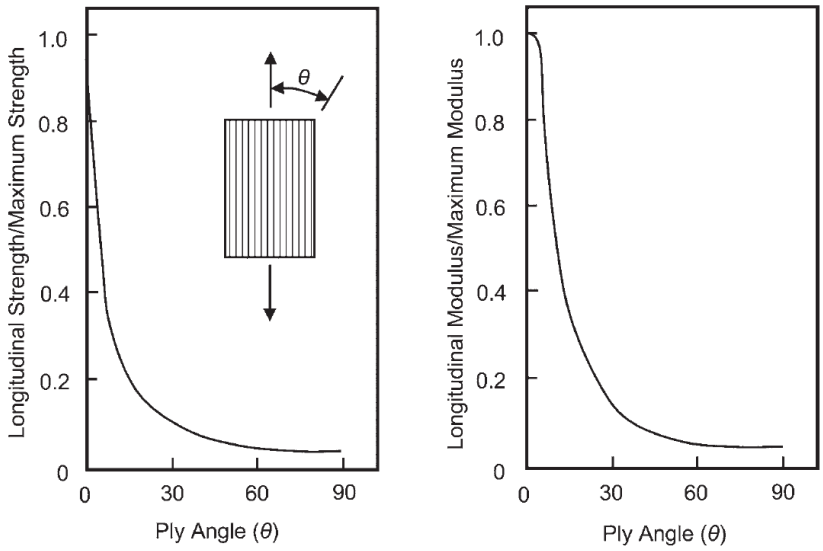

Figure 2.4: Influence of ply angle on strength and modulus

It's clear the dominant role of the fibers in determining the lamina strength and stiffness. When loads are parallel to the fibers (0°), the ply is much stronger and stiffer than when loads are transverse (90°) to the fiber direction. There is a dramatic decrease in strength and stiffness resulting from only a few degrees of misalignment off of 0°. When the lamina shown in Fig. 2.4 is loaded in the transverse (90° or 22-direction), the fibers and the matrix function in series, with both carrying the same load. The transverse modulus of elasticity E_{22} is given as:

$$\frac{1}{E_{22}} = \frac{V_f}{E_f} + \frac{V_m}{E_m} \tag{2.5}$$

Figure 2.5 shows the variation of modulus as a function of fiber volume percentage. When the fiber percentage is zero, the modulus is essentially the modulus of the polymer, which increases up to 100 percent (where it is the modulus of the fiber). At all other fiber volumes, the E_{22} or 90^o modulus is lower than the E_{11} or zero degrees modulus, because it is dependent on the

much weaker matrix. Other rule of mixture expressions for lamina properties include those for the Poisson's ratio ν_{12} and for the shear modulus G_{12}:

$$\nu_{12} = \nu_f V_f + \nu_m V_m \tag{2.6}$$

$$\frac{1}{G_{12}} = \frac{V_f}{G_f} + \frac{V_m}{G_m} \tag{2.7}$$

These expressions are somewhat less useful than the previous ones, because the values for Poisson's ratio ν_f and the shear modulus G_f of the fibers are usually not readily available. Physical properties, such as density ρ, can also be expressed using rule of mixture relations:

$$\rho_{12} = \rho_f V_f + \rho_m V_m \tag{2.8}$$

While these micromechanics equations are useful for a first estimation of lamina properties when no data are available, they generally do not yield sufficiently accurate values for design purposes. For design purposes, basic lamina and laminate properties should be determined using actual mechanical property testing.

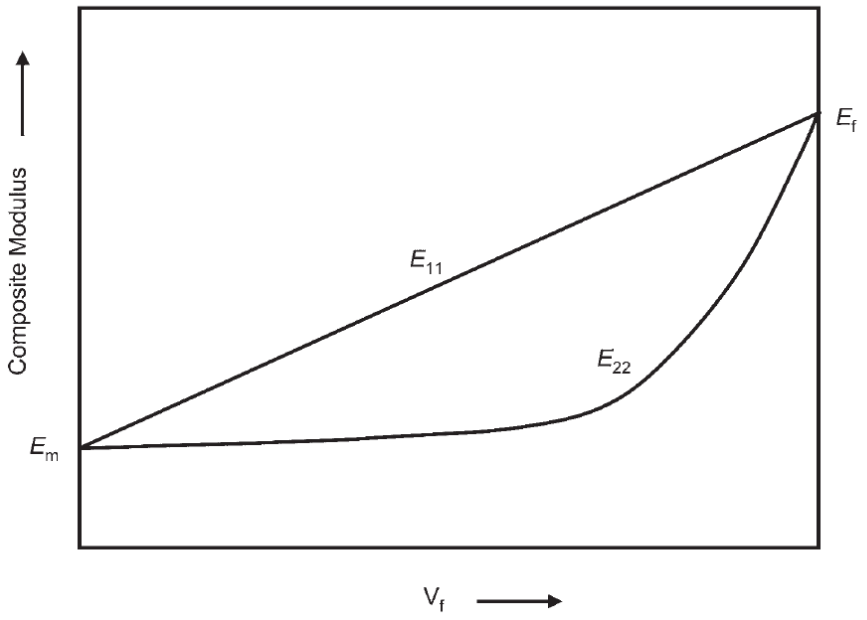

Figure 2.5: Variation of composite modulus of a unidirectional 0° lamina as a function of fiber volume fraction

Composite Laminate Theory

In a typical structural application of a composite, multiple layers (or laminae) of unidirectional composite are stacked together at various angles to form a laminate. The stacking sequence and orientations of the individual layers give the laminate designer additional degrees of freedom to optimize the design with respect to the strength, stiffness, buckling load, vibration response, panel flutter or other desired performance objective. The purpose of lamination theory is to predict the behavior of a laminate from a knowledge of the material properties of the individual layers and the laminate geometry.
Classical lamination theory is based upon certain simplified engineering assumptions: (1) each layer is thin and constructed of macroscopically homogeneous, orthotropic, linear-elastic material, (2) the entire laminate and all of the individual layers are assumed to be in a state of plane stress, (3) layers are perfectly bonded together, (4) the Kirchoff hypothesis is invoked, plane, normal cross sections of the entire laminate before deformations remain plane, normal to the deflected middle surface, and do not change in thickness. A corollary of this last hypothesis is that the in-plane displacements vary linearly through the entire thickness of the laminate, while the normal deflection is uniform through the thickness.

A thin composite laminate could then be effectively studied as a plate whose state of deformation is described by equation:

$$\{\varepsilon\} = \{\varepsilon_0\} + z\{k\} \tag{2.9}$$

The laminate is composed by N laminae or plies, each one of them possess a coordinate system coincident with the axes of symmetry of the material, which defines the laminae axes. Laminae axes are rotated with respect to the laminate axes in XY plane. While the all plate is defined according to this XYZ coordinate system, in an individual ply, the direction 11 usually indicates the fiber direction, and the 22 direction is normal to the fiber direction.

Defined the first hypothesis and coordinate systems is possible to introduce the first step of the CLT calculation: the definition of the ABD matrix. This Matrix is a 6x6 matrix that serves as a connection between the applied loads and the associated strains in the laminate. It essentially defines the elastic properties of the entire laminate.

First the reduced stiffness matrix Q_{ij} is calculated for each material used in the laminate (if a laminate uses only one type of composite material, there will be only one stiffness matrix). The stiffness matrix describes the elastic behavior of the ply in plane loading:

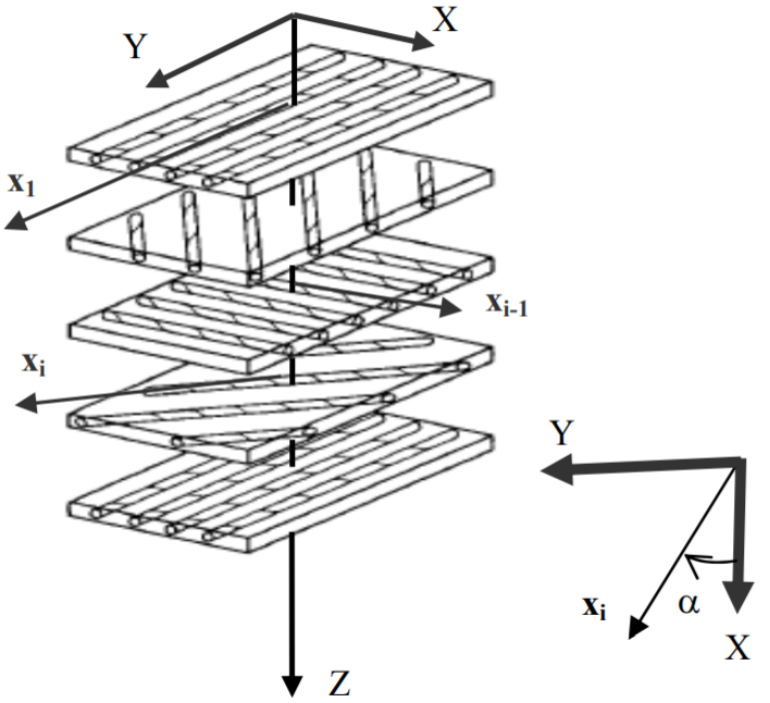

Figure 2.6: Laminae and Laminate axes

$$Q_{ij} = \begin{bmatrix} Q_{11} & Q_{12} & 0 \\ Q_{12} & Q_{22} & 0 \\ 0 & 0 & Q_{66} \end{bmatrix} \tag{2.10}$$

where

$$Q_{11} = \frac{{E_{11}}^2}{E_{11} - \nu_{12} E_{22}} \tag{2.11}$$

$$Q_{12} = \frac{\nu_{12} E_{11} E_{22}}{E_{11} - {\nu_{12}}^2 E_{22}} \tag{2.12}$$

$$Q_{12} = \frac{E_{11} E_{22}}{E_{11} - {\nu_{12}}^2 E_{22}} \tag{2.13}$$

$$Q_{66} = G_{12} \tag{2.14}$$

Now it's possible to calculate the transformed reduced stiffness matrix $\overline{Q_{ij}}$ for each ply based on the reduced stiffness matrix and fiber angle.

$$\overline{Q_{11}} = Q_{11}cos(\theta)^4 + 2(Q_{12} + 2Q_{66})cos(\theta)^2sin(\theta)^2 + Q_{22}sin(\theta)^4 \tag{2.15}$$

$$\overline{Q_{12}} = \overline{Q_{21}} = Q_{12}(cos(\theta)^4 + sin(\theta)^4) + (Q_{11} + Q_{22} - 4Q_{66})cos(\theta)^2sin(\theta)^2 \tag{2.16}$$

$$\overline{Q_{16}} = \overline{Q_{61}} = (Q_{11} - Q_{12} - 2Q_{66})cos(\theta)^3sin(\theta) - (Q_{22} - Q_{12} - 2Q_{66})cos(\theta)sin(\theta)^3 \tag{2.17}$$

$$\overline{Q_{22}} = Q_{11}sin(\theta)^4 + 2(Q_{12} + 2Q_{66})cos(\theta)^2sin(\theta)^2 + Q_{22}cos(\theta)^4 \tag{2.18}$$

$$\overline{Q_{26}} = \overline{Q_{62}} = (Q_{11} - Q_{12} - 2Q_{66})cos(\theta)sin(\theta)^3 - (Q_{22} - Q_{12} - 2Q_{66})cos(\theta)^3sin(\theta) \tag{2.19}$$

$$\overline{Q_{66}} = (Q_{11} + Q_{22} - 2Q_{12} - 2Q_{66})cos(\theta)^2sin(\theta)^2 + Q_{66}(cos(\theta)^4 + sin(\theta)^4) \tag{2.20}$$

$$\overline{Q_{ij}} = \begin{bmatrix} \overline{Q_{11}} & \overline{Q_{12}} & \overline{Q_{16}} \\ \overline{Q_{12}} & \overline{Q_{22}} & \overline{Q_{26}} \\ \overline{Q_{16}} & \overline{Q_{26}} & \overline{Q_{66}} \end{bmatrix} \tag{2.21}$$

Now calculate the A_{ij}, B_{ij},D_{ij} matrices using the following equations where z represents the position in the ply from the midplane:

$$A_{ij} = \sum_{k=1}^{n} \{Q_{ij}\}_n (z_k - z_{k-1}) \tag{2.22}$$

$$B_{ij} = \frac{1}{2} \sum_{k=1}^{n} \{Q_{ij}\}_n ({z_k}^2 - {z_{k-1}}^2) \tag{2.23}$$

$$D_{ij} = \frac{1}{3} \sum_{k=1}^{n} \{Q_{ij}\}_n ({z_k}^3 - {z_{k-1}}^3) \tag{2.24}$$

and assemble ABD and its inverse

$$ABD = \begin{bmatrix} A & B \\ B & D \end{bmatrix} \tag{2.25}$$

$$abd = ABD^{-1} \tag{2.26}$$

The midplane Strains and Curvatues induced in the laminate which represents the deflections of the laminate:

$$\begin{bmatrix} \varepsilon^0_{xx} \\ \varepsilon^0_{yy} \\ \varepsilon^0_{xy} \\ k_{xx} \\ k_{yy} \\ k_{xy} \end{bmatrix} = \begin{bmatrix} a_{11} & a_{12} & a_{16} & b_{11} & b_{12} & b_{16} \\ a_{12} & a_{22} & a_{26} & b_{12} & b_{22} & b_{26} \\ a_{16} & a_{26} & a_{66} & b_{16} & b_{26} & b_{66} \\ b_{11} & b_{12} & b_{16} & d_{11} & d_{12} & d_{16} \\ b_{12} & b_{22} & b_{26} & d_{12} & d_{22} & d_{26} \\ b_{16} & b_{26} & b_{66} & d_{16} & d_{26} & d_{66} \end{bmatrix} \begin{bmatrix} N_{xx} \\ N_{yy} \\ N_{xy} \\ M_{xx} \\ M_{yy} \\ M_{xy} \end{bmatrix} \tag{2.27}$$

X-Y plane strains for each ply:

$$\begin{bmatrix} \varepsilon_{xx} \\ \varepsilon_{yy} \\ \gamma_{xy} \end{bmatrix} = \begin{bmatrix} \varepsilon^0_{xx} \\ \varepsilon^0_{yy} \\ \gamma^0_{xt} \end{bmatrix} + z \begin{bmatrix} K_{xx} \\ K_{yy} \\ K_{xy} \end{bmatrix} \tag{2.28}$$

$$\tag{2.29}$$

and ply stresses in the X-Y coordinate system:

$$\begin{bmatrix} \sigma_{xx} \\ \sigma_{yy} \\ \tau_{xy} \end{bmatrix} = \begin{bmatrix} \overline{Q_{11}} & \overline{Q_{12}} & \overline{Q_{16}} \\ \overline{Q_{12}} & \overline{Q_{22}} & \overline{Q_{26}} \\ \overline{Q_{16}} & \overline{Q_{26}} & \overline{Q_{66}} \end{bmatrix} \begin{bmatrix} \varepsilon_{xx} \\ \varepsilon_{yy} \\ \varepsilon_{xy} \end{bmatrix} \tag{2.30}$$

Chapter 3

Development of the multiscale stochastic computational framework

The core of this research is the creation of an analytic procedure able to introduce into impact simulations the probabilistic nature of certain characteristics at the microscale level of composite materials in order to understand their influence on the penetration impact response. This framework should be available and useful for most of the actual standard composite materials architecture. Stochastic variations of material constituent properties could be introduced directly into FEM models using microscale level modeling but this will increase immensely the computation cost of the simulation that is based on a code not optimized for this discretization level.
Multiscale modeling can then increment the efficiency of the numerical simulation without neglecting the microscale level of the system. By considering simultaneously models at different length scale, could be possible to arrive at an approach that shares the efficiency of the macroscopic models as well as the the accuracy of the microscopic models. Multiscale modeling is a process based on the bridging between different scale lengths and could be applied whenever this connection is relevant to the final results.
In structural analysis, historically, engineers have studied the response to loading conditions focusing on the use of average material properties. This because the macroscale level stiffness and strength are directly related to the average values of the constituent properties. Whit the diffusion of fracture mechanics the importance of material constituents local properties has become much more influential on simulations results. Fracture initiation is an event driven by the local properties of the material (in case of homogeneous material) or the ma-

terial constituents (in the case of a composite material). Penetration response of structures to ballistic impact is no exception and with the use of composite materials, comprehending different constituents and thousands of fibers these aspects are even more relevant.

Multiscale modeling in this study is used to introduce the probabilistic nature of composite material constituents into FEM simulations with differentiation of analysis at the microscale and macroscale level. Splitting the different length scale onto different software and codes create a more efficient and flexible way to analyze these problems.

3.1 State of the Art in Multiscale Modeling

Due to the diminishing effect of microscale randomness at higher length scales, microstructural variability is often ignored when studying structural behaviour, however in some type of composite structures under particular concentrated loading conditions such as in impact resistant structures the local properties are highly dominant for the failure generation. As experimental data of impact simulations show for a precise impact velocity on a chosen component is possible to define the probability of penetration. For this reason, especially in composite materials, due to their complex microscale nature studies about the influence of stochastic variations of their properties are becoming more and more common.

The numerical investigation of the effects of variability of microscale characteristics has to be supported by an efficient computational framework. A direct introduction of microscale level modeling into classic FEM analysis most of the time can be computationally too expensive especially in impact analysis.

Multiscale modeling allow the scaling of information between different length scales using homogenization and localization techniques without incrementing sensibly the computational cost of the simulation. Micromechanical methods such as asymptotic field expansion separate the fields of the large scale model into small scale ones (Fish, Shek, Pandheeradi,Shephard, 1997 [12]; Fish,Yu, Shek,1999 [13]; Suquet, 1987 [25]). The bridging of these scales is performed using the homogenization functions obtainable from a variety of techniques. The Voronoi cell method (Ghosh, 2011 [7]; Ghosh, Lee, Moorthy, 1995[20]; Ghosh Liu, 1995[8]; Ghosh Moorthy, 1995 [9], Ghosh Mukhopadhyay, 1991[10]) analyzes the microscale by explicitly accounting for the composite microstructure using tessellation of polygons containing a single fiber or particle within a FEA formulation. This approach has been used by Ghosh, Liu and Raghavan (2001) [21] to develop a multiscale analysis that uses random microstructures to an-

alyze composite failure. Xu [27] and Shen and Xu [22] developed the Multiscale Stochastic Finite element Method (MSFEM) to simulate random heterogeneous material from the micro-to-meso-to-macroscales. The Generalized Method of Cells by Paley and Aboudi [17] has been then implemented by Bednarcyk Arnold [4] to create the Micromechanics Analysis Code, MAC/GMC, that uses GMC and HFGMC (High Fidelity Generalized Method of Cells) techniques as well as classical laminate theory to conduct multiscale analyses of composites.
Considering impact resistant structures J.P. Johnston [14] developed a stochastic computational framework with scale dependent constitutive laws and an appropriate failure theory to simulate the behavior and failure of polymer matrix composite structures subjected to complex loading showing the influence of variations in properties such as fiber volume fraction, fiber dimensions, fiber waviness, pure resin pockets, and void distributions to the composite impact performance. G. Nilankantan [15] has also performed a research about the prediction of the impact performance of flexible textile composite using multiscale and probabilistic methods. Here a yarn model comprised of a filament level architecture is developed to investigate the feasibility of solid element based homogenized yarn models as well as the effect of filament strength, spreading and intern-filament friction on the impact response and the numerical determination of the probabilistic velocity response curve. Ricks and Lacy have developed a multiscale modeling methodology that incorporates a statistical distributions of fiber strength into coupled micromechanics/finite element analysis. Here has been investigated the effect of a statistical fiber strength distribution and microscale architecture on the failure behavior of a dogbone specimen of SCS-6 / TIMETAL 21S material. Goldberg and Bonacuse [18] investigated the effects of the microstructural variations of woven ceramic matrix composites on the effective properties and response of the material and Arnold et Al.studied the microstructural Influence on Deformation and Fatigue Life of Composites.

For this work the code MAC/GMC will be used to introduce the probabilistic nature of material characteristic and to generate the input for the Material Card in LS-Dyna helping the bridging from microscale to macroscale.

3.2 Structure

The computational framework used to perform the probabilistic analysis is composed by three main software: NASA MAC/GMC, LS-OPT and LS-DYNA. Next to this sofwares Matlab has been used to manage, automatize and post-process data and output of the simulations.

This architecture allows to start from the probabilistic definitions of the

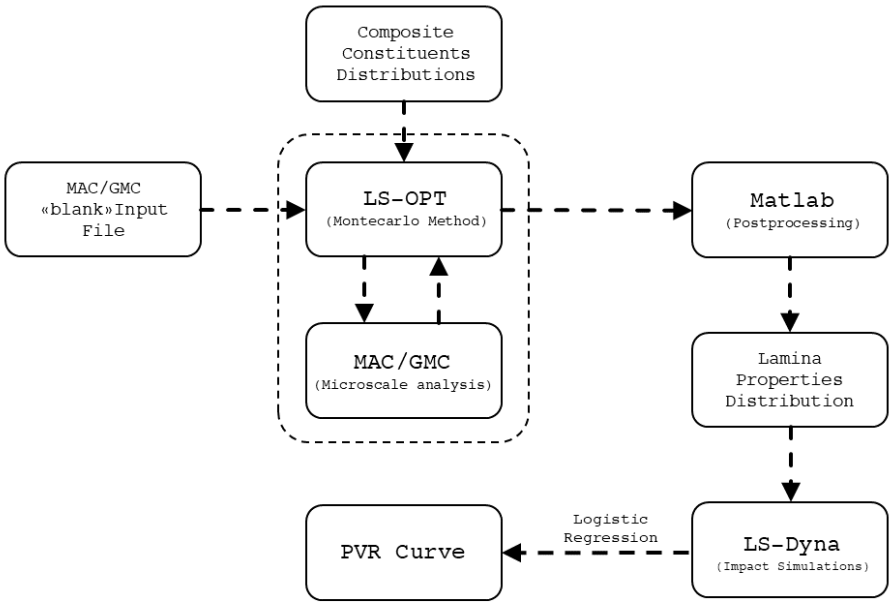

Figure 3.1: Computational framework structure.

composite constituent properties and obtain as a result the probabilistic velocity response curve of the structure under the studied ballistic impact and is also possible to determine through sensitivity analysis which of the lamina properties are more relevant in fracture initiation.

3.3 Software

3.3.1 MAC/GMC

MAC/GMC is a computer code developed at NASA Glenn Research Center that analyzes the thermoelastic behavior of composite materials and laminates. The code is based on the micromechanics theory known as the generalized method of cells (GMC). GMC models the response of composite materials using a doubly or triply periodic repeating unit cell (RUC), which is composed of a number of subcells (see Figure 3.2 and Figure 3.2).

By placing distinct constituent materials within the subcells, an heterogeneous (composite) material can be modeled, provided an RUC can be identified in the material's micro scale architecture. The main advantages of the generalized method of cells over other micromechanics theories and approaches are: 1) its fully multi-axial formulation, 2) the availability of local (constituent level) stress and strain fields, and 3) its computational efficiency. The availability of the local fields makes the method attractive in situations where more

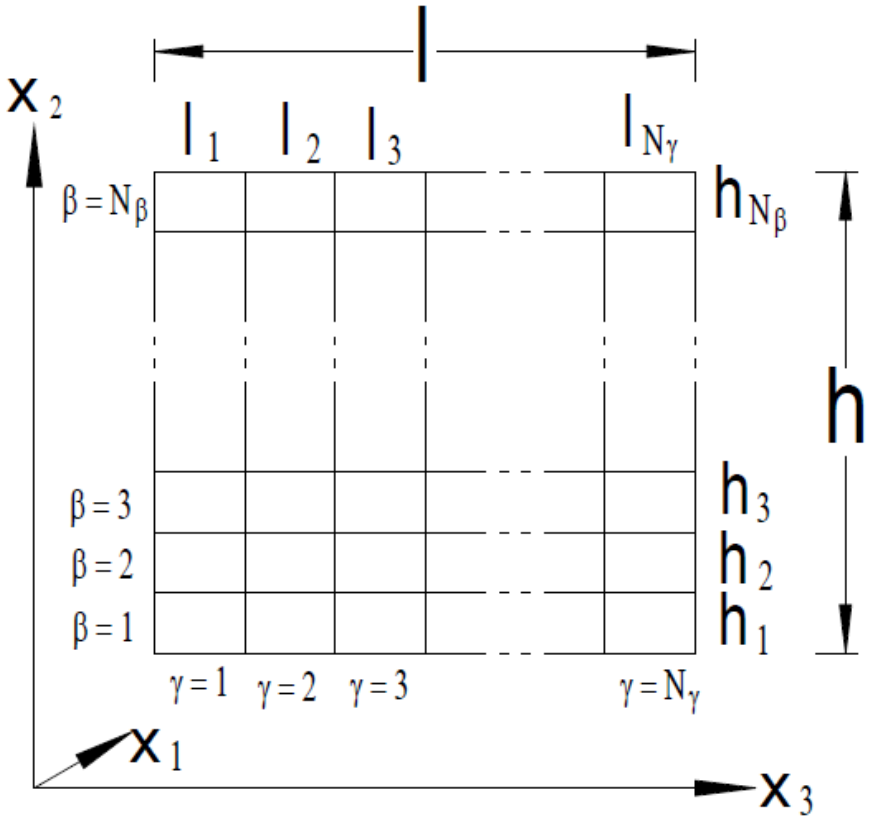

Figure 3.2: 2D RUC

detailed composite analysis, beyond simple determination of effective thermoelastic properties, is necessary. In such situations, when matrix inelasticity, constituent damage or failure, or fiber-matrix debonding is important, the availability of the local fields is critical in order to account for these effects appropriately. It is the purpose of the MAC/GMC code to provide a convenient and user-friendly "package" for the GMC theories, in addition to providing significant added value through a library of inelastic constitutive models, repeating unit cells, thermo-mechanical and yield surface loading options, failure and damage analysis capabilities, and results generation options. The original method of cells (which allowed only four subcells) was developed by Aboudi [3] in 1989, the doubly periodic version of GMC by Paley and Aboudi (1992) [17], and the triply periodic version of GMC by Aboudi (1995) [2]. The actual GMC theories implemented within MAC/GMC 4.0 were reformulated for maximum computational efficiency by Pindera and Bednarcyk (1999) and Bednarcyk and Pindera (2000). A recent advancement in the GMC technology has significantly

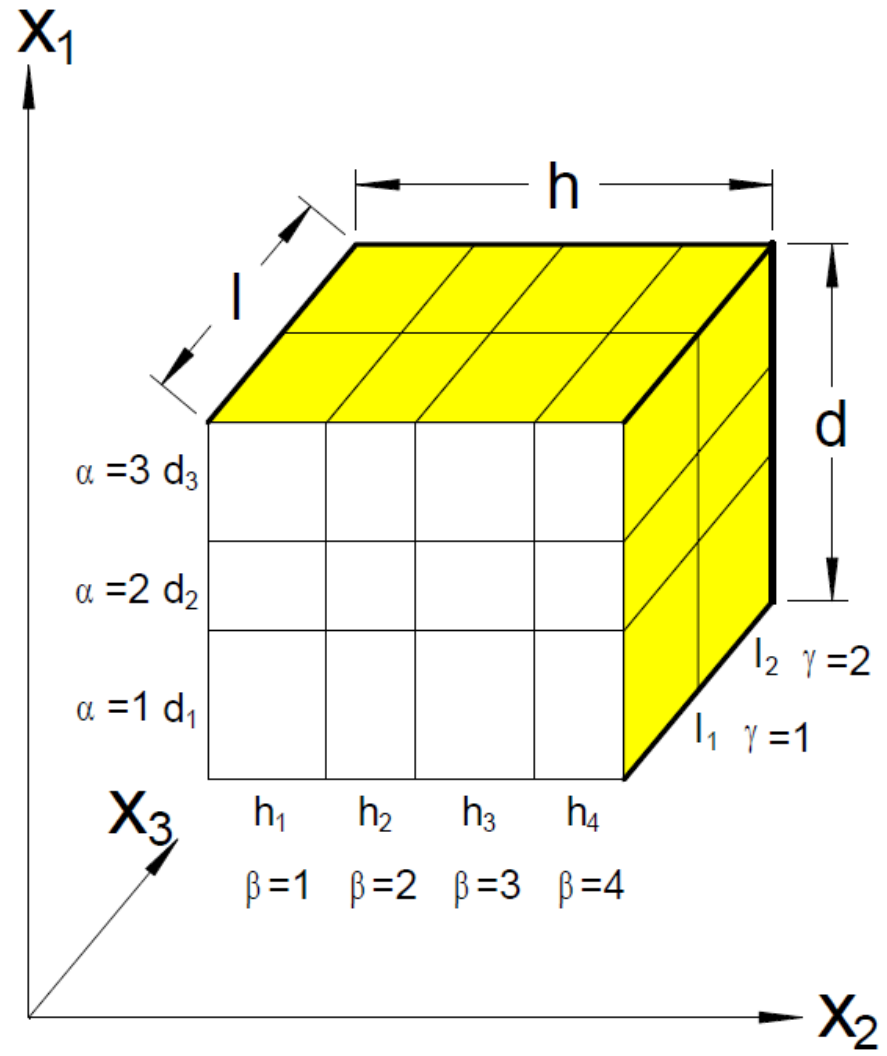

Figure 3.3: 3D RUC

improved the local accuracy of the doubly periodic version of the model. This new micromechanics theory, called the high-fidelity generalized method of cells (HFGMC), developed by Aboudi et al. (2001, 2002), has also been implemented with MAC/GMC. As mentioned, MAC/GMC 4.0 is also capable of analyzing composite laminates. The composite laminate analysis capabilities also rely on the GMC composite material model. The doubly and triply periodic versions of GMC function within the context of classical lamination theory (Jones, 1975; Herakovich, 1998) to model the ply level composite material. Thus, the code can analyze the thermo-inelastic behavior of arbitrary laminate configurations.

Microscale Modeling with Generalized Method of cells

The ability to accurately predict the thermomechanical properties of of advanced multi-phase composites plays a critical role in the development and practical implementation of these strategic materials. The analytical models that predict the effective behavior of composites are used both by engineers to perform structural analysis and by material scientist to develop new material systems. To fulfill this two different functions the analytical model must be based on a micromechanics approach which utilizes physically based deformation and life constitutive models and generates the average (macro) response of a composite material given the properties of the individual constituents and their geometric arrangement. Only then can such a model be used to investigate the effect of different deformation mechanisms on the overall response of the composite in order to identify the appropriate constituents for a given application. Alternatively, if a microscale method is to be used in a large scale structural analysis it must be: computation efficient, able to generate accurate displacement and stress field at both macro and microscale level and must be compatible with the finite element method. Also, as advancements in processing and fabrication of techniques make it possible to more accurately engineer the architectures of these advanced composite systems the importance of an accurate and computationally efficient multiscale analysis capable of accurately predict the effect of microstructural details on the internal and macroscopic behavior of composite becomes even more relevant.
Aboudis's method of cells and its continuous/discontinuous reinforcement generalization present the required computational efficiency and a sufficient accuracy both at the micro and macro scale level and for this reasons represent the base of the MAC/GMC software. GMC is capable of predicting the response of both continuous and discontinuous multi-phase composites with arbitrary internal microstructures and reinforcement shapes. GMC is a continuum-based micromechanics model that provides closed-form expressions for the macroscopic composite response in terms of properties, size, shape, distribution and response of the individual constituents or phases that make up the material. Furthermore, expressions relating the internal stress and strain fields in the individual constituents in term of the macroscopically applied stresses and strains are available through strain or stress concentration factors. These expressions make possible the investigation of failure processes at the microscopic level at each step of an applied load history.

In the original formulations of the method of cells a continuously or discontinuously reinforced, unidirectional fibrous composite was modeled as a rectangular double periodic (or triple periodic) array of fibers embedded in a matrix phase. The periodic character of the assemblage allowed identification of a repeating

unit cell that can be used as a building block to construct the entire composite.

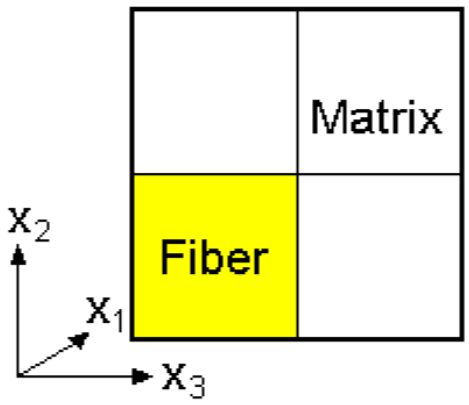

Figure 3.4: Double periodic RUC.

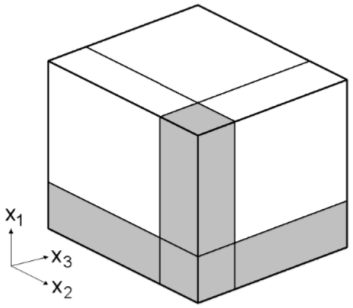

Figure 3.5: Triple periodic RUC.

The properties of the repeating unit cell were thus representative of the properties of the entire assemblage. The unit cell consisted of a single fiber subcell surrounded by three matrix subcells for continuous and seven for discontinuous composites, hence the name method of cells. The rectangular geometry of the repeating unit cell allowed one to to obtain an approximate solution for the stresses and strains in the individual subcells given some macroscopically homogeneous state of strain or stress applied to the composite. The approximate solution to the posed boundary value problem was, in turn, used to determine macroscopic (average) properties, traditionally referred to as effective properties of the composite. The method of cell has then been used the develop the generalized method of cells for continuous or discontinuous fibrous composites. The repeating unit cell can consist of an arbitrary number of phases. This generalization extend the modeling capability of the original method including modeling various fiber architectures (including both shape and packing arrangements), modeling of porosities and damage and modeling of interfacial regions around inclusions.

The basic homogenization approach taken in the micromechanical analysis consists essentially of four steps. First, the representative volume element of the periodic composite is identified. Second, the macroscopic or average stress and strain states in terms of the individual microscopic (subcell) stress and strain states is defined. Third, the continuity of tractions and displacements are imposed at the boundaries between the constituents. These three steps, in conjunction with micro-equilibrium, establish the relationship between micro (sub-

cell) total, thermal and inelastic strains and macro (composite strains) via the relevant concentration tensors. In the fourth and final step,the overall macro constitutive equations of the composite are determined. These four steps form the basis of the micro-to-macromechanics analysis which describes the behavior of heterogeneous media. The resulting micromechanical analysis establishes the overall (macro) behavior of the multi-phase composite which is expressed as a constitutive relation between the average stress, strain, thermal, and inelastic strains, in conjunction with the effective elastic stiffness matrix.

$$\underset{\sim}{\bar{\boldsymbol{\sigma}}} = \underset{\sim}{\boldsymbol{B}}^{*}(\underset{\sim}{\bar{\boldsymbol{\varepsilon}}} - \underset{\sim}{\bar{\boldsymbol{\varepsilon}}}^{I} - \underset{\sim}{\bar{\boldsymbol{\varepsilon}}}^{T}) \tag{3.1}$$

Where for the most general case of discontinuous reinforcements with N_α by N_β by N_γ number of subcells, the effective elastic stiffness matrix, $\underset{\sim}{\boldsymbol{B}}^{*}$ of the composite is given by:

$$\underset{\sim}{\boldsymbol{B}}^{*} = \frac{1}{dhl}\sum_{\alpha=1}^{N_\alpha}\sum_{\beta=1}^{N_\beta}\sum_{\gamma=1}^{N_\gamma} d_\alpha h_\beta l_\gamma \underset{\sim}{\boldsymbol{C}}^{(\alpha\beta\gamma)} \underset{\sim}{\boldsymbol{A}}^{(\alpha\beta\gamma)} \tag{3.2}$$

the composite inelastic strain vector is defined as:

$$\underset{\sim}{\bar{\boldsymbol{\varepsilon}}}^{I} = \frac{-\underset{\sim}{\boldsymbol{B}}^{*-1}}{dhl}\sum_{\alpha=1}^{N_\alpha}\sum_{\beta=1}^{N_\beta}\sum_{\gamma=1}^{N_\gamma} d_\alpha h_\beta l_\gamma \underset{\sim}{\boldsymbol{C}}^{(\alpha\beta\gamma)}(\underset{\sim}{\boldsymbol{D}}^{(\alpha\beta\gamma)}\underset{\sim}{\boldsymbol{\varepsilon}}_s^{I} - \underset{\sim}{\bar{\boldsymbol{\varepsilon}}}^{I(\alpha\beta\gamma)}) \tag{3.3}$$

the average thermal strain vector as,

$$\underset{\sim}{\bar{\boldsymbol{\varepsilon}}}^{T} = \frac{-\underset{\sim}{\boldsymbol{B}}^{*-1}}{dhl}\sum_{\alpha=1}^{N_\alpha}\sum_{\beta=1}^{N_\beta}\sum_{\gamma=1}^{N_\gamma} d_\alpha h_\beta l_\gamma \underset{\sim}{\boldsymbol{C}}^{(\alpha\beta\gamma)}(\underset{\sim}{\boldsymbol{D}}^{(\alpha\beta\gamma)}\underset{\sim}{\boldsymbol{\varepsilon}}_s^{T} - \underset{\sim}{\bar{\boldsymbol{\varepsilon}}}^{T(\alpha\beta\gamma)}) \tag{3.4}$$

and $\bar{\varepsilon}$ is the uniform applied macro (composite) strain. In the component analyzed in this study the reinforcement is not discontinuous but continuous. In this case the number of subcell is only N_β by N_γ and the previous equations reduces to the following:

$$\underset{\sim}{\boldsymbol{B}}^{*} = \frac{1}{hl}\sum_{\beta=1}^{N_\beta}\sum_{\gamma=1}^{N_\gamma} h_\beta l_\gamma \underset{\sim}{\boldsymbol{C}}^{\beta\gamma} \underset{\sim}{\boldsymbol{A}}^{\beta\gamma} \tag{3.5}$$

$$\underset{\sim}{\bar{\boldsymbol{\varepsilon}}}^{I} = \frac{-\underset{\sim}{\boldsymbol{B}}^{*-1}}{hl}\sum_{\beta=1}^{N_\beta}\sum_{\gamma=1}^{N_\gamma} h_\beta l_\gamma \underset{\sim}{\boldsymbol{C}}^{(\beta\gamma)}(\underset{\sim}{\boldsymbol{D}}^{(\beta\gamma)}\underset{\sim}{\boldsymbol{\varepsilon}}_s^{I} - \underset{\sim}{\bar{\boldsymbol{\varepsilon}}}^{I(\beta\gamma)}) \tag{3.6}$$

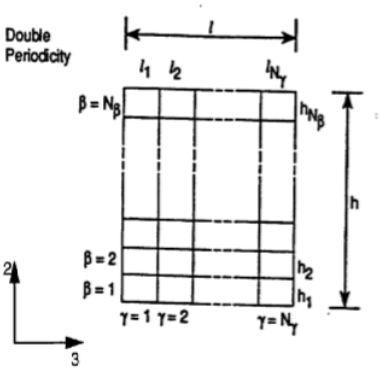

Figure 3.6: Double periodicicty

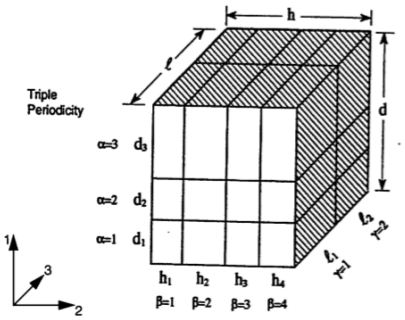

Figure 3.7: Triple periodicity

$$\underset{\sim}{\bar{\varepsilon}}^T = \frac{-\underset{\sim}{\boldsymbol{B}}^{*-1}}{hl} \sum_{\beta=1}^{N_\beta} \sum_{\gamma=1}^{N_\gamma} h_\beta l_\gamma \underset{\sim}{\boldsymbol{C}}^{(\beta\gamma)} (\underset{\sim}{\boldsymbol{D}}^{(\beta\gamma)} \underset{\sim}{\varepsilon}_s^T - \underset{\sim}{\bar{\varepsilon}}^{T(\beta\gamma)}) \tag{3.7}$$

In the above equations matrix notation is employed; where, for example, the average stress, $\underset{\sim}{\bar{\sigma}}$, average strain, $\underset{\sim}{\bar{\varepsilon}}$, and inelastic subcell strain, $\underset{\sim}{\varepsilon}_s^I$, vectors represent:

$$\underset{\sim}{\bar{\sigma}} = \{\bar{\sigma}_{11}, \bar{\sigma}_{22}, \bar{\sigma}_{33}, \bar{\sigma}_{23}, \bar{\sigma}_{13}, \bar{\sigma}_{12}\} \tag{3.8}$$

$$\underset{\sim}{\bar{\varepsilon}} = \{\bar{\varepsilon}_{11}, \bar{\varepsilon}_{22}, \bar{\varepsilon}_{23}, \bar{\varepsilon}_{23}, \bar{\varepsilon}_{13}, \bar{\varepsilon}_{12}\} \tag{3.9}$$

$$\underset{\sim}{\varepsilon}_s^I = \{\underset{\sim}{\bar{\varepsilon}}_s^{I(111)}, \underset{\sim}{\bar{\varepsilon}}_s^{I(222)}, ..., \underset{\sim}{\bar{\varepsilon}}_s^{I(N_\alpha N_\beta N_\gamma)}\} \tag{3.10}$$

where the six components of the vector $\underset{\sim}{\varepsilon}^{I(\alpha\beta\gamma)}$ are arranged as in eq. 3.9. Similar definitions for $\underset{\sim}{\varepsilon}_s^T$, $\underset{\sim}{\varepsilon}^{T(\alpha\beta\gamma)}$ also exist. Note that the key ingredient in the construction of this macro constitutive law is the derivation of the appropriate concentration matrices, $\underset{\sim}{\boldsymbol{A}}^{(\alpha\beta\gamma)}$ and $\underset{\sim}{\boldsymbol{D}}^{(\alpha\beta\gamma)}$ having the dimensions 6x6 and by $N_\alpha N_{beta} N_{gamma}$ respectively, at the micro (subcell) level. The matrix $\underset{\sim}{\boldsymbol{C}}^{(\alpha\beta\gamma)}$ represents the elastic stiffness tensor of each subcell $(\alpha\beta\gamma)$ and $d_\alpha, h_\beta, l_\gamma$ the respective subcell dimensions wherein,

$$d = \sum_{\alpha=1}^{N_\alpha} d_\alpha \tag{3.11}$$

$$h = \sum_{\beta=1}^{N_\beta} h_\beta \tag{3.12}$$

$$l = \sum_{\gamma=1}^{N_\gamma} l_\gamma \tag{3.13}$$

Similarly, given the concentration matrices $\underset{\sim}{\boldsymbol{A}}^{(\alpha\beta\gamma)}$ and $\underset{\sim}{\boldsymbol{D}}^{(\alpha\beta\gamma)}$,expressions for the average strain in each subcell can be constructed, i.e.,

$$\underset{\sim}{\boldsymbol{\varepsilon}}^{(\alpha\beta\gamma)} = \underset{\sim}{\boldsymbol{A}}^{(\alpha\beta\gamma)} \underset{\sim}{\overline{\boldsymbol{\varepsilon}}} + \underset{\sim}{\boldsymbol{D}}^{(\alpha\beta\gamma)} (\underset{\sim}{\boldsymbol{\varepsilon}}_s^{I(\alpha\beta\gamma)} + \underset{\sim}{\boldsymbol{\varepsilon}}_s^{T(\alpha\beta\gamma)}) \tag{3.14}$$

as well as average stress

$$\underset{\sim}{\overline{\boldsymbol{\sigma}}}^{\alpha\beta\gamma} = \underset{\sim}{\boldsymbol{C}}^{(\alpha\beta\gamma)} (\underset{\sim}{\boldsymbol{A}}^{(\alpha\beta\gamma)} \underset{\sim}{\overline{\boldsymbol{\varepsilon}}} + \underset{\sim}{\boldsymbol{D}}^{(\alpha\beta\gamma)} (\underset{\sim}{\boldsymbol{\varepsilon}}_s^{I(\alpha\beta\gamma)} + \underset{\sim}{\boldsymbol{\varepsilon}}_s^{T(\alpha\beta\gamma)}) - (\underset{\sim}{\boldsymbol{\varepsilon}}^{I(\alpha\beta\gamma)} + \underset{\sim}{\boldsymbol{\varepsilon}}^{T(\alpha\beta\gamma)})) \tag{3.15}$$

The analytic constitutive law (equation 3.1), may be readily applied to investigate the behavior of various types of composites, given knowledge of the behavior of the individual phases. Within MAC/GMC an incremental tangent solution scheme is utilized, therefore the appropriate rate forms of these equation are employed.

Numerous advantages can be stated regarding the current macro/micro constitutive laws as compared to the other numerical micromechanical approaches in the literature, e.g. the finite element unit cell approach. One advantage is that any type of simple or combined loading (multiaxial state of stress) can be applied irrespective of whether symmetry exists or not, as well as without resorting to different boundary condition application strategies as in the case of the finite element unit cell procedure. Another, advantage concerns the availability of an analytical expression representing the macro elastic-thermo-inelastic constitutive law, thus ensuring a reduction in memory requirements

when implementing this formulation into a structural finite element analysis code. Furthermore, this formulation has been shown to predict accurate macro behavior given only a few subcells, within the repeating cell.

The equations of GMC-3D (and consequently through appropriate specialization GMC-2D) have been reformulated to improve the computational efficiency and are implemented into MAC/GMC becoming the default setting. By nature of the traction continuity conditions within the original generalized method, all six stress components are not unique in every subcell. Normal stress components are constant in certain rows of subcells, while shear stress components are constant in certain layers of subcells. The unique subcell stress components are denoted as,

$$T_{11}{}^{\beta\gamma}, T_{22}{}^{\alpha\gamma}, T_{33}{}^{\alpha\beta}, T_{23}{}^{\alpha}, T_{13}{}^{\beta}, T_{12}{}^{\gamma} \tag{3.16}$$

Consequently, a more efficient formulation of GMC can be obtained by applying traction continuity directly (i.e. recognizing that traction continuity conditions require no more and no less than the aforementioned reduction in subcell stress components) and using subcell stresses rather than strains as the basic unknown quantities. Accordingly, the continuity of displacement conditions are formed in terms of subcell stresses (through the use of the subcell constitutive and kinematic equations), and the mixed concentration equations for the unit cell are constructed,

$$\underset{\sim}{\boldsymbol{T}} = \underset{\sim}{\boldsymbol{G}}^{\alpha\beta\gamma}\underset{\approx}{\boldsymbol{\varepsilon}} + \underset{\sim}{\boldsymbol{G}}^{IT(\alpha\beta\gamma)}(\underset{\approx}{\boldsymbol{\varepsilon}}_s{}^{I} + \underset{\approx}{\boldsymbol{\varepsilon}}_s{}^{T}) \tag{3.17}$$

Here, $\underset{\sim}{\boldsymbol{T}}$ is the vector of all subcell stress components listed in eq 3.16, $\underset{\sim}{\boldsymbol{G}}^{(\alpha\beta\gamma)}$ is the subcell mixed concentration matrix, and $\underset{\sim}{\boldsymbol{G}}^{IT(\alpha\beta\gamma)}$ is the subcell inelastic-thermal mixed concentration matrix. The term *mixed* is used here because eq 3.17 relates local subcell stresses to global strains. Clearly this equation contrasts with its original formulation counterpart, eq 3.14, which relates local strains to global strains and is this the unit cell strain concentration equation. The increased efficiency of the reformulation of GMC emerges mainly due to the increased efficiency of forming eq. 3.17 versus forming eq 3.14. The formation of eq 3.14 requires solution (of linear equations) for the unknown independent subcell stress components listed in eq 3.16, numbering $N_\beta N_\gamma + N_\alpha N_\gamma + N_\alpha N_\beta + N_\alpha + N_\beta + N_\gamma$. The formation of eq 3.14 requires solution for 6 unknown strain components for each subcell, or a total of $6N_\alpha N_\beta N_\gamma$

unknowns. Solution of linear equations, in essence, amounts to the inversion of a matrix which has the rank of the number of unknown quantities. Since the computational effort associated with matrix inversion increases approximately as the cube of the matrix rank, reducing the number of unknown quantities has a major impact on computational efficiency. The reduction in unknowns due to the reformulation is shown in Figure 3.8 and can be quite significant. For example, a 10x10xl0 unit cell originally required solution for 6000 unknowns. In the reformulated version of GMC-3D the number of unknowns is reduced to 330. Consequently, the corresponding execution times are reduced as well. Clearly, as the number of subcells in the repeating unit cell increases, the increase in efficiency attributable to the reformulation becomes astronomical.

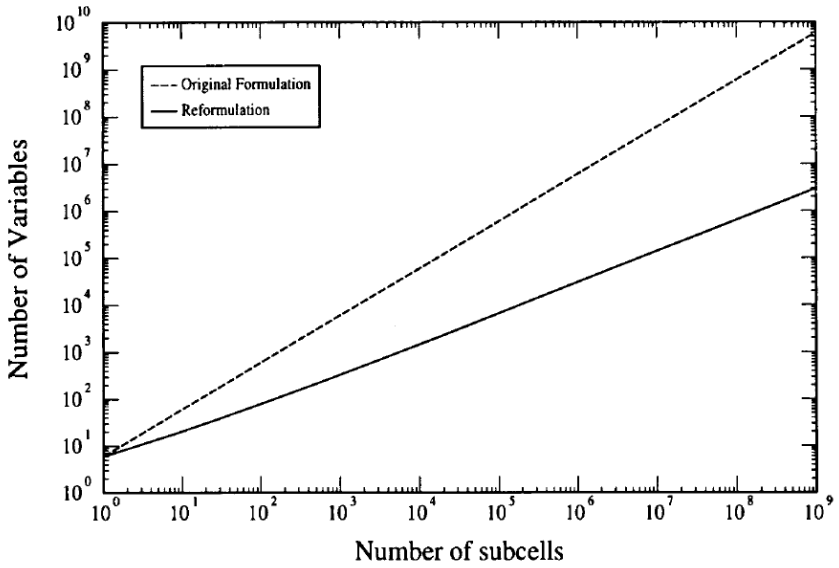

Figure 3.8: Number of subcells vs. number of unknown variables for the original and reformulated versions of GMC-3D for $N_\alpha = N_\beta = N_\gamma$

3.3.2 LS-OPT

Ls-OPT is a product of LSTC (Livermore software Technology Corporation) born to solve optimization and probabilistic problems. LS-OPT can be linked with any simulation code and used for a different number of tasks like:

- Successive Response Surface method
- Multidisciplinary optimization
- Genetic Algorithm
- Numerical/analytical based sensitivities
- Stochastic/Probabilistic Analysis
- Monte Carlo Analysis using Metamodels
- Analysis of Variance (ANOVA)

This optimization and stochastic software offers a very complete package but in this research the focus will be mainly on the Stochastic/Monte Carlo capabilities and the Sensitivity Analysis instruments.

In stochastic simulations the interest in obtaining probabilistic quantities of the Output (Response) due to variation of Input (Parameter). Input are not defined as deterministic values but are described from a proper probabilistic distribution function (PDF) characterized from mean value and standard deviation.

LS-OPT allows the user after linking with the desired software (MAC/GMC in this specific case) to automatize the Stochastic/Monte Carlo analysis offering multiple sampling options for the input PDF and automatically runs the solver applying a random combination of sampled input. Using the same approach it is also possible to perform variance based sensitivity analysis. This simulations, based on metamodels can compute the influence of the input variances on the response variance giving the user a direct feedback on which are the most predominant probabilistic parameters. The basic theory behind ANOVA analysis will be discussed in chapter 5.

Monte Carlo Method History and formulation

No system will be manufactured and operated exactly as designed. Diverse combinations of design and loading variation may lead to undesirable behavior or failure; therefore, if significant variation exists, probabilistic evaluation may be

desirable. This is the main problem at the base of Monte Carlo Method whose core is to learn about a system by simulating it with random sampling. This approach is powerful, flexible and very direct. It is often the simplest way to solve a problem, and sometimes the only feasible way. Monte Carlo method is used in almost every quantitative subject of study: physical sciences, engineering, statistics, finance, and computing, including machine learning and graphics.

The Monte Carlo method has a long history. In statistics it was called *model sampling* and used to verify the properties of estimates by mimicking the settings for which they were designed. W. S. Gosset, writing as Student (1908) derived what is now called Student's t distribution. Before finding his analytic result, he did some simulations, using height and left middle finger measurements from 3000 criminals as written on pieces of cardboard. Tippett (1927) is an early source of numbers to use as if they were random in sampling. Sampling was also used by physicists. Hammersley and Handscomb (1964) describe some computations done by Kelvin (1901) on the Boltzmann equation. There is more history in Kalos and Whitlock (2008) including computations made by Fermi in the 1930s. An even earlier idea was the famous Buffon needle method for estimating π by throwing needles randomly on a wooden floor and counting the fraction of needles that touch the line between two planks. Monte Carlo sampling became far more prominent in the 1940s and early 1950s. It was used to solve problems in physics related to atomic weapons. The name itself is from this era, taken from the famous casino located in Monte Carlo. Many of the problems studied had a deterministic origin. By now it is standard to use random sampling on problems stated deterministically but early on that was a major innovation, and was even considered to be part of the definition of a Monte Carlo method. There are numerous landmark papers in which the Monte Carlo method catches on and becomes widely used for a new class of problems. Here are some examples. Metropolis et al. (1953) presented the Metropolis algorithm, the first Markov chain Monte Carlo method, for studying the relative positions of atoms. Boyle (1977) shows how to use Monte Carlo methods to value financial options. Gillespie (1977) uses Monte Carlo simulation for chemical reactions in which the number of molecules is so small that differential equations are not accurate enough to describe them. Efron's (1979) bootstrap uses Monte Carlo sampling to give statistical answers with few distributional assumptions. There are undoubtedly more major milestones that could be added to the list above and most of those ideas had precursors.

Among the various formulations of the Monte Carlo Methods, Simple Monte Carlo is used for the purposes of this work. Simple Monte Carlo is often called crude Monte Carlo to distinguish it from more sophisticated methods and its

general goal is to estimate a population expectation by the corresponding sample expectation, in this study this task is related to defining the distribution of the composite material T800/F3900 starting from it's estimated constituents characteristics distributions.

In a simple Monte Carlo problem we express the quantity we want to know as the expected value of a random variable Y, such as $\mu = E(Y)$. Then the values Y_1,...,Y_n are generated independently and randomly from the distribution of Y and their average:

$$\hat{\mu}_n = \frac{1}{n}\sum_{i=1}^{n} Y_i \tag{3.18}$$

is taken as the estimate of μ. In practice, there is usually a bit more to the story. Commonly $Y = f(X)$ where the random variable $X \in D \in R^d$ has a probability density function $p(x)$, and f is a real-valued function defined over D. Then:

$$\mu = \int_D f(x)p(x)d(x) \tag{3.19}$$

For some problems it is easier to work with expectations while for other tasks it is simpler to work directly with the integrals. In still other settings X is a discrete random variable with a probability mass function that we also call p. The input X need not even to be a point in Euclidean space at all. It could be the path taken by a wandering particle or it could be an image. But so long as $Y = f(X)$ is a quantity that can be averaged, such as a real number or vector,we can apply simple Monte Carlo. The primary justification for simple Monte Carlo is through the laws of large numbers. Let Y be a random variable for which $\mu = E(Y)$ exists, and suppose that Y_1,...,Y_n are independent and identically distributed with the same distribution as Y. Then under the weak law of large numbers:

$$\lim_{n\to+\infty} P(|\hat{\mu}_n - \mu| \leq \epsilon) = 1, \tag{3.20}$$

holds for any $\epsilon > 0$. The weak law tells us that our chance of missing by more than ϵ goes to zero. The strong law of large numbers tells us a bit more. The absolute error $|\hat{\mu}_n - \mu|$ will eventually get below ϵ and then stay there forever:

$$P(\lim_{n\to\infty} |\hat{\mu}_n - \mu| = 0) = 1 \tag{3.21}$$

While both laws of large numbers tell that Monte Carlo will eventually produce an error as small as we like, neither tells how large n has to be for this to happen. They also don't say for a given sample Y_1,...,Y_n whether the error is likely to be small. The situation improves when Y has a finite variance. Suppose that $Var(Y) = \sigma^2 < \infty$. When sampling, $\hat{mu}_n$ is a random variable and it has its own mean and variance. The mean of $\hat{mu}_n$ is

$$E(\hat{\mu}_n) = \frac{1}{n}\sum_{i=1}^{n} E(Y_i) = \mu \tag{3.22}$$

Because the expected value of $\hat{\mu_n}$ is equal to μ we say that simple Monte Carlo is unbiased. The variance of $\hat{\mu}_n$ is then

$$E((\hat{\mu}^n - \mu)^2) = \frac{\sigma^2}{n} \tag{3.23}$$

While it is intuitively obvious that the answer should get worse with increased variance and better with increased sample size, equation 3.23 gives the exact rate of exchange. The root mean square error (RMSE) of $\hat{\mu}_n$ is:

$$\sqrt{E((\hat{\mu}^n - \mu)^2)} = \frac{\sigma}{\sqrt{n}} \tag{3.24}$$

To get one more decimal digit of accuracy is like asking for an RMSE one tenth as large, and that requires a 100-fold increase in computation. To get three more digits of accuracy requires one million times as much computation. It is clear that simple Monte Carlo computation is poorly suited for problems that must be answered with high precision. Equation 3.23 also shows that if we

can change the problem in some way that reduces σ^2 by a factor of two while leaving μ unchanged, then we gain just as much as we would by doubling n. If we can recode the function to make it twice as fast, or switch to a computer that is twice as fast, then we make the same gain as we would get by cutting σ^2 in two. The economics of the $\frac{\sigma}{\sqrt{n}}$ error rate also work in reverse. If raising n from n_1 to n_2 only makes our accuracy a little better, then reducing n from n_2 to n_1 must only make our accuracy a little worse. An interesting feature about the formula $\frac{\sigma}{\sqrt{n}}$ is that the dimension d of the argument x does not appear in it anywhere. In applications d can be 2 or 1000 and the RMSE is still $\frac{\sigma}{\sqrt{n}}$.

One of the great strengths of the Monte Carlo method is that the sample values themselves can be used to get a rough idea of the error $\hat{\mu_n} - \mu$. It it usually more interesting a good estimate of μ itself than of the error. The average squared error in Monte Carlo sampling is σ^2/n. σ^2 is seldom known but it is easy to get an estimate from the sample values. The most commonly used estimate of σ^2 are:

$$s^2 = \frac{1}{n-1}\sum_{i=1}^{n}(Y_i - \hat{\mu_n})^2 \tag{3.25}$$

$$\hat{\sigma^2} = \frac{1}{n}\sum_{i=1}^{n}(Y_i - \hat{\mu_n})^2 \tag{3.26}$$

Monte Carlo sampling typically uses such large values of n that this two equations will be much closer to each other than either of them is to actual variance σ^2.

3.3.3 LS-DYNA

LS-DYNA is a general purpose finite element analysis software developed by LSTC capable of simulating complex real world problems. The code's origins lie in highly nonlinear, transient dynamic finite element analysis using explicit time integration and for this reason is one the most diffused software for impact simulation in the automotive and aerospace industry. In this study after the determination of the statistical properties of the material, this variations will be introduced in a series of ballistic impact simulations on a carbon fiber composite plate.

The result of the LS-Dyna impact analysis will give information about the PVR curve and will also be used to develop the new material card MAT213, specifically designed for composite material with the option for the user of modeling with probabilistic input variables.

Ballistic Impact and the PVR curve

The impact and penetration behavior of woven composite structure is probabilistic in nature. This implies that conducting multiple fabric impact tests for the same impact scenario could yield different outcomes. This outcome may refer to a penetration or non-penetration, or may refer to the magnitude of the projectile residual velocity for penetrating tests. This is a serious concern for penetration resistant applications comprised of these high strength fabrics which are used to protect critical structural elements and often, human life against high energy impact projectiles. In these applications, it is vital to know at what impacting velocity a particular type of projectile will be defeated each and every time. Since every design is constrained by consideration of costs and weight, the amount of fabric material used in the protective structure must be estimated correctly. For example in the application of engine containment systems the weight of the composite structure is an important design constraint. An overestimation of the amount of required plies will provide superior protection; however it will also lead to higher weight which will decrease the efficiency of the system, increase fuel consumption and overall costs for production on operation. An underestimation of the amount of required fabric will minimize the protective capability of the clothing and put the safety of the system. This leads to an important question: How much fabric material is needed to consistently defeat a particular type of projectile at a particular impact velocity?

Since the penetration behavior of fabric system is probabilistic in nature, there exists a probability of penetration at each projectile impact velocity. This behavior can be represented by a continuous probabilistic velocity response (PVR) curve, known as the $V_0 - V_{100}$ curve as shown in figure.

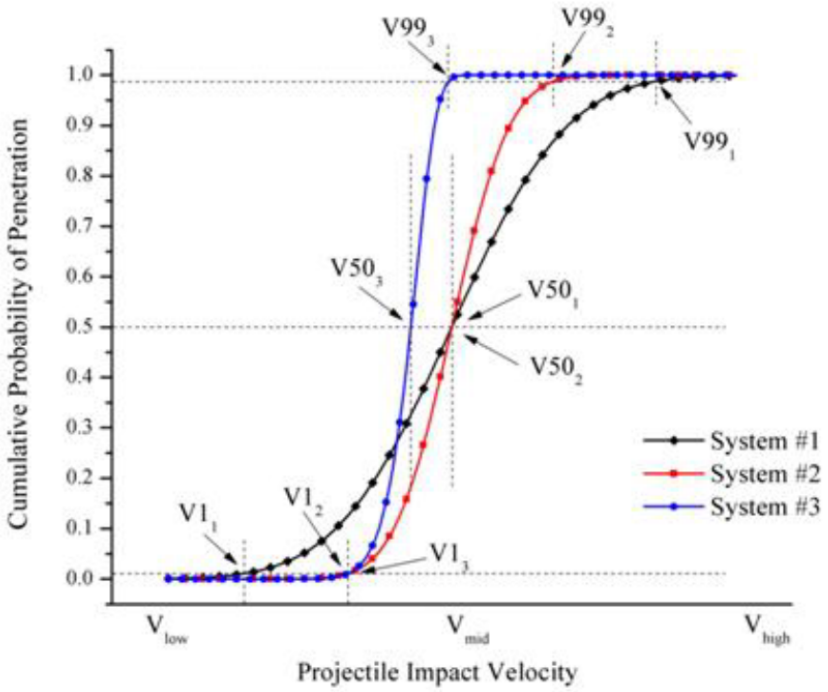

Figure 3.9: Probabilistic Velocity Response Curve

The V_{50} velocity, at which penetration occurs during 50% of impacts, requires the fewest number of impact tests to determine experimentally. Therefore V_{50} values are the popular choice to characterize and compare the performance of protective systems. For the design of practical protective systems, it is more preferable to determine the V_0 velocity which would imply a 0% probability of projectile penetration. However from a statistically rigorous standpoint the V_0 velocity is zero and so probabilities very close to zero are selected leading to parameters such as the V_1 or the $V_{0.1}$ velocities, representing velocities at which penetration respectively occurs at 1% and 0.1% of impacts. These two parameters are much better suited to estimate the correct amount of fabric requires in a protective system. However the precise limiting V_x value used as a design point is chosen based on desired margins of safety and acceptable risks. Compared to V_{50} characterization, considerably more experiments are required to determine these values with confidence, and so the V_{50} velocity still remains a popular indicator of penetration performance even if in order to fully understand the probabilistic impact performance of a system, the PVR curve or $V_0 - V_{100}$ curve must be generated from which the three most important parameters ($V_1 V_{50} V_{99}$) can be easily obtained. LS-Dyna can use the curves obtained with the probabilistic microscale analyses to create a set of ballistic simulation capable of

recreate numerically the PVR curve without the necessity of very expensive test campaigns.

During this process there will exist a few cases wherein the impact velocity of certain non-penetrating shots (V_{NP}) will be higher than the impact velocity of certain penetrating shots (V_P). We refer to the region between the lowest penetrating shot (V_{P_min}) and the highest non penetrating shot (V_{P_max}) as the zone of mixed results or ZMR. While it would seem to be intuitive for a non penetrating shot to have an impact velocity lower than a penetrating shot, this counter-intuitive phenomenon ($V_{NP} > V_P$) that leads to the existence of the ZMR is because of certain sources of variability, discussed in chapter 4. Figure 3.9 displays typical experimental impact data during the testing of fabrics. Data points which represents the PVR curve. Thus the PVR curve describes the probability of fabric penetration (Y-axis) as a function of impact velocity (X-axis). The wider the ZMR the greater the degree of variability in the system. A wide ZMR results implies widely separated V_1 and V_{99} velocities. From the performance standpoint of a fabric based protective structure, it is desirable to have as high a V_1 or V_{50} velocity as possible and as narrow a ZMR as possible.

Chapter 4

Microscale Analysis

Microscale analysis based on the generalized method of cells allows to compute composite material properties starting from its constituents characteristics. The generalized method of cells (GMC) is based on the possibility of representing the micro-scale structure of a material with a repeating unit cell. This approach has been implemented in the NASA MAC/GMC code that is used for this purpose. Within MAC/GMC code there are three separate micro-mechanics models that can be employed in RUC analyses: 1) Doubly periodic generalized method of cells (GMC), 2) Triply periodic GMC and 3) Doubly periodic high-fidelity GMC (HFGMC). The nature of this study and the material structure of the unidirectional T800/F3900 makes the doubly periodic GMC the most suitable and efficient micro-mechanic model.
By assigning the different constituents materials to the sub-cells within the RUC, these elements are organized to represent the composite material structure. As the name indicates, the RUC repeats infinitely in two Cartesian coordinate directions. The Doubly periodic is infinitely long in the third out of plane X_1 direction and represent an infinite heterogeneous (composite) medium with a periodic microstructure. Thus GMC may be thought of as a model for a material point that may be part of a larger overall structure. These micromechanics model not only computes the effective properties of the composite material located at a particular material point, but also allows the simulation of applied loading conditions (in the form of global stresses, global strains, a uniform temperature change) on the composite material to perform failure analysis for different loading histories and directions.

Two types of simulations are studied in this chapter: Elastic Properties Estimation and Static Failure Analysis. Elastic properties estimation is the simplest form of analysis available in MAC/GMC 4.0 and requires only the definition of the Elastic properties of constituents materials while Static failure analy-

sis within MAC/GMC 4.0 (via the FAILURE_SUBCELL and FAILURE_CELL keywords) is less immediate and requires a more dedicated set up. The static failure analysis monitors the stress and strain components in the composite or laminate (on the subcell or RUC level) and checks for failures using the specified failure criteria. Thus, the static failure analysis (like an actual experimental test) is inherently linked to the loading applied to the RUC or laminate and the predicted failure stress and strain are not truly material properties.
To do so the failure subcell simulation is used to perform static failure analysis based on the local stress and strain fields in the subcells without strain rate dependency. Static failure analysis involves checking the specified failure criteria during application of a simulated thermomechanical loading history. The static failure predictions are inherently linked to the specifics of the simulated loading applied to the composite. The maximum stress, maximum strain, and Tsai-Hill failure criteria are available within the software.

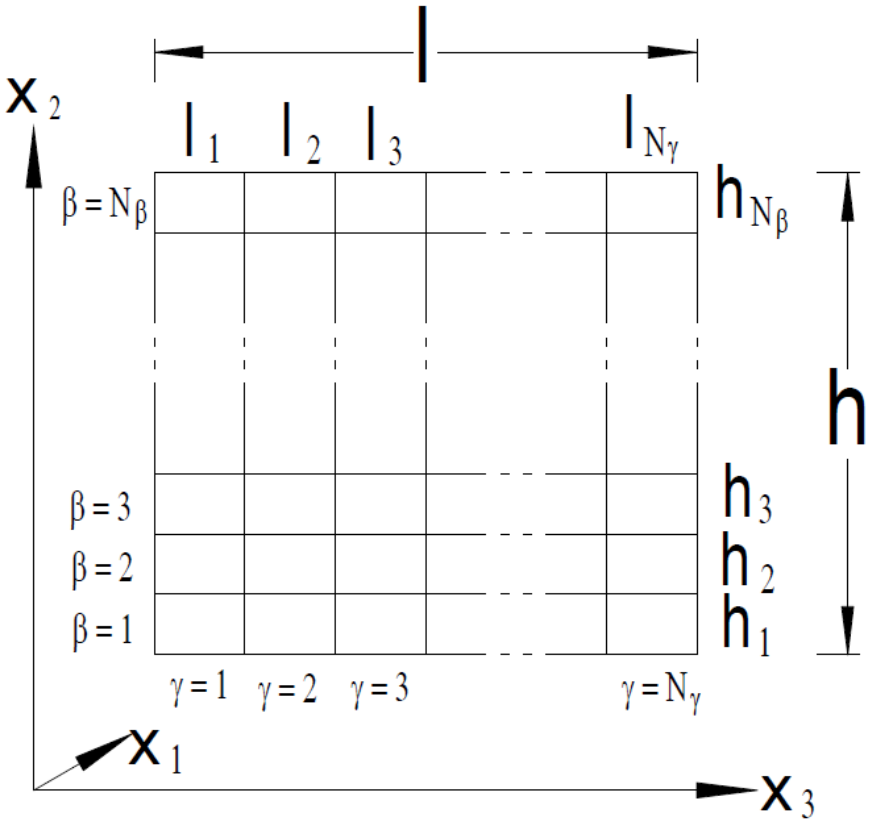

Figure 4.1: RUC Charachteristic Parameters

After assigning material models, and failure criteria the microscale simu-

lation of MAC/GMC is coupled with LS-OPT to perform the Monte Carlo Microscale analysis. Here the input properties of the constituents material are no more defined with their mean values but with a vector of samples computed to represent the proper probability density function of the observed characteristic. The outputs of this process will be as well a probability density functions of the composite properties. The computed output of the composite obtained from the constituents properties (discussed in the next section) are:

	Description
E_a	Axial Elastic Modulus
E_b	Transverse Elastic Modulus
PR_{ba}	Axial Poisson Ratio
PR_{cb}	Transvese Poisson Ratio
G_{ab}	Axial Shear Modulus
G_{bc}	Transverse Shear Modulus
ε_{11}	Axial Ultimate Strain
γ_{23}	Utimate Shear Strain

Table 4.1: Microscale Elastic Properties

4.1 Composite Constituent Properties Identification

To run microscale simulations it's necessary to have a certain number of input characteristics of the composite material constituent properties. The studied material is constituted from two materials: carbon fiber T800 and the epoxy resin system F3900. MAC/GMC have a number of different available constituents models and the most appropriate had to be identified to describe the behaviour of the composite constituents. Fibers can be modeled as having a purely elastic response and which direction is aligned with a specific axis 1 shown in figure 4.1. According to these considerations for fibers a transversely isotropic elastic model is used.

$$\begin{bmatrix} \sigma_{11} \\ \sigma_{22} \\ \sigma_{33} \\ \sigma_{23} \\ \sigma_{13} \\ \sigma_{12} \end{bmatrix} = \begin{bmatrix} C_{11} & C_{12} & C_{12} & 0 & 0 & 0 \\ C_{12} & C_{22} & C_{23} & 0 & 0 & 0 \\ C_{12} & C_2 & C_{22} & 0 & 0 & 0 \\ 0 & 0 & 0 & C_{44} & 0 & 0 \\ 0 & 0 & 0 & 0 & C_{44} & 0 \\ 0 & 0 & 0 & 0 & 0 & C_{66} \end{bmatrix} \left(\begin{bmatrix} \varepsilon_{11} \\ \varepsilon_{22} \\ \varepsilon_{33} \\ \gamma_{23} \\ \gamma_{13} \\ \gamma_{12} \end{bmatrix} - \begin{bmatrix} \alpha_L \Delta T \\ \alpha_T \Delta T \\ \alpha_T \Delta T \\ 0 \\ 0 \\ 0 \end{bmatrix} \right) \tag{4.1}$$

where components C_{ij} can be expressed in terms of five indipended constants,

$$E_a, E_t, \nu_a, \nu_t, G_a \tag{4.2}$$

and the longitudinal and transverse thermal expansion coefficient are not used as the dependence on temperature is neglected.

A similar set of properties is required to describe the behaviour of the matrix, which is still considered as a brittle material but the more "general" standard isotropic elastic material model is used in MAC/GMC, reducing the necessary input from 5 to three as the difference in the longitudinal and transverse behaviour is lost.

4.1.1 T800/F3900 Microscale Elastic Properties

T800/F3900 composite has already been characterized and used for the study of a specific ballistic impact simulation which is the base for the last part of this study (Chapter 6). The material model used so far was a classic deterministic model whose properties have been estimated through common dogbone experimental material testing performed at Arizona State University.

Property	Value
E_{11}	161,751 GPa
E_{22}	7,349 GPa
E_{33}	7,349 GPa
PR_{12}	0,0168
PR_{13}	0,439
PR_{23}	0,439
G_{12}	3,9955
G_{13}	2,2476
G_{23}	2,2476

Table 4.2: T800/F3900 Experimental Engineering Moduli

A comparable set of engineering properties of the composite has to be obtained from the constituent properties using MAC/GMC. Most of the fiber and resin values have been obtained using documents as the Torayca T800/F3900 data-sheet and literature [5] [23] but for some of them, like the transverse Poisson ratio and Transverse Elastic Modulus of single fibers, which are normally very hard to obtain through experimental testing, a process of reverse engineering has been done to estimate the proper values. Using the most refined single fiber RUC architecture internally defined in MAC/GMC (Archid 13, Figure 4.5) it's possible to make a quick verification of the input used. An error between the MAC/GMC output and ASU baseline is acceptable as the focus it's not on the perfect correlation between MAC/GMG output and ASU experimental results but the ability to predict the standard variation of the the composite properties which are not influenced by the mean values just computed. The microscale simulation input are divided in three categories: Fiber properties, resin properties, fiber volume fraction:

ID	Description	Value
E_{a_f}	Axial Elastic Modulus	284.895 GPa
E_{t_f}	Transverse Elastic Modulus	15.513 GPa
PR_{a_f}	Axial Poisson Ratio	0.305
PR_{t_f}	Transverse Poisson Ratio	0.35
G_{a_f}	Axial Shear Modulus	103.42 GPa
α_a	Axial coefficient of thermal expansion	0
α_t	Transverse coefficient of thermal expansion	0
D(d_1, d_2, d_3)	Components of vector normal to the plane of transverse isotropy	1,0,0

Table 4.3: T800 Fiber Elastic Properties

ID	Description	Value
E_r	Elastic Modulus	3.447 GPa
PR_r	Poisson Ratio	0.35
G_r	Shear Modulus	1.275 GPa
α_a	Axial coefficient of thermal expansion	0
α_t	Transverse coefficient of thermal expansion	0

Table 4.4: F3900 Resin Elastic Properties

ID	Description	Value
V_f	Fiber Volume Fraction	0,54

Table 4.5: T800/F3900 Composite Fiber Volume Fraction

Before comparing the two set of results it's important to pay attention to the Poisson Ratio: MAC/GMC output it's for direction 12 when ASU baseline is for direction 21. The relationship to transform PR_{12} into PR_{21} is:

$$PR_{21} = \frac{E_{22}}{E_{11}} PR_{12} \tag{4.3}$$

and finally the results obtained from microscale simulation using a ARCHID13 fiber arrangement compared with experimental testing of T800/F3900 samples:

ID	MAC/GMC	ASU Test	err%
E_{11}	159.203 GPa	161.751 GPa	1.57%
PR_{21}	0.0171	0.0168	1.78%
PR_{13}	0.44298	0.4390	0.88%
E_{22}	8.07132 GPa	7.3498 GPa	9.81%
G_{13}	2.25641 GPa	2.2476 GPa	0.39%
G_{12}	4.0527 GPa	3.9955 GPa	1.43%

Table 4.6: MAC/GMC Output vs Experimental Testing

Now That the deterministic microscale input to compute elastic properties are defined it's time to identify their standard deviations and subsequently their probabilistic distribution functions. Finding information relative to PDF it's particularly difficult considering that very few studies have been done on this subject and for this specific materials. Some approximations and arbitrary values based on some literature background will then be used to fill the lack of information. As described before, these approximations will not influence the effectiveness of the computational framework that has the possibility to be adapted and utilized with different distributions shapes according to the studied material.

Let's begin from the probability distribution function relative to fiber volume fraction which variation can be easily computed and associated with changes of the mesoscale behaviour [1]. For this reason a larger set of information is avail-

able compared to resin and fiber moduli. Jonston et al. [14] using imagine quantification techniques on unidirectional carbon fiber reinforced polymeric matrix composite using optical microscopy has been able to estimate the variability of fiber volume fraction for the specimens analysed. For the local area V_f analysis a normal distribution was found to be the best fit. With this information related to the possible best fit distribution and the standard deviation computed using a set of V_f values obtained for different specimen of T800/F3900 material reported in NASA Technical Paper 3102 [23] has been possible to generate a valid fiber volume fraction PDF:

ID	Mean Value	Standard Deviation	Standard Deviation%
V_f	0.54	0.0338	3.381%

Table 4.7: Fiber volume fraction distribution

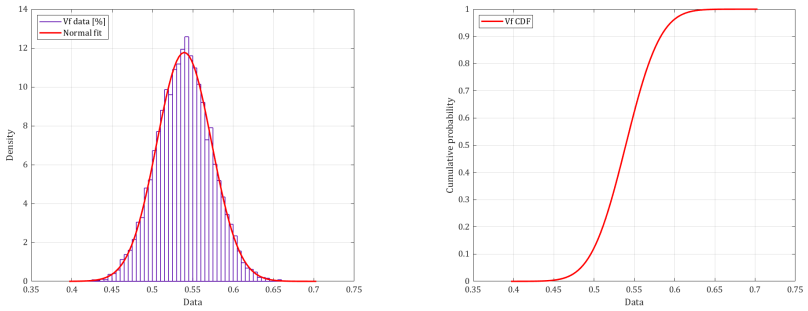

(a) PDF (b) CDF

Figure 4.2: V_f Normal Distribution fit

Engineering moduli distributions for fiber filaments and Epoxy resin matrix are more difficult to be found in literature. Statistical analysis historically where performed on single fiber filaments focusing on ultimate strain and stress variability and not on elastic properties because of their lower influence in failure initiation. To be able to estimate if and when elastic properties variability will have an influence on the plate impact response has been decided to apply the

same standard deviation found for capon fiber axial elastic modulus to all the other properties of the T800 fiber and F3900 Matrix. As for variation in fiber volume fraction this probability density functions are normal or Gaussian.

ID	Mean Value	Standard Deviation
Ea_f	284.895GPa	16.72333 GPa
Et_f	15.513GPa	0.91061 GPa
PRa_f	0.305	0.0179
PRt_f	0.35	0.0205
Ga_f	103.42GPa	6.0707 GPa

Table 4.8: Fiber Elastic Properties Distribution

ID	Mean Value	Standard Deviation
Ea_m	3.477 GPa	0.17235 GPa
Et_m	3.477 GPa	0.17235 GPa
PRa_m	0.35	0.0175
PRt_m	0.35	0.0175
Ga_m	1.275 GPa	0.06375 GPa

Table 4.9: Resin Elastic Properties Distribution

4.1.2 T800/F3900 Microscale Static Failure Properties

The same identification process for mean values and standard deviations has to be applied to failure properties. The rupture properties of high performance filaments are complex parameters hardly described by a single value. Instead of Gaussian distributions, the Weibull model is used to describe the statistical nature of the fracture limits. [30] [29] [16]. Here a two parameters (λ, k) Weibull distribution is applied to model the variability of ultimate strains:

$$f(x) = \frac{k}{\lambda^k} x^{k-1} e^{-(\frac{x}{\lambda})^k} \tag{4.4}$$

T800/F3900 has already been studied and accurately characterized for ballistic impact response by Ohio State University. During experimental tests has been observed how the ultimate penetration is driven by the very high ultimate strain of the epoxy matrix under this particular conditions. In impact events the very high concentrated energy rises the temperature of the resin above the glass transition temperature increasing it's ultimate strain. Due to this particular behavior for microscale failure analysis will be used a strain based failure criteria and subsequently the probabilistic failure properties analysed and described are the ultimate strains of both fibers and matrix.

Fiber	Matrix	Description
ε_{11}	ε_{11}	Ultimate Axial Strain Dir. 11
ε_{22}	ε_{22}	Ultimate Axial Strain Dir. 22
ε_{33}	ε_{33}	Ultimate Axial Strain Dir. 33
γ_{23}	γ_{23}	Ultimate Shear Strain Dir. 23
γ_{13}	γ_{13}	Ultimate Shear Strain Dir. 13
γ_{32}	γ_{32}	Ultimate Shear Strain Dir. 32

Table 4.10: Microscale Failure Properties

ID	Mean Value [Strain]	StD [Strain]	Shape Factor(k)	Scale Factor(λ)
ε_{11}	0.019	0.002958	7.6	0.02023
ε_{22}	0.019	0.002958	7.6	0.02023
ε_{33}	0.019	0.002958	7.6	0.02023
γ_{23}	0.01222	0.001868	7.75	0.013
γ_{13}	0.01222	0.001868	7.75	0.013
γ_{32}	0.01222	0.001868	7.75	0.013

Table 4.11: Fiber ultimate strains distribution

ID	Mean Value [Strain]	StD [Strain]	Shape Factor	Scale Factor
ε_{11}	0.0215	0.001073	25	0.02197
ε_{22}	0.0215	0.001073	25	0.02197
ε_{33}	0.0215	0.001073	25	0.02197
γ_{23}	0.06609	0.003304	24.95	0.06755
γ_{13}	0.06609	0.003304	24.95	0.06755
γ_{32}	0.06609	0.003304	24.95	0.06755

Table 4.12: Matrix ultimate strains distribution

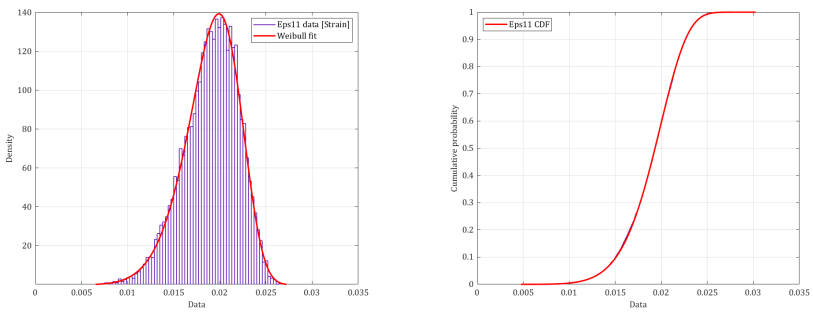

(a) PDF

(b) CDF

Figure 4.3: Fiber ε_{11} Weibull distribution fit

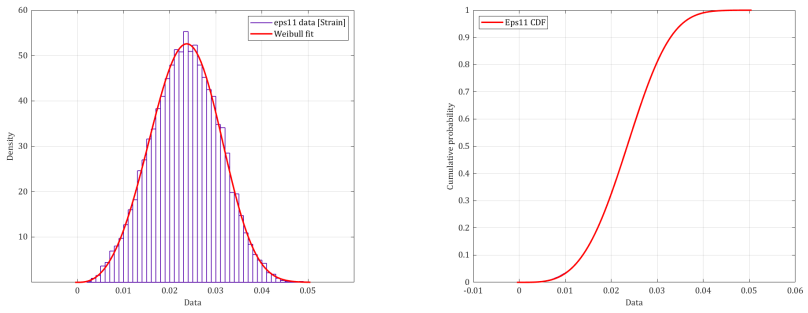

(a) PDF (b) CDF

Figure 4.4: Matrix ε_{11} Weibull distribution fit

4.2 Probabilistic Microscale Simulations Set Up

The distributions of the constituents properties obtained from the stochastic generalized method of cells is utilized to compute the distributions of axial modulus, shear modulus, Poisson ratios and ultimate failure strains of the composite. These curves will be defined for different Repeating Unit Cells architecture types to investigate how different length scales impact the output distributions. Increasing the length scale, the unit cell of material will contain more and more fibers leading to more homogeneous values which are closer to the deterministic (i.e. averages) material parameters. This trend explains how the effort to define stochastic variations of material properties is justified especially when the length scale of the analyzed event is small to the point where the probabilistic behavior of a particular portion of structure is not anymore negligible. In the next paragraphs are presented the result for architectures containing 1, 4, 16 and 25 fiber filaments.

4.2.1 RUC Architectures Definition

Single Fiber RUC discretization

As it happens is classic meshing techniques in FEM models, at the microscale level it is possible to discretize the repeating unit cell using a different number of subcells. Starting from the simplest representation, which contains 4 subcells, one modeling the fiber and three modeling the surrounding matrix, 4 level of refinement are analyzed. Both the results and computational time are observed to pick the proper architecture to use in the more articulated multi fiber simulations.

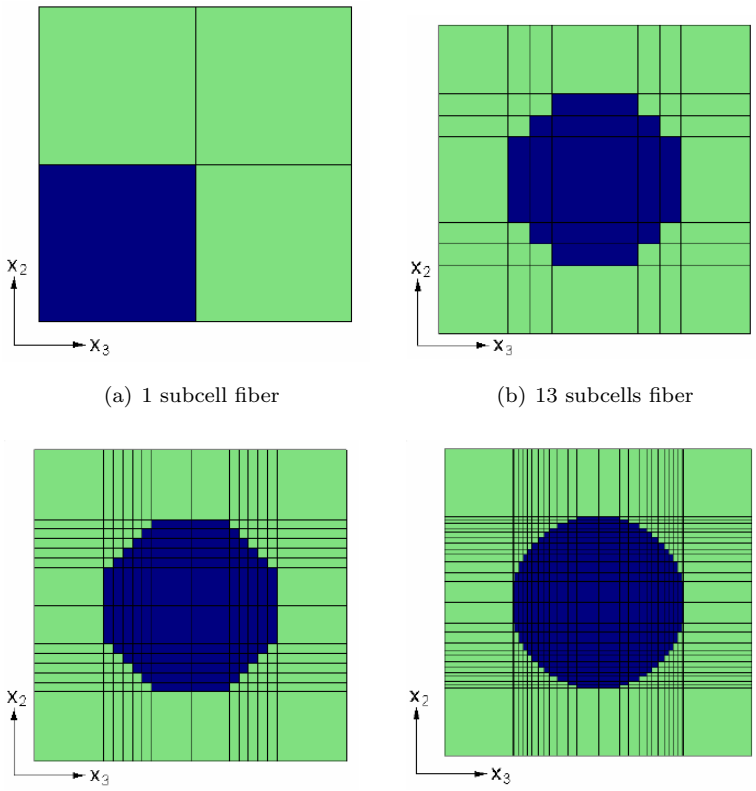

(a) 1 subcell fiber

(b) 13 subcells fiber

(c) 84 subcells fiber

(d) 312 subcells fiber

Figure 4.5: RUCs discretization

The results obtained by computing these four RUC properties show a small influence of the refinement level on the fiber on the calculated engineering moduli. The differences are larger between the four subcells and thirteen subcells architecture but overall negligible for the scope of this study. In static failure analysis, the rupture values are not changing but a different failure behaviour can be observed in the curves of figure 4.6.

With the possibility of neglecting the differences resulting by changing the fiber plus matrix modeling precision the main criteria for selecting the most efficient RUC is computational time. It is obvious that the simplest architecture will then require the least computational effort (table 4.15) making it extremely useful especially in stochastic microscale simulation where a large number of samples will be required (i.e. 10^4 as will be shown later). An even larger impact can be observed when assembling multiple repeating unit cells to simulate larger length scales.

ID	1 subcells	13 subcells	84 subcells	312 subcells
E11	0.155430E+06	0.155430E+06	0.155430E+06	0.155430E+06
N12	0.3241939944	0.3240658522	0.3241120199	0.3241635773
N13	0.3241939944	0.3240658522	0.3241120199	0.3241635773
E22	0.792844E+04	0.783739E+04	0.781435E+04	0.779624E+04
N23	0.4044057475	0.4129550660	0.4140672226	0.4147404726
E33	0.792844E+04	0.783739E+04	0.781435E+04	0.779624E+04
G23	0.220119E+04	0.220119E+04	0.220119E+04	0.220119E+04
G13	0.375487E+04	0.399436E+04	0.393976E+04	0.387440E+04
G12	0.375487E+04	0.399436E+04	0.393976E+04	0.387440E+04

Table 4.13: Deterministic engineering moduli for single fiber RUCs

ID	1 Subcells vs 16 Subcells	13 Subcells vs 84 Subcells 7	84 Subcells vs 312 Subcells
E11	-	-	-
N12	0.02%	0.008%	0.01%
E33	1.18%	0.295%	0.231%
N23	1.89%	0.235%	0.138%
G23	-	-	-
G13	7.29%	1.601%	1.98%

Table 4.14: Difference between RUCs elastic properties

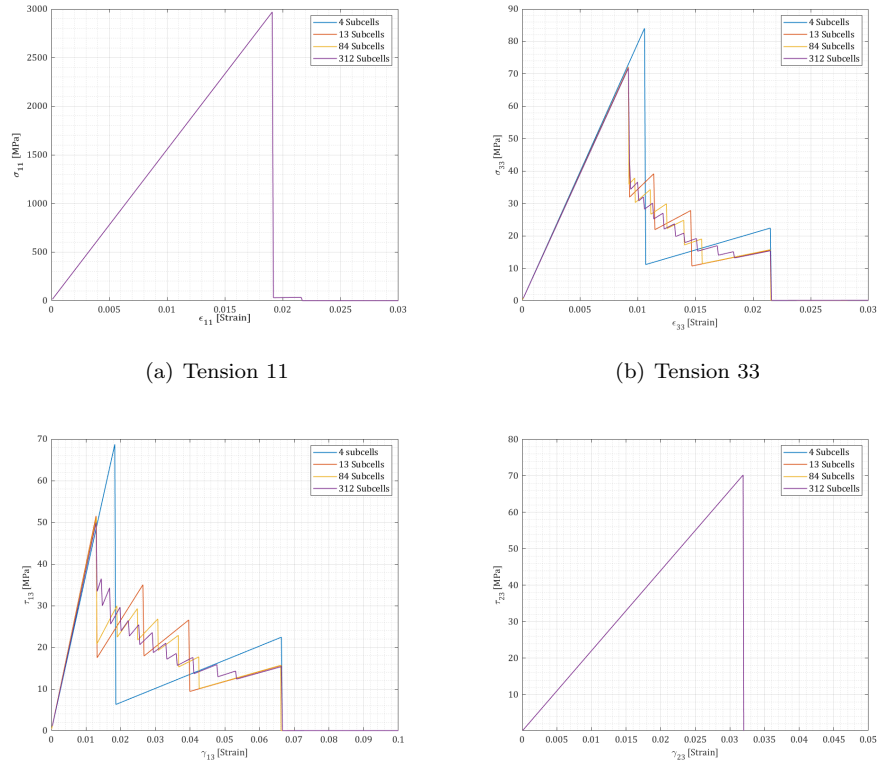

(a) Tension 11

(b) Tension 33

(c) Shear 13

(d) Shear 23

Figure 4.6: Stress vs Strain curves of single fibers RUC

	1 Subcells	13 Sub	84 Subcells	312 Subcells
Time $[s]$	0.265	0.395	0.399	1.657

Table 4.15: Average Execution time for Single Fiber RUC simulation

	1 Subcells	13 Sub	84 Subcells	312 Subcells
Time $[s]$	5650	6950	6990	19570

Table 4.16: Execution time for Single Fiber RUC Monte Carlo simulation

Multifiber RUC

Selected the modeling architecture for the single RUC, larger length scales will be analyzed assembling multiple single fiber elements. Models contacting four,

sixteen and 25 fibers will be simulated and the effect on the output distributions assessed. In the simulations, each filament is treated as an independent stochastic variable while fiber volume fraction variation if obtained by changing the thickness of matrix subcells. Simulating different length scale is important to better understand the probability of failure initiation with respect to the number of fibers involved in the first phases of the impact. To a smaller length scale, excited by small projectile, variability is higher as failure will start from a small number of fibers. With increasing length scales, the variability will decrease. Already with 25 fibers it has been possible to observe a tendency of the mean value of the simulation results to reach stability. With twenty five filaments in the material cell the computational cost increases sensibly and the the limitation of the hardware used made not possible to explore larger length scales. Anyway, the obtained results can be considered sufficient for the scope of this thesis.

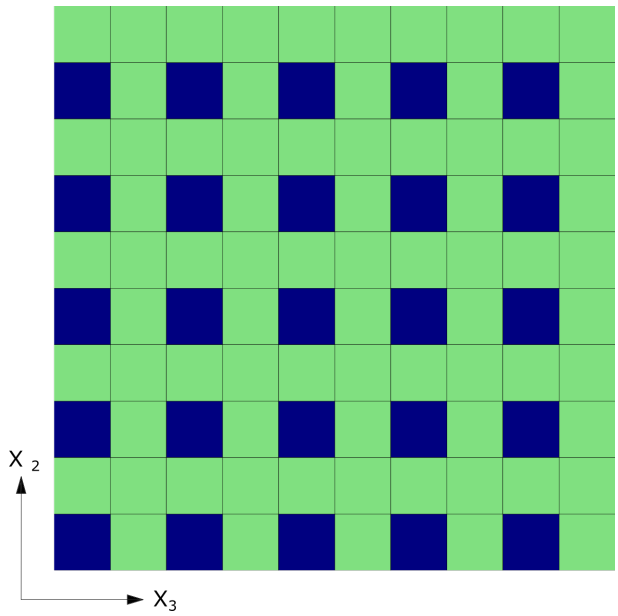

Figure 4.7: 25 Fibers RUC scheme

4.2.2 Mote Carlo simulation Sampling

In direct Monte Carlo analysis Sampling is based on the distribution of random variables. The probabilistic input are defined as noise variables. These variables are completely described by the associated probabilistic distribution and are not controlled at the design and production level, but only at the analysis level.

A probabilistic variable can be defined as a noise variable either because the user chooses to study the effect of uncertainty around a fixed mean value or because it may not be possible to control the variable. A noise variable will have the nominal value as specified by the distribution. These Noise variables are sampled using a the Monte Carlo sampling technique: random samples are obtained from the input distribution. To complete an accurate simulation it's required to define the correct amount of samples for the convergence of the analysis. The convergence criteria is arbitrarily defined at corresponds to when the difference between standard deviation of two consecutive sets is close to 1%.

Sets of 100,1000, 5000, 10000, and 15000 samples are simulated to evaluate the convergence both for elastic and failure parameters. Only the single fiber RUC results are used for this evaluation because multifiber RUCs reach convergence with fewer samples due it's intrinsic structure.

Composite Elastic Properties sampling infleunce

Elastic Properties Mean Values reach convergence very quickly. With only 1000 samples point the mean output values are already showing a stable trend. On the contrary when analyzing the standard deviations a higher number of samples is required. As seen, only when increasing the sampling point above 10000 the variations becomes small enough to be considered negligible and therefore this is fixed as the convergence threshold. Following, the results of the stochastic microscale analysis for a single fiber RUC and five different sampling sets:

ID	100	1000	5000	10000	15000
Ea [GPa]	157.0063	155.4495	155.2254	155.3588	155.3935
Eb [GPa]	7.8422	7.8223	7.8099	7.8071	7.8079
PRba	0.0163	0.0164	0.0164	0.0164	0.0164
PRcb	0.4149	0.4151	0.4162	0.4162	0.4161
Gab [GPa]	3.9557	3.9272	3.9153	3.9118	3.9128
Gbc [GPa]	2.2166	2.2089	2.2037	2.2035	2.2043

Table 4.17: Mean Value - single fiber RUC

ID	100	1000	5000	10000	15000
Ea [GPa]	13.2774	12.8194	13.1277	13.1763	13.2259
Eb [GPa]	0.5125	0.4841	0.4984	0.5011	0.5029
PRba	0.0016	0.0014	0.0015	0.0015	0.0015
PRcb	0.0289	0.0277	0.0281	0.0284	0.0285
Gab [GPa]	0.5029	0.4884	0.4797	0.4799	0.4817
Gbc [GPa]	0.1498	0.1370	0.1369	0.1374	0.1381

Table 4.18: Standard Deviation - Single Fiber RUC

ID	100	1000	5000	10000	15000
Ea [GPa]	8.4566 %	8.2467 %	8.4572 %	8.4812 %	8.5113 %
Eb [GPa]	6.5348 %	6.1888 %	6.3822 %	6.4190 %	6.4412 %
PRba	9.6238 %	8.5749 %	8.9389 %	9.0259 %	8.9838 %
PRcb	6.9615 %	6.6809 %	6.7573 %	6.8328 %	6.8444 %
Gab [GPa]	12.713 %	12.436 %	12.251 %	12.267 %	12.311 %
Gbc [GPa]	6.7575 %	6.2004 %	6.2108 %	6.2337 %	6.2653 %

Table 4.19: Standard deviation % - Single Fiber RUC

ID	100	1000	5000	10000	15000
Ea [GPa]	131.0428	119.8716	112.4751	105.5929	105.5929
Eb [GPa]	6.7231	6.2584	6.1270	6.1270	6.1270
PRba	0.0130	0.0122	0.0121	0.0119	0.0118
PRcb	0.3448	0.3375	0.3330	0.3271	0.3271
Gab [GPa]	3.1103	2.6600	2.6600	2.5269	2.5230
Gbc [GPa]	1.8972	1.7697	1.7697	1.7653	1.7324

Table 4.20: Minimum Value - Single Fiber RUC

ID	100	1000	5000	10000	15000
Ea [GPa]	205.3254	205.3254	207.5751	211.4342	211.4342
Eb [GPa]	9.0769	9.4879	10.1190	10.1190	10.1190
PRba	0.0209	0.0209	0.0223	0.0228	0.0229
PRcb	0.4936	0.5001	0.5186	0.5293	0.5342
Gab [GPa]	5.8359	6.3826	6.4664	6.6931	6.6931
Gbc [GPa]	2.6058	2.8060	2.8810	2.8810	2.8810

Table 4.21: Maximum Value - Single Fiber RUC

ID	100vs1000	1000vs5000	5000vs10000	10000vs150000
Ea	2.54 %	2.48 %	0.2 %	0.35 %
Eb	5.59 %	3.03 %	0.57 %	0.34 %
PRba	12.23 %	4.07 %	0.96 %	0.46 %
PRcb	4.20 %	1.13 %	1.10 %	0.16 %
Gab	2.22 %	1.51 %	0.13 %	0.35 %
Gbc	8.98 %	0.16 %	0.36 %	0.50 %

Table 4.22: Difference between StD.%

ID	100vs1000	1000vs5000	5000vs10000	10000vs150000
Ea	9.31 %	6.57 %	6.51 %	– %
Eb	7.42 %	2.14 %	– %	– %
PRba	6.55 %	0.82 %	1.68 %	0.84 %
PRcb	2.12 %	1.35 %	1.80 %	– %
Gab	16.92 %	– %	5.26 %	0.15 %
Gbc	7.92 %	– %	0.24 %	1.84 %

Table 4.23: Difference between Min. Values

ID	100vs1000	1000vs5000	5000vs10000	10000vs150000
Ea	– %	1.08 %	1.82 %	– %
Eb	4.33 %	6.23 %	– %	– %
PRba	– %	6.27 %	2.19 %	0.43 %
PRcb	1.29 %	3.56 %	2.02 %	0.91 %
Gab	8.56 %	1.29 %	3.38 %	– %
Gbc	7.13 %	2.6 %	– %	– %

Table 4.24: Difference between Max. Values

Composite Static Failure Properties sampling influence

The same trend for PDF properties vs sampling number is not as linear as for elastic properties, at least up to the the limit of 15000 samples.This is observable in particular with standard deviation while for mean and extreme values the behaviour is more stable with the samples increase.

ID	100	1000	5000	10000
mean	0.0217	0.0219	0.0219	0.0219
StD	1.317E-3	1.112E-3	1.1007E-3	1.122E-3
StD%	6.057	5.077	5.0146	5.111
min	0.0179	0.0179	0.0171	0.0161
max	0.0257	0.0257	0.0263	0.0268

Table 4.25: ε_{11} Static Failure - Single Fiber RUC

ID	100vs1000	1000vs5000	5000vs10000
StD%	16	1.22	1.92

Table 4.26: ε_{11} StD difference

ID	100	1000	5000	10000
mean	0.032	0.0318	0.0317	0.0317
StD	6.1120E-3	5.2270E-3	5.110E-3	5.0087E-3
StD%	19.1	16.01	15.80	15.77
min	0.01295	0.0129	0.0120	0.0114
max	0.0444	0.0446	0.0450	0.0452

Table 4.27: γ_{23} Static Failure - Single Fiber RUC

ID	100vs1000	1000vs5000	5000vs10000
$StD\%$	16.17	1.311	0.189

Table 4.28: γ_{23} StD difference

4.3 Microscale analysis results

Following the previous considerations, it is not possible to complete the Microscale Monte Carlo Simulations, which results are the stochastic composite properties starting from probabilistic microscale level properties describing the two constituents, fiber and matrix, and their volume fraction. The following results are obtained using inputs from table 4.8 and 4.9 for Elastic properties, and 4.11 and 4.12 for ultimate strain in failure analysis. The ultimate goal is then to understand which of the composite distributions and consequently which microscale properties are influencing the most the ballistic penetration response of a composite plate. For the final part of the study, LS Dyna is used for impact simulations and regarding the specif failure parameters to be given as input, only axial and shear strains are required. Because of this, the microscale failure results are limited to these two characteristics of the material. Simulations are completed using 10000 sampling points. To show the influence of the length scale, results for architectures composed by 1, 4,16 and 25 fibers are shown. The base architecture, used in the smaller length scale is four subcell repeating unit cell (figure 4.5 (a)) comprehending one subcell simulating the fiber and three subcells representing the matrix which thickness is changing to emulate the fiber volume fraction distribution. Larger length scales are obtained by assembling multiple single fiber repeating unit cells.

4.3.1 Elastic Properties

Axial Elastic Modulus

	1 Fiber	4 Fibers	16 Fibers	25 Fibers
Mean	155.3588	155.8608	155.9152	155.7619
StD	13.1763	10.7253	9.8279	9.5787
StD%	8.4812	6.8813	6.3033	6.1496
Min	105.5929	125.1903	128.4908	130.3614
Max	211.4342	193.1717	188.0893	191.6561

Table 4.29: Ea Distribution [GPa]

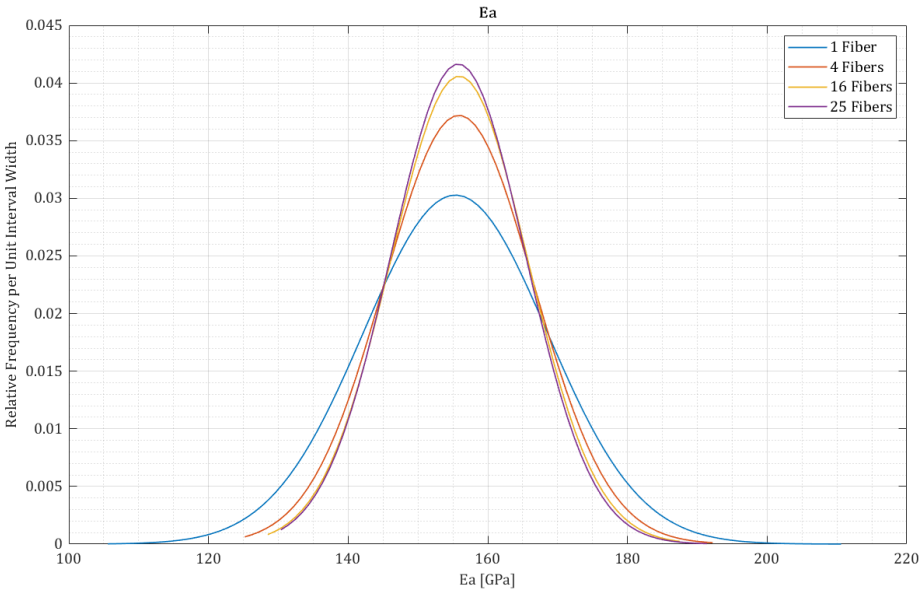

Figure 4.8: Ea Distributions

Transverse Elastic Modulus

	1 Fiber	4 Fibers	16 Fibers	25 Fibers
Mean	7.8071	7.9390	7.94191	7.9443
StD	0.5011	0.4980	0.4769	0.4859
StD%	6.4190	6.2728	6.0045	6.1158
Min	6.1270	6.3910	6.6742	6.2461
Max	10.1190	9.8860	9.5399	10.0275

Table 4.30: Eb Distributions [GPa]

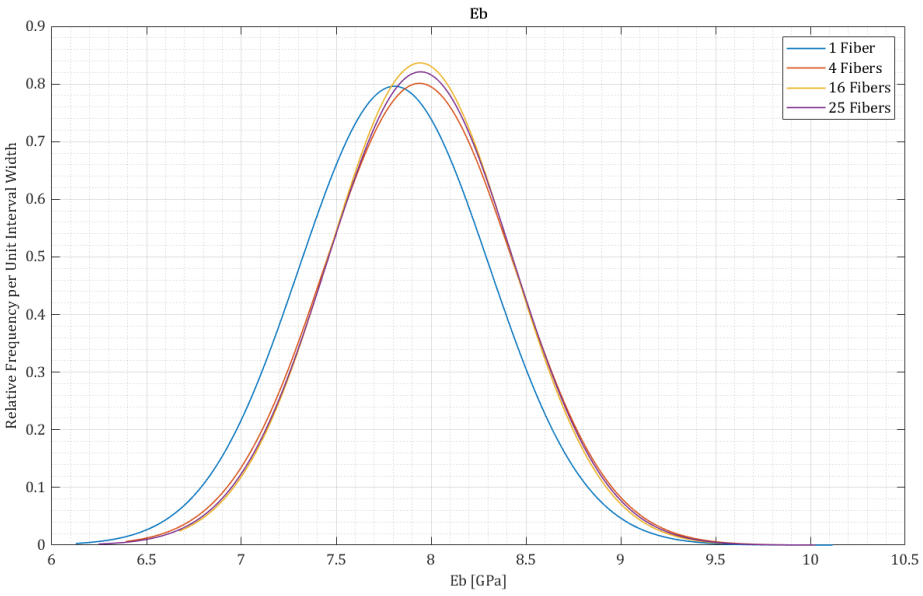

Figure 4.9: Eb Distributions

Axial Poisson Ration (direction ba)

	1 Fiber	4 Fibers	16 Fibers	25 Fibers
Mean	0.0164	0.0166	0.0165	0.0166
StD	0.0015	0.0011	0.0010	0.0009
StD%	9.0259	6.5140	5.8412	5.4224
Min	0.0119	0.0137	0.0140	0.0141
Max	0.0228	0.0209	0.0202	0.0200

Table 4.31: PRba Distributions

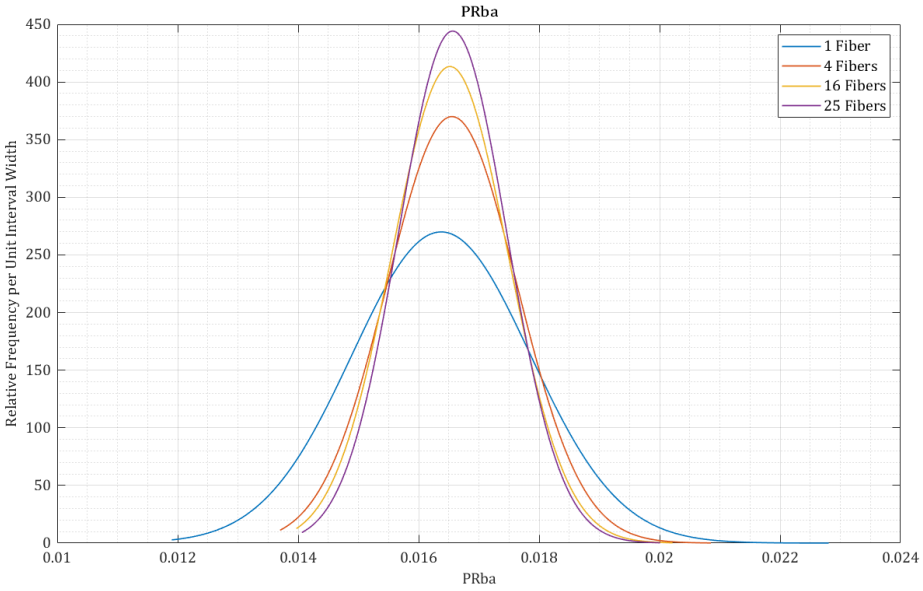

Figure 4.10: PRba Distributions

Transverse Poisson Ration (Direction *cb*)

	1 Fiber	4 Fibers	16 Fibers	25 Fibers
Mean	0.4162	0.4053	0.4039	0.4060
StD	0.0284	0.0268	0.0270	0.0263
StD%	6.8328	6.6160	6.6923	6.4737
Min	0.3271	0.3277	2.8002	2.8557
Max	0.5293	0.5019	5.5244	5.3865

Table 4.32: PRcb Distributions

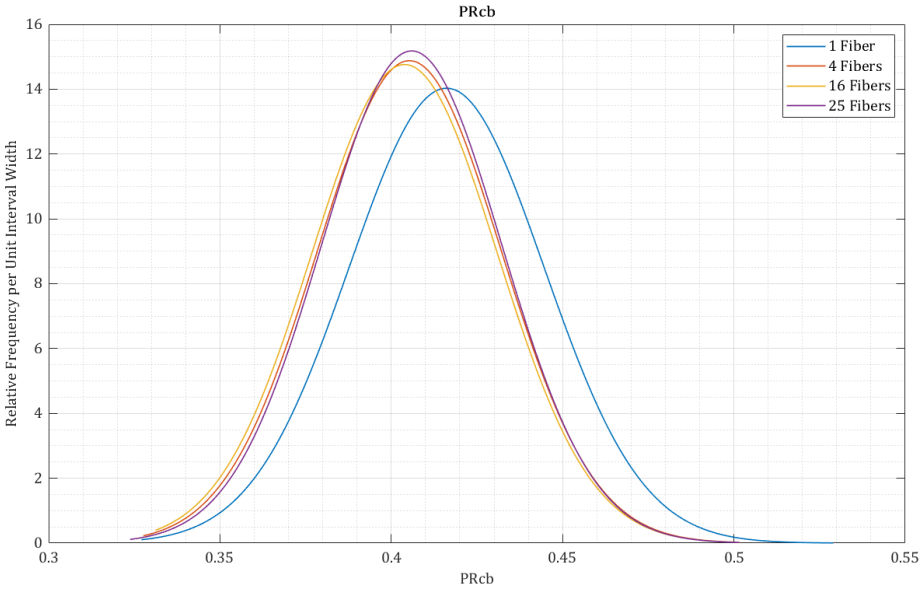

Figure 4.11: PRcb Distributions

Axial Shear Modulus (Direction ab)

	1 Fiber	4 Fibers	16 Fibers	25 Fibers
Mean	3.9118	3.7907	3.8093	3.7941
StD	0.4799	0.4345	0.4291	0.4165
StD%	12.2678	11.4627	11.2658	10.9772
Min	2.5269	2.8278	2.8002	2.8557
Max	6.6931	5.6967	5.5244	5.3865

Table 4.33: Gab Distributions

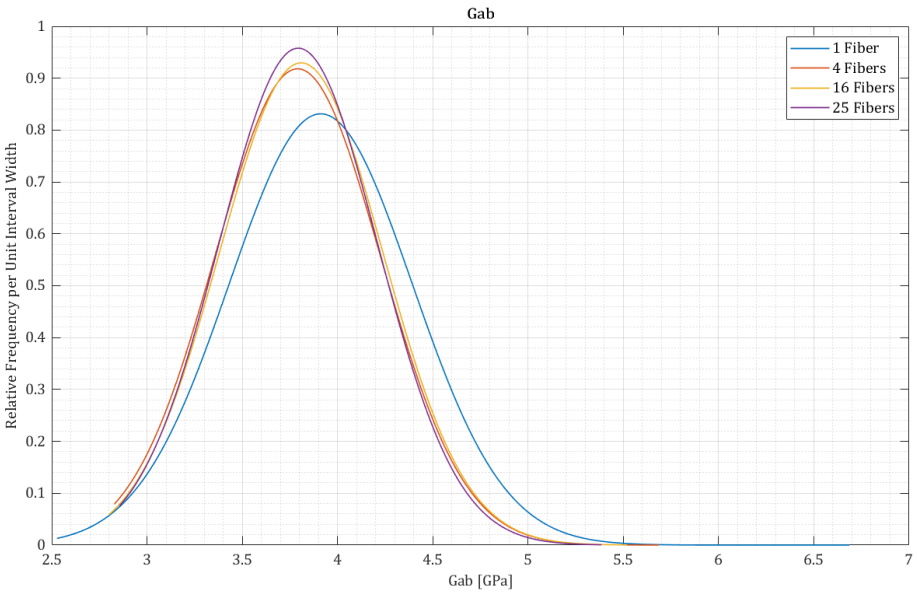

Figure 4.12: Gab Distributions

Transverse Shear Modulus (Direction bc)

	1 Fiber	4 Fibers	16 Fibers	25 Fibers
Mean	2.2035	2.2022	2.2091	2.2041
StD	0.1374	0.1403	0.1395	0.1394
StD%	6.2337	6.3719	6.3138	6.3252
Min	1.7653	1.7646	1.8222	1.7067
Max	2.8810	2.8916	2.7347	2.7104

Table 4.34: Gbc Distributions

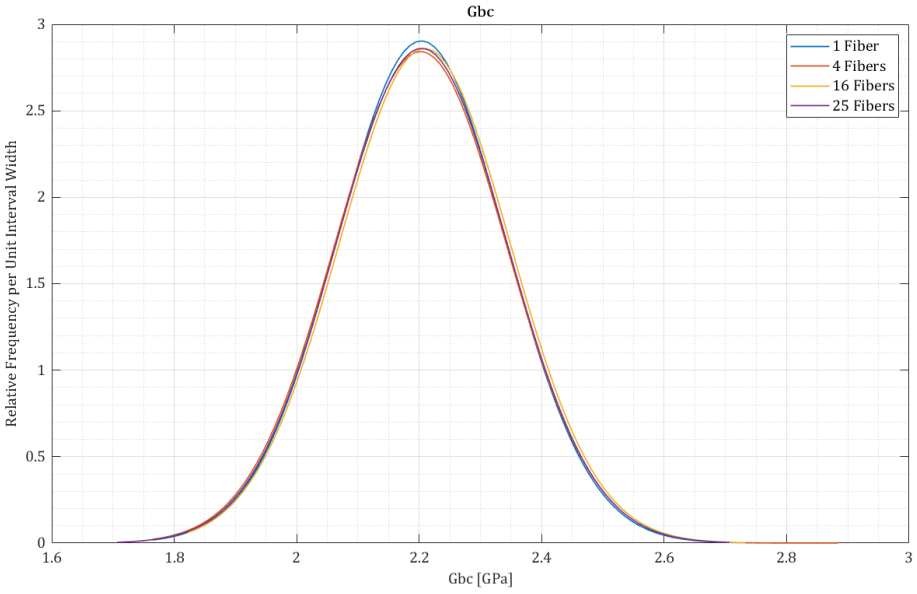

Figure 4.13: Gbc Distributions

4.3.2 Static Failure

Static failure behaviour shows a greater variability with respect to fiber content. Figure 4.16 shows a plot of the RUCs failure trends resulting from simulations using a statistical distribution of individual fiber properties in repeating unit cells containing one, four, sixteen and twenty five simulated filaments.

For the single fiber RUC, average RUC ultimate failure became highly dependent on the selected fiber properties. As the number of the simulated fiber was increased, the RUC averaged failure became less depended on the individual fiber strengths. Essentially, the load carried by one fiber at failure was redistributed among the remaining fibers. Additionally, if the number of fibers is large, the distributions of fibers ultimate strength and strain withing a given RUCs become more similar, resulting in less variation in the predicted rupture limit. Consequently, as the number of fibers increases and exceeds 25 fibers, the mean value and variation in the RUc averaged response asymptotically approaches those of the representative volume elements.Simulating larger fiber contents therefore would results in additional computation costs without giving particular benefits the the final results.

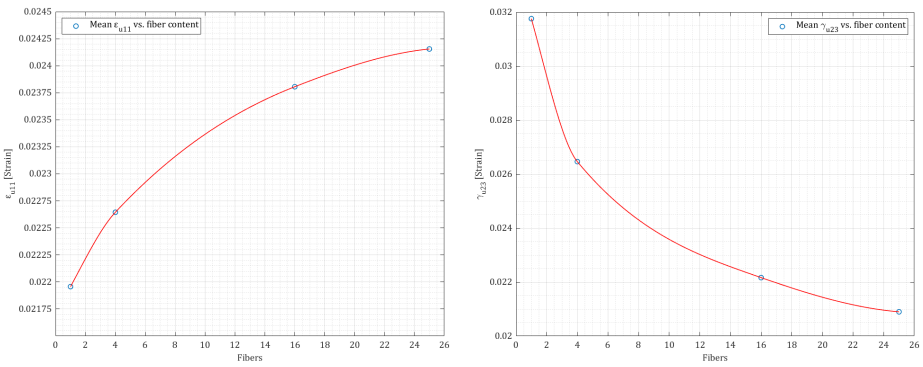

(a) ε_{11} (b) γ_{23}

Figure 4.14: Mean Ultimate Strain vs Fiber Content

Axial ultimate strain (ε_{11})

	1 Fiber	4 Fibers	16 Fibers	25 Fibers
Mean	2.1957e-02	2.2645e-02	2.3806e-02	2.4155e-02
StD	1.1223e-03	1.1630e-03	1.0627e-03	9.8031e-04
Min	1.6100e-02	1.8300e-02	2.0400e-02	2.0900e-02
Max	2.6800e-02	2.8600e-02	2.8600e-02	2.8700e-02

Table 4.35: ε_{11} Distributions

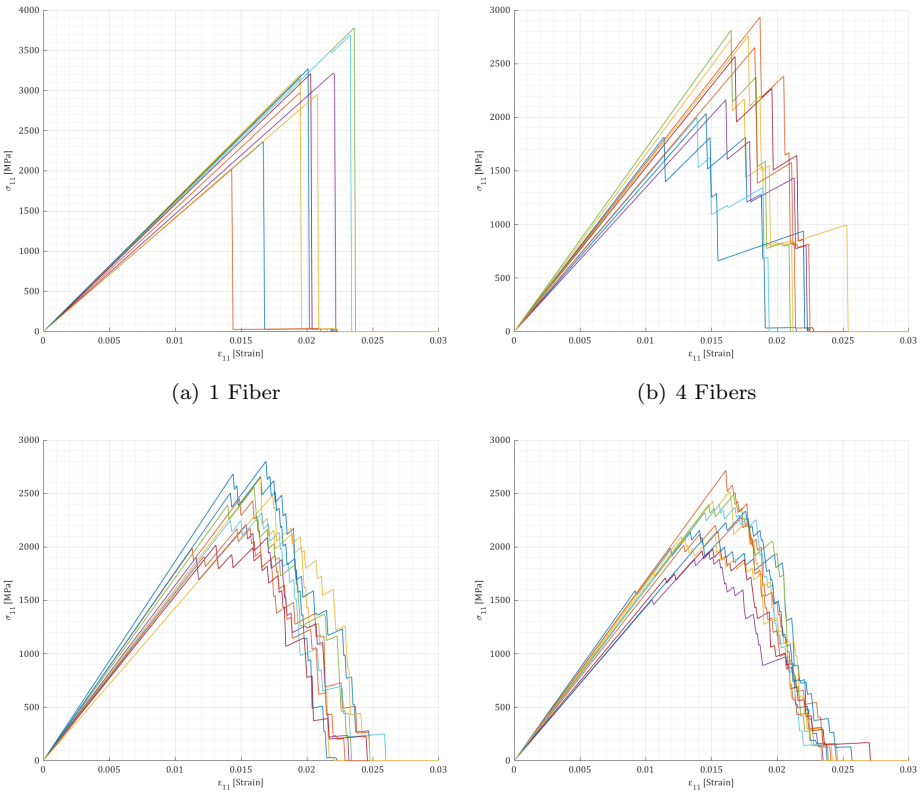

(a) 1 Fiber

(b) 4 Fibers

(c) 16 Fibers

(d) 25 Fibers

Figure 4.15: 10 random Tension$_{11}$ Static Failure Simulation

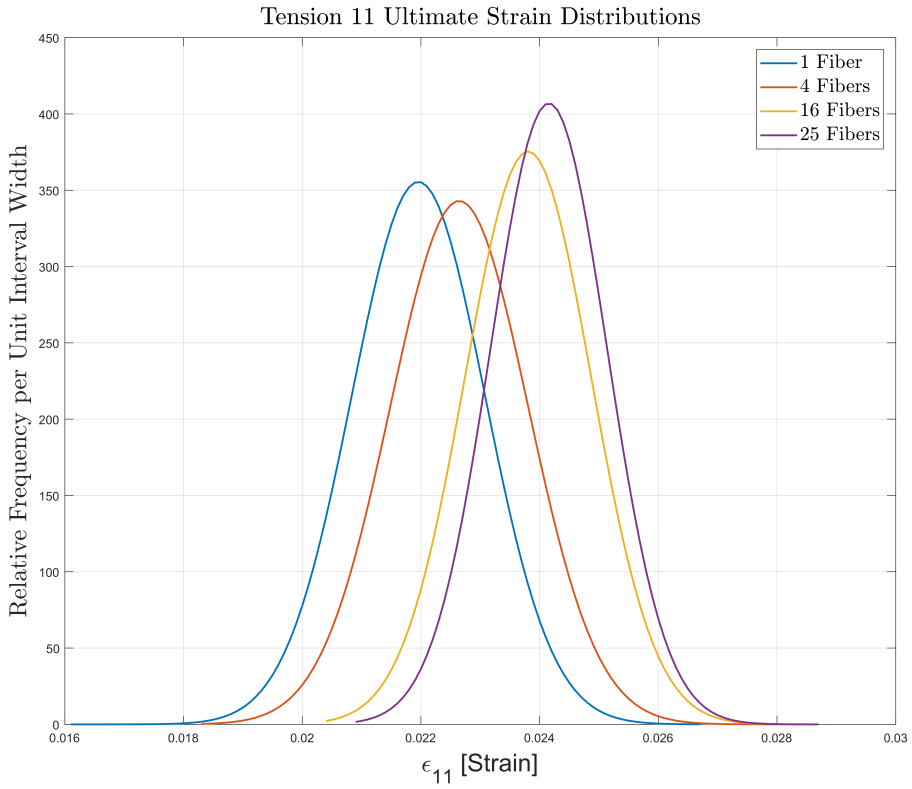

Figure 4.16: Failure Distributions

Ultimate shear strain (γ_{23})

	1 Fiber	4 Fibers	16 Fibers	25 Fibers
Mean	3.1759e-02	2.6463e-02	2.2165e-02	2.0898e-02
StD	5.0087e-03	4.4160e-03	3.5911e-03	3.4524e-03
Min	1.1400e-02	9.1000e-03	7.5000e-03	6.5000e-03
Max	4.5200e-02	4.0800e-02	3.3700e-02	3.2800e-02

Table 4.36: γ_{23} Distributions

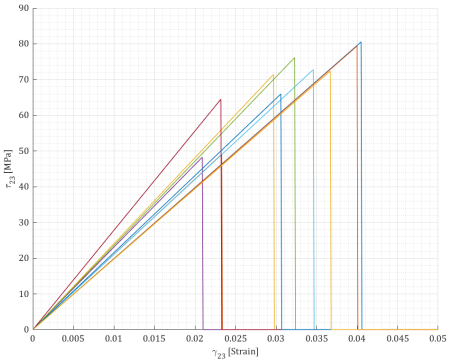

(a) 1 Fiber

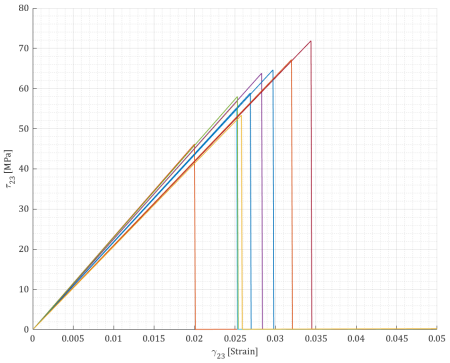

(b) 4 Fibers

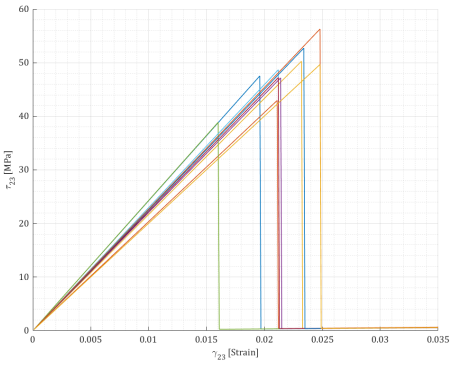

(c) 16 Fibers

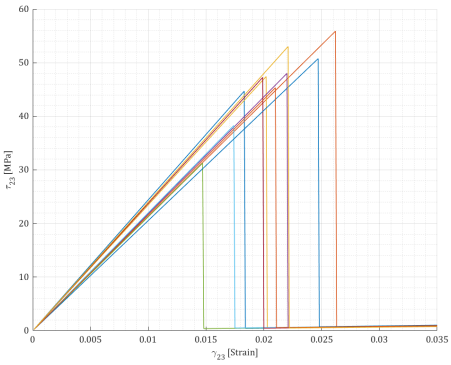

(d) 25 Fibers

Figure 4.17: 10 random Shear$_{23}$ Static Failure Simulation

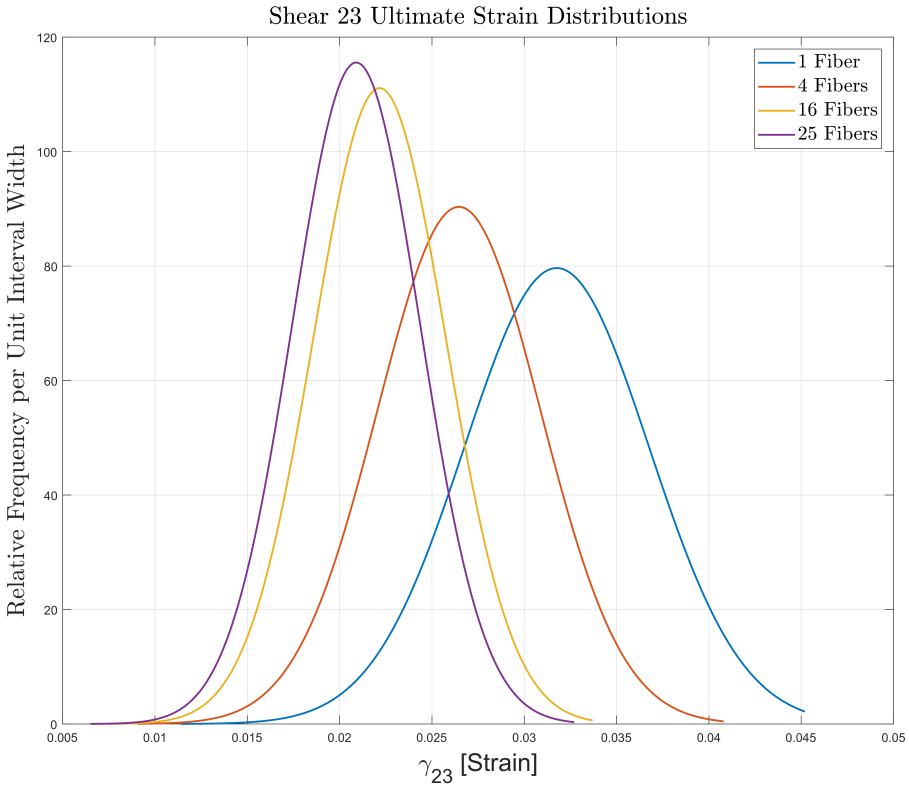

Figure 4.18: Failure Distributions

Chapter 5

Sensitivity analysis

The quantity of stochastic input are directly related to the computational cost of the the simulations. Keeping some input deterministic and and focus the effort of studying variations only on specific parameters is one of the strategies that can be pursued to increase the efficiency of the framework. To understand the criteria behind this selection, the global sensitivity analysis using the Sobol's method, is one of the available methods. Through this variance based sensitivity study it possible to correlate the variance of the output to specific input variances, as each input, will have a larger or smaller influence on specific outputs. For Properties like the axial elastic modulus, it is obvious that the axial elastic modulus of fibers will have an important role and it is less immediate comprehending the influence of other parameters like Poisson ratios or fiber volume fraction. This dependence can becomes even less straightforward when applied to the final structure.

Using the sensitivity analysis module integrated in LS-OPT it is possible to directly perform sensitivity analysis during the stochastic microscale simulation. The method is based on methamodels which have to be chosen and tuned properly as the accuracy of the result depends on the quality of the methamodel. The sampling method, sampling point number and integration points are the parameters to set-up for the methamodel. Here, the Sobol's indexes are computed through quadratic polynomial methamodel where the sampling point are the one used for the Monte Carlo simulation and twenty thousand integration points. Following is presented the mathematical fundamentals of the method and the results obtained for for elastic and failure properties.

5.1 Fundamentals of Variance Based Sensitivity Analysis

The variation of the response can be broken down in contributions from each design variable and its variance assuming independent variables, can be written using the Sobol's indices approach. This technique will rank the influence of the input variance on the response variance using the so called Sobol Indexes.

Considering the following model:

$$Y = f(X_1, ..., X_p) \tag{5.1}$$

where the output Y is a scalar and the input factors $X_1, ..., X_p$ are supposed to be independent random variables described by known probability distributions. These distributions reflect the uncertain knowledge of the system. The naun idea of this method is to decompose the output variance into the contributions associated with each input factor.

In order to quantify the importance of an input factor X_i on the variance of Y, imagine that it's possible to fix it as its "true" value, x_i^*. How much would this assumption change the variance of Y? This is the conditional variance

$$V_{X_{-i}}(Y|X_i = x_i^*) \tag{5.2}$$

where the variance is taken over the $(p-1)$-dimensional parameter space X_{-i}, consisting in all factors but X_i. Because the true value of X_i is unknown, we average over all possible values of X_i.

$$E_{X_i}(V_{X_{-i}}(Y|X_i)) \tag{5.3}$$

The smaller this quantity, the more important the contribution of X_i to the variance of Y. Indeed, using the law of total variance, it's possible to write:

$$V(Y) = V_{X_i}(E_{X_{-i}}(Y|X_i)) + E_{X_i}(V_{X_{-i}}(Y|X_i)) \tag{5.4}$$

and normalizing,

$$1 = \frac{V_{X_i}(E_{X_{-i}}(Y|X_i))}{V(Y)} + \frac{E_{X_i}(V_{X_{-i}}(Y|X_i))}{V(Y)} \tag{5.5}$$

The first-order sensitivity index for factor X_i is given by the first term in equation 5.5:

$$S_i = \frac{V_{X_i}(E_{X_{-i}}(Y|X_i))}{V(Y)} \tag{5.6}$$

From equation 5.5 we get that the first order sensitivity index verifies $S_i \leq 1$. As proved in eq 1, if the function in 1 is integrable over $[0,1]^p$ then it can be decomposed into terms of increasing dimensionality as follows:

$$f(X_1, ..., X_p) = f_0 + \sum_{i=1}^{p} f_i(X_i) + \sum_{1 \leq i < j \leq p} f_{ij}(X_1, ..., X_p) \tag{5.7}$$

Moreover, if the input factors are mutually independent then there exists a unique decomposition of 5.5 such that all the summands are mutually orthogonal. Using this result, it can be shown that the variance of the output, V_Y, can also be decomposed into:

$$V(Y) = \sum_{i=1}^{p} V_i + \sum_{1 \leq i < j \leq p} V_{ij} + ... + V_{1,...,p} \tag{5.8}$$

where $V_i, V_{ij}, ..., V_{1,2,...,p}$ denote the variance of $f_i, f_{ij}, ..., f_{1,...,p}$ respectively:

$$V_i = V(E(Y|X_i)) \tag{5.9}$$

$$V_{ij} = V(E(Y|X_i, X_j)) - V_i - V_j \tag{5.10}$$

$$V_{ijk} = V(E(Y|X_i, X_j, X_k)) - V_{ij} - V_{ik} - V_{jk} - V_i - V_j - V_k \tag{5.11}$$

$$... \tag{5.12}$$

$$V_{1,...,p} = V(Y) - \sum_{i=1}^{p} V_i - \sum_{1 \leq i < j \leq p} V_{ij} - ... - \sum_{1 \leq i_1 < ... < i_{p-1} \leq p} V_{i_1,...,i_{p-1}} \tag{5.13}$$

where, for simplicity, the indices for the variance and the mean were omitted. From this decomposition, sensitivity indexes can be deduced from the first p terms of the decomposition 5.8:

$$s_i = \frac{V_i}{V(Y)} = \frac{V(E(Y|X_i))}{V(Y)} \tag{5.14}$$

The other terms of the decomposition 5 can similarly be interpreted in terms of higher order sensitivity indexes. The second-order sensitivity index, S_{ij}, expresses the amount of variance of Y explained by the interaction of the factorsX_i and X_j

$$S_{ij} = \frac{V_{ij}}{V(Y)} \tag{5.15}$$

and so on until order p. Therefore, for p input factors, we have defined $2^p - 1$ sensitivity indexes. With these definitions of the indexes, we can get the relation:

$$1 = \sum_{i=1}^{p} S_i + \sum_{1 \leq i < j \leq p} S_{ij} + ... + S_{1,...,p} \tag{5.16}$$

5.2 Microscale Analysis Global Sensitivity Results

Starting from a total of seventeen microscale properties, it possible to reduce sensibly the actual properties which have to be considered as probabilistic despite their nature. This selection becomes even more effective, when coupled with a study which identifies which of the composite properties are the most influential in penetration response and behaviour. Anticipating the next chapter content, in low velocity impacts, when penetration does not occur, the Elastic modulus has the highest impact on projectile velocity. For the more interesting cases, when penetration occurs, shear moduli and ultimate tensorial shear strain are the parameters to consider.

Property	ID	Event
Axial Elastic Modulus	Ea	Low Velocity, no penetration
Shear Elastic Moduli	Gab/Gbc	High velocity, penetration
Tensorial Shear Strain	γ_{23}	High velocity, penetration

Table 5.1: Ballistic Impact Response Main Stochastic influences

5.2.1 Elastic Properties

Following the Sobol's indexes obtained for Elastic The elastic properties. Between the various inputs, only the shear modulus of the fiber contribution can be considered negligible (as can be easily understood), and when focusing on the three main elastic parameters in ballistic impact, only five of the eight total inputs distributions have a tangible effect on the out variances. As expected, fiber volume fraction always plays an important role in the overall composite characteristics.

Summarizing: the main probabilistic microscale input which affects the ballistic response of the composite plate that is described in chapter 6 are:

- Fiber Volume fraction (V_f)
- Fiber Axial modulus (E_{a_f})
- Fiber Transverse modulus (E_{t_f})
- Matrix Elastic modulus (E_m)
- Matrix Poisson's ratio (ν_m)

In table 5.2 are reported all the indexes resulting for the variance based sensitivity analysis ranked, red, yellow, blue, green, from the most impacting parameters to the lowest. White cells in table 5.2 represent the negligible probabilistic properties.

	E11	E33	G23	G13	ν_{12}	ν_{23}
V_f	5.273e-1	5.725e-1	5.298e-1	8.435e-1	2.009e-2	7.243e-2
E_{a_f}	4.751e-1	1.290e-5	4.821e-8	1.367e-6	5.335e-9	1.248e-4
E_{t_f}	5.95e-12	1.479e-1	4.100e-2	1.036e-6	3.296e-5	6.523e-3
ν_{a_f}	1.508e-8	4.638e-6	1.401e-7	1.958e-6	6.306e-1	5.891e-5
ν_{t_f}	2.60e-13	4.174e-4	2.738e-3	1.091e-6	6.435e-6	6.318e-2
G_{a_f}	4.84e-14	1.586e-7	1.521e-7	3.830e-4	2.160e-9	7.126e-8
E_m	3.679e-5	2.025e-1	4.014e-1	2.034e-6	2.309e-5	3.608e-3
G_m	2.24e-13	5.474e-7	4.429e-7	1.584e-1	2.694e-9	7.466e-8
ν_m	1.488e-8	8.113e-2	2.695e-2	1.277e-6	3.552e-1	8.582e-1

Table 5.2: Elastic Properties Sensitivity Indexes

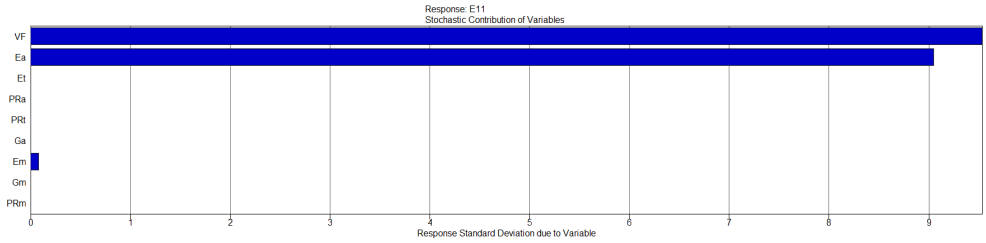

Figure 5.1: Sensitivity Indexes E11

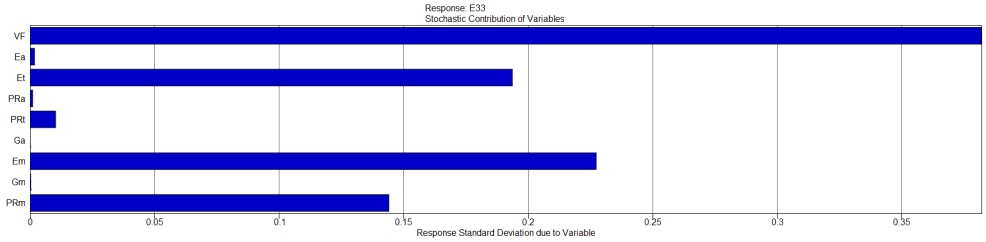

Figure 5.2: Sensitivity Indexes E33

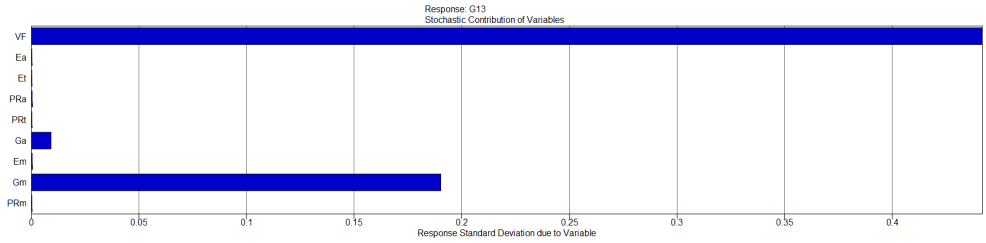

Figure 5.3: Sensitivity Indexes G13

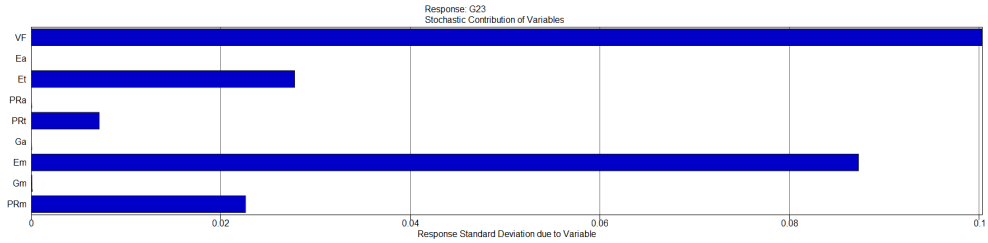

Figure 5.4: Sensitivity Indexes G23

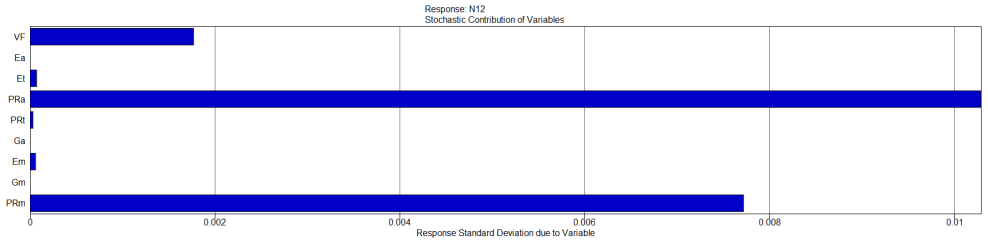

Figure 5.5: Sensitivity Indexes ν_{12}

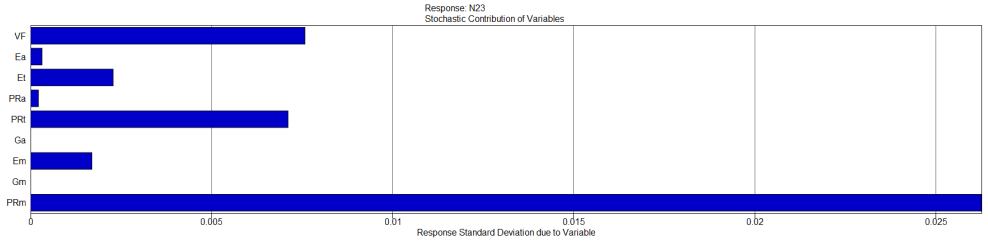

Figure 5.6: Sensitivity Indexes ν_{23}

5.2.2 Failure Properties

Failure properties are showing a similar behaviour and only a few of the microscale inputs are really affecting the output distributions. It is interesting observing how for shear strain in direction 2-3, a partial influence is dictated also by some of the properties classified as elastic characteristics in the previous section. Composite failure distributions are then mainly affected by:

- Fiber axial tensorial strain
- Matrix tensorial strain
- Fiber shear strain
- Matrix Shear Strain
- Fiber volume fraction
- Fiber transverse elastic modulus
- Matrix Elastic modulus

	ε_{12}	γ_{23}
ε_{11f}	5.489e-1	3.394e-4
ε_{22f}	1.514e-3	3.394e-4
ε_{33f}	1.205e-3	4.772e-4
γ_{23f}	1.509e-3	7.995e-1
γ_{13f}	9.132e-4	4.650e-4
γ_{12f}	1.21e-33.384e-4	
ε_m	5.444e-1	5.871e-4
γ_m	1.642e-3	1.637e-2
V_f	-	9.393e-2
E_{tf}	-	5.694e-2
E_m	-	4.180e-2

Table 5.3: Failure Properties Sensitivity Indexes

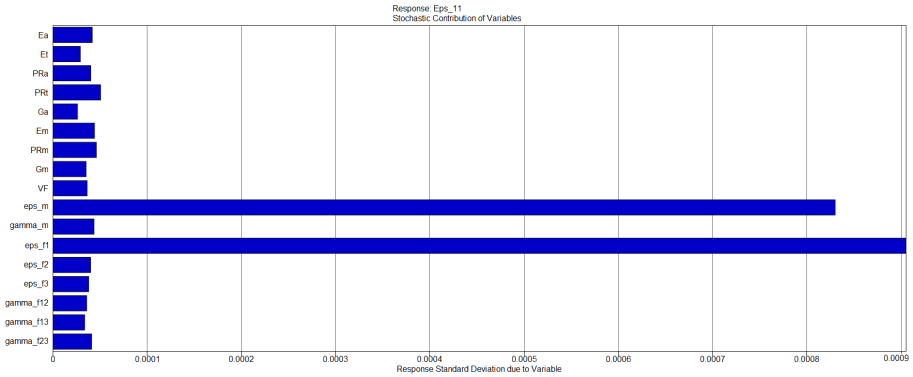

Figure 5.7: Sensitivity Indexes ε_{11}

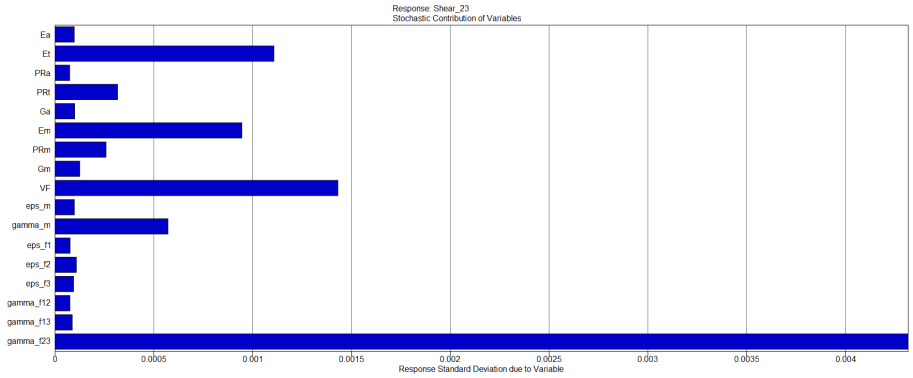

Figure 5.8: Sensitivity Indexes γ_{23}

Chapter 6

Macro-Scale Impact Simulations

In general, Finite Element simulation provide deterministic results. In the case of ballistic impact simulations, for a specific set of inputs (material model and parameter, geometry, mesh, impact velocity and others) the result should always be the same. For a specific simulated impact velocity the result will be either penetration or containment. In reality, however, due to several effects like fore example impurities, inclusions, variations in constituent properties and other source of variation, composite material properties show statistical variations. Therefore a zone of mixed results exists, in which, for a given impact velocity, the projectile sometimes penetrate the composite plate and sometimes not. Deterministic simulations are not able to reproduce or predict this probability of penetration. To replicate this behavior, the goal was to use stochastic variations of the material properties of the composites as input to the simulations.

The probability distributions functions obtained through the micromechanics code are applied to an LS-Dyna FEM model simulating a specific ballistic impact test. The widely used LS-Dyna MAT54 material model is used in combination with the material stochastic properties. After the validation of the material model, the sensitivity to scaling of individual material properties is analyzed to identify which parameters showed a higher influence in low and high velocity impact simulations as anticipated in the previous chapter.

Finally, using the validated MAT54 material card as a baseline, a specific number of material cards have been crated through sampling of the stochastic input distributions obtained from microscale material properties distributions. This new set of material cards are then randomly assigned to the plate elements building the FEM model. By shuffling the assignment of materials to elements, a variation in the response of the composite is observed and using logistic re-

gression analysis a probability of penetration for different impact velocities is defined.

6.1 LS-Dyna FEM Model

For the purpose of studying the variability in structural behaviour as a function a material properties distributions, an already existing and validated model has been used. This model, is representative of an experimental ballistic test where a target (a T800/F3900 Carbon Epoxy Plate) is hit by a 50.8 grams projectile. The composite plate is fabricated using 16 layers resulting in a thickness of 3.098mm and has a 254mm circular clamping patterns. The hollow projectile is made of AL-2024 and has a radiused face.

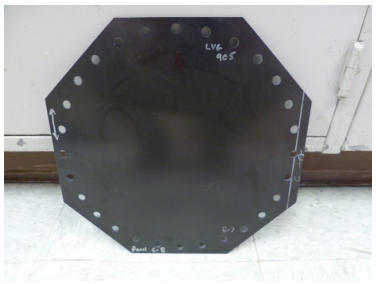

Figure 6.1: A figure

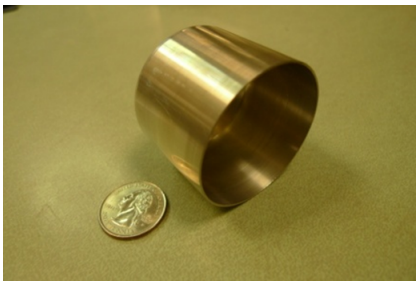

Figure 6.2: Another figure

In LS-Dyna the plate has been modeled using 16 elements (one per layer) through the thickness with the addition of cohesive elements between each layer. A symmetric layup of $[0, 90, +45, -45]_{2s}$ is used (Figure 6.4). A finer mesh is used to model the central section of the plate using an element aspect ration of approximately 8:1 while the aspect ration in the outer part is 16:1 when considering element longest edge. This results in a total of 370.000 plate element and 350.000 cohesive elements. Boundary conditions (figure 6.3) are achieved by constraining the round plate in the clamping region in impact direction modeling the interaction between the clamping plates and the composite plate. Additionally, the nodes in the region where the bolts would be located are constrained in plane.

The aluminium impactor was modeled with 27200, 8-noded hexaedral elements using a piecewise linear plasticity model (MAT24). The influence of friction between projectile ad plate and the influence on the angular impact. In the first case, the coefficient of friction has been varied from 0.1 to 0.3 without showing any variation in the simulation output.For angular impact, both the impact axis and the velocity vector were rotted around the y-axis (perpendicu-

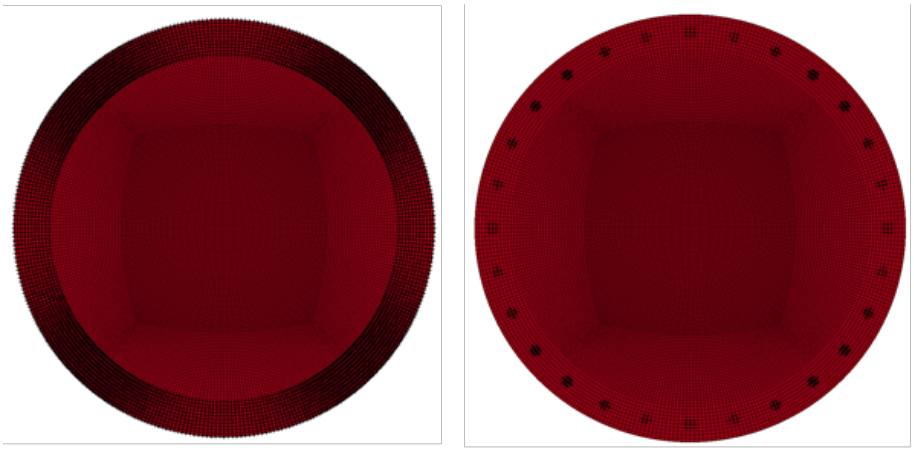

Figure 6.3: Constraint Representation

Figure 6.4: FEM model layup

lar to the fiber direction) about 5deg. In figure is shown the rotated projectile and the nodal velocity vectors with the short black arrows. The results do not show a Major impact on the displacement results. Normal impact and angular result in very similar output for the center of impact point and the maximum displacement point

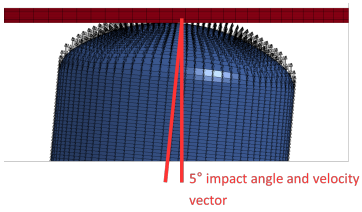

Figure 6.5: A figure

Figure 6.6: Another figure

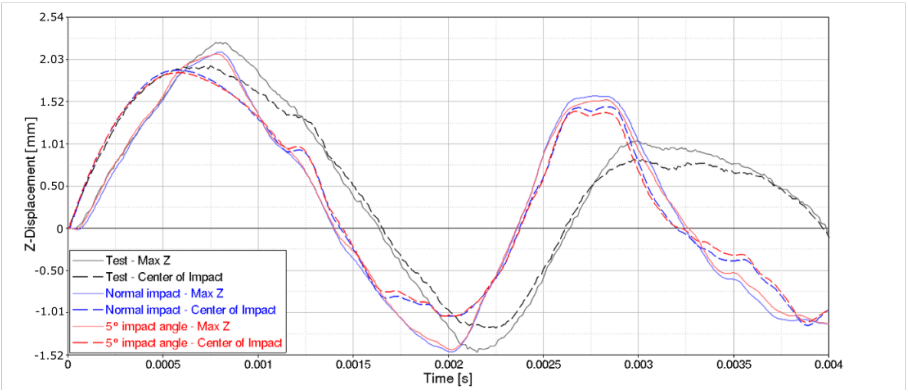

Figure 6.7: Impactor angular deflection plot

6.2 MAT54 material card and single element verification

6.2.1 Single element verification

Single element simulations were used to verify the baseline material card is working as expected and to highlight some of the current capabilities of MAT54. Figure 1 shows the used input to the MAT54 material card while Table 1 lists how these values were obtained and, if applicable, the source. The material tests to get the elastic properties of the T800/F3900 composite were performed by Arizona State University and The Ohio State University.

Input	Description	Source	Value
ro	Mass Density	Material Test	1.4521E-4
ea	Young's modulus - longitudinal	Material Test	161.751GPa
eb	Young's modulus - transverse	Material Test	7.3498GPa
prba	Poisson's ratio ba	Material Test	0.0168
prcb	Poisson's ration cb	Material Test	0.4390
gab	Shear modulus ab	Material Test	3.9955GPa
gbc	Shear modulus bc	Material Test	2.2476GPa
ti	Flag to turn on transversal isotropic behavior	Assumption	1
alph	Shear stress paraeter for nonlinear term	Wade et al. [26]	0.1
fbrt	Softening for fiber tensile strength	Wade et al. [26]	0.5
ycfac	Reduction factor for compressive fiber strength after matrix compressive failure	Wade et al. [26]	1.2
dfailt	Maximum strain for fiber tension	De Facto Deactivated	300.0
dfailc	Maximum strain for fiber compression	De Facto Deactivated	-300.0
xc	Longitudinal compressive strength	Material Test	0.727GPa
xt	Longitudinal tensile strength	Material Test	2.523GPa
yc	Transverse compressive strength	Material Test	0.175GPa
yt	Transverse tensile strength	Material Test	0.044GPa
sc	Shear strength, ab plane	Material Test	0.128GPa
crit	Failure criterion	Computational	54
beta	Weighting factor for shear term in tensile fiber mode	Wade et al. [26]	0.5

Input	Description	Source	Value
slimt1	Factor to determine the minimum stress limit after stress maximum (fiber tension)	Assumption – generally requires extensive calibration [19]	0.5
slimt1	Factor to determine the minimum stress limit after stress maximum (fiber tension)	Assumption – generally requires extensive calibration [19]	0.2834
slimc1	Factor to determine the minimum stress limit after stress maximum (fiber compression)	Assumption – generally requires extensive calibration [19]	1.0
slimt2	Factor to determine the minimum stress limit after stress maximum	Assumption – generally requires extensive calibration [19]	0.6402
slimc2	Factor to determine the minimum stress limit after stress maximum (matrix compression)	Assumption – generally requires extensive calibration [19]	1.0
slims	Factor to determine the minimum stress limit after stress maximum (shear)	Assumption – generally requires extensive calibration [19]	1.0

Table 6.1: FEM Impact Tests Results

Apart from the elastic properties that were obtained using material tests (shaded blue), several material parameters had to be taken from literature (shaded red). Obtaining good values for these parameters can be time and resource intensive and requires extensive calibration efforts to reverse engineer the correct values for the used material. As many of these parameters were obtained for a different fiber/matrix combination, they might not be the best values possible and could be improved. Due to time constraints, an extensive calibration of these parameters was not performed in this study. To verify the material is responding as expected, single element simulations were performed. The material was loaded in 1, 2 and 3-direction in tension and compression as well as in 12, 23, and 31 shear. Table 2 shows the results of the 9 single element simulations. In 1-direction tension, the material responds linear elastic until the longitudinal tensile strength (XT) is reached. The stress then drops to XT*SLIMT1 and stays perfectly plastic. As the transverse isotropic behavior flag is turned on (TI=1), the response in the 2 and 3 direction is expected to be the same, which is the case. In both the 2 and 3 direction tension, the stress increases linear elastic until the transverse tensile strength (YT) is reached and then drops to a perfectly plastic level of YT*SLIMT2. In compression, the SLIM values were chosen to be 1 (assumption) and therefore, after the compressive

strengths (XC and YC) are reached, the stress does not drop but stays perfectly plastic at the level of XC and YC respectively. The response in shear 12 and 31 directions are the same due to transverse isotropy with stresses reaching SC and then staying perfectly plastic at that level due to SLIMS being chosen as 1. In shear 23 the material seems to respond similar to tension in transverse direction with stresses reaching a level of YT and then dropping to YT*SLIMT2.

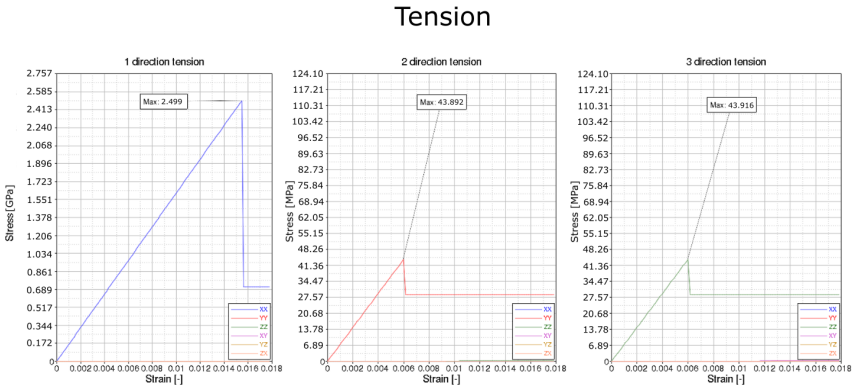

Figure 6.8: Single Element Tension Verification

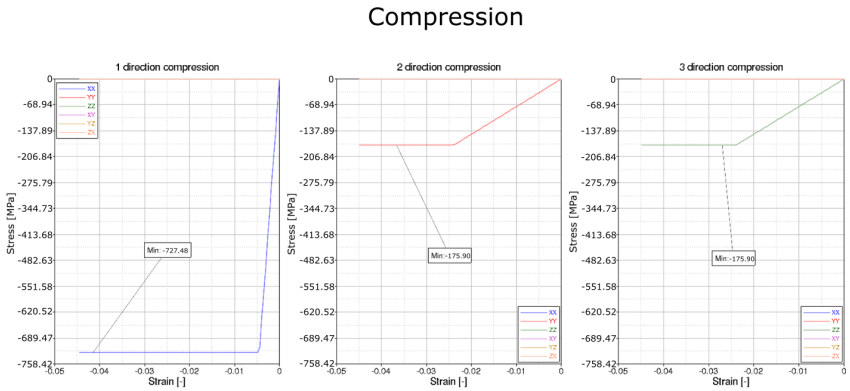

Figure 6.9: Single Element Compression verification

6.2.2 Impact Simulations Verification

For validation of the elastic response of the material, a relatively low velocity impact was chosen (LVG1067/1071 – 47.244m/s). To calibrate the failure criterion, three high velocity impacts were chosen:

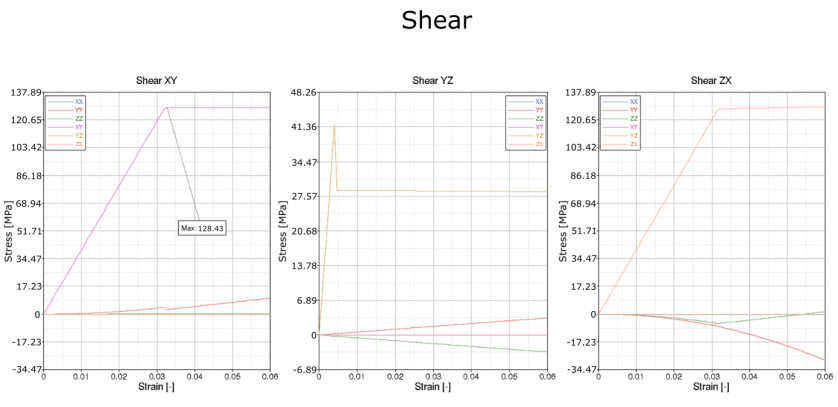

Figure 6.10: Single element Shear verification

- LVG1075 - 117.34 m/s, in which the projectile caused significant damage to the plate but was contained.
- LVG1074 - 127.10 m/s, where the projectile penetrated the plate and exited with a low velocity ($\sim$ 7.62m/s)
- LVG1076 - 138.37 m/s, which was the second highest velocity tested by NASA where the projectile penetrated the plate and exited with a high velocity.

Figure 6.11 shows a plot of impact velocity (abscissa) vs. exit velocity (ordinate) in the penetration cases or rebound velocity (ordinate) in the cases where the projectile was contained.

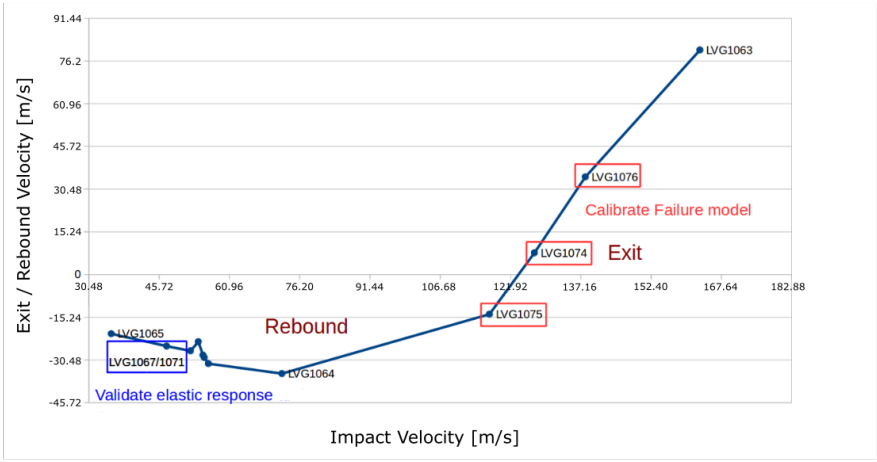

Figure 6.11: Impact Velocities plot

Low Velocity Impacts

The elastic response of the material model was validated using the low velocity impact tests LVG1067 and LVG1071 with projectile velocities of 47.24 m/s and 47.35 m/s respectively. The impact caused no visible damage to the plate in both tests. Figure 6.12 shows the displacement in impact direction in the center of the back side of the plate in the test (blue), simulated using MAT22 (purple), an early version of MAT213 and the material card MAT54 described earlier in this document. The response of MAT54 was considered "close enough" to the test results and therefore could be used in the higher velocity impacts to calibrate a failure model.

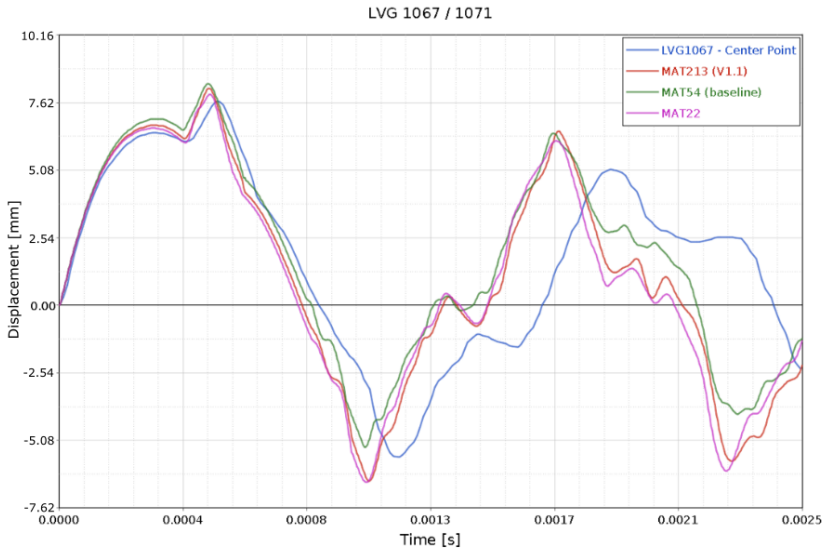

Figure 6.12: Low Velocity Impact calibration

High Velocity Impacts

For this study failure was considered using the LS-DYNA Erosion card, which provides an option to include different failure criteria with existing material models. The options chosen were minimum and maximum principal strain at failure and tensorial shear strain at failure. To calibrate this failure model, three higher velocity impacts were simulated. As a first step, the lowest of the three velocities was simulated with failure disabled. Plotting the minimum and maximum principal strain at failure and the shear strain in this simulation provided a first starting point to identify failure parameters that allow for an accurate modeling of the failure patterns. By trial and error approximately 10 different combinations of the three failure parameters were simulated at the three different impact velocities. The total amount of simulations determine

the final set of values was therefore around 30s. The projectile velocities pre-and-post-impact are plotted in Figure 6.13 with the horizontal datum lines representing the exit velocity that was measured in the test. A good fit of the simulation is therefore obtained if the post-impact velocity of the projectile is close to the datum line of the specific test. As Figure 6.13 shows, the material is capable of modeling the projectile rebound in LVG1075 and the penetration and exit velocities in both LVG1074 and LVG1076.

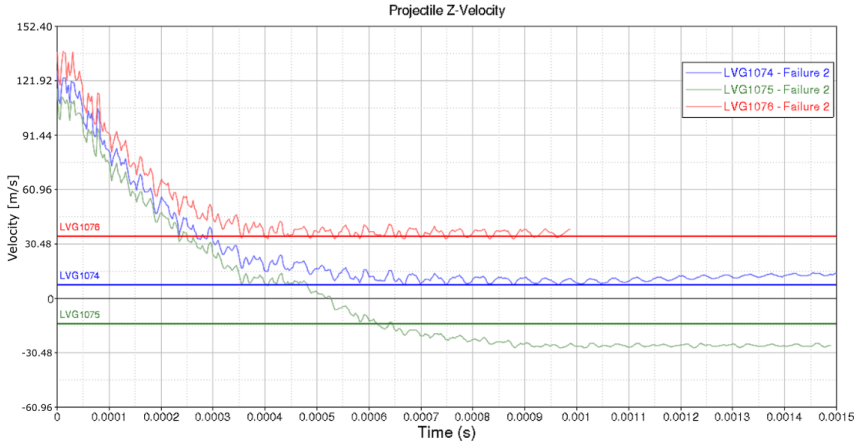

Figure 6.13: High Velocity Impact calibration

The failure pattern in the test and the simulation are shown in Figure 6.14. In the top, the top view (impacted side) of the plate in the simulation (left) and test (right) is shown and in the two pictures below the bottom view. In both, test and simulation, the plate fails in a cross-like pattern with significant delamination between the layers. The failure patterns in the higher speed impacts looked similar in the tests and simulations.

Figure 6.14: FEM vs Test fracture pattern

6.2.3 Delamination

As described above, delamination was accounted for by the use of cohesive elements that were calibrated extensively in an earlier study based on Double Cantilever Beam, End Notched Flexure tests and ballistic impact simulations. However, this was the first time the calibrated cohesive material was used in high velocity impacts. As the images in Figure 6.15, 6.16, 6.17 show, the predicted delaminated areas in the simulations (left) are close to the delaminated areas that can be seen in scans of the tested specimen (right). The importance to account for delamination in ballistic impact simulations of composite plates is demonstrated by the comparison of a simulation without cohesive elements to the baseline simulation. Figure 6.18 shows the projectile velocity in the LVG1074 case. Just like in the test, the projectile penetrated the panel in the simulation in which delamination was accounted for by cohesive elements (blue). In the simulation without cohesive elements (red), the projectile is contained and now rebounds the plate (negative post-impact velocity). This highlights the need to account for delamination in impact simulations of composites.

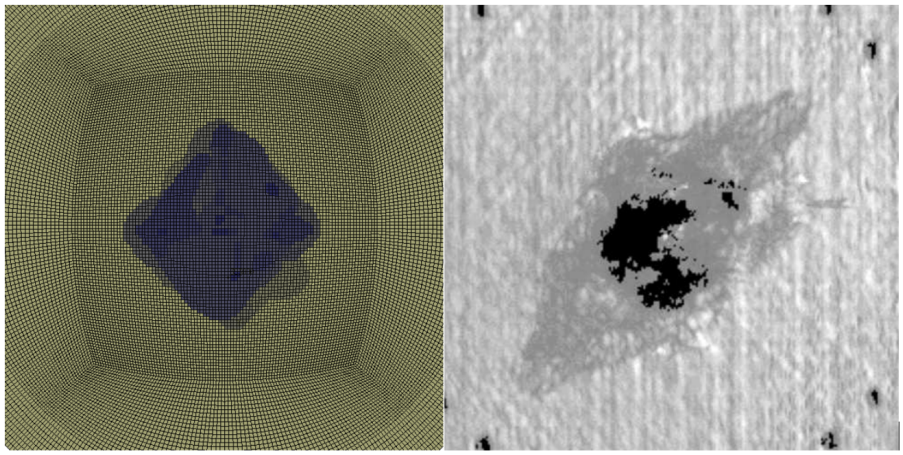

Figure 6.15: LV1075 Delamination

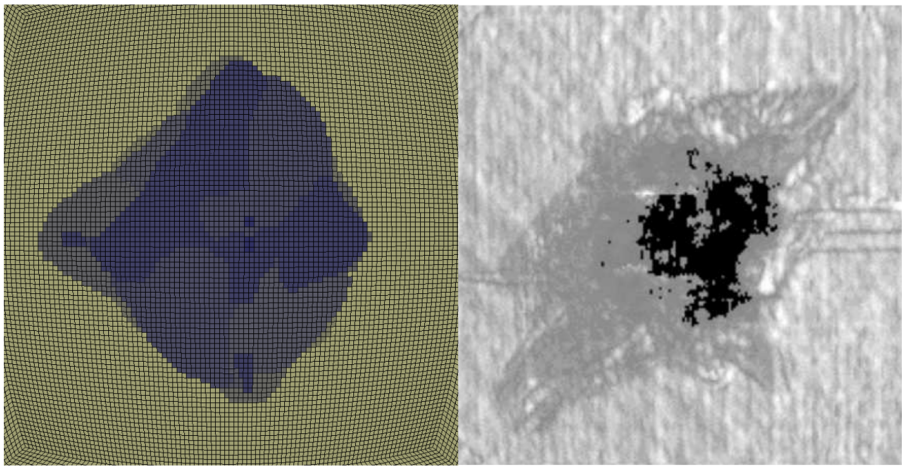

Figure 6.16: LVG1074 Delamination

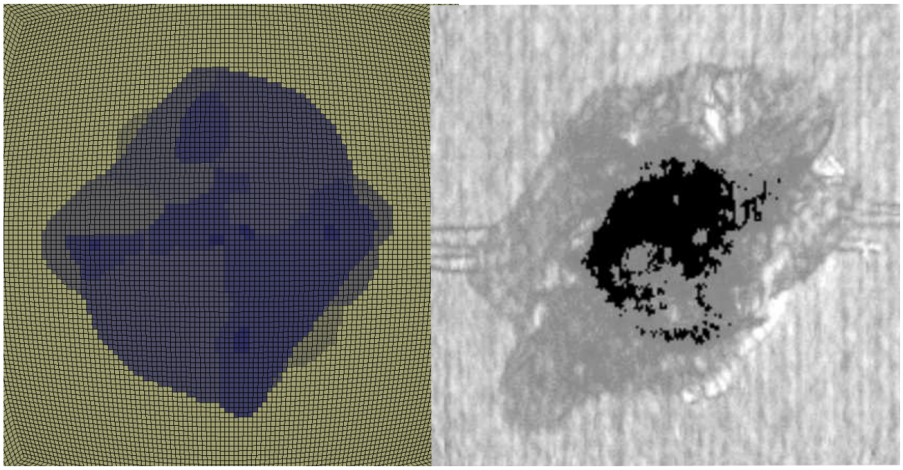

Figure 6.17: LVG076 Delamination

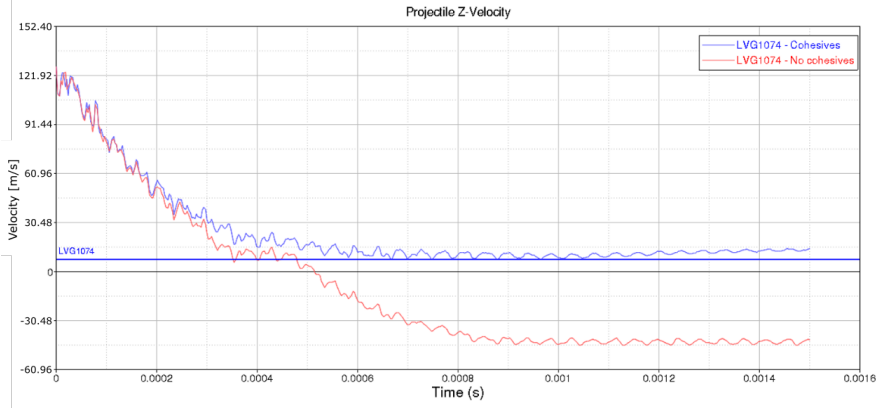

Figure 6.18: LVG1074 Simulation - Cohesive vs Non-cohesive elements

6.2.4 Assumption and Limitations

Due to the limited scope of this study, some assumptions were made to simplify the analysis. As mentioned earlier, several material parameters were taken from literature where these values were optimized for different fiber/matrix pairings. In addition, the material and failure model were calibrated on a specific use case with a certain mesh size and orientation. Variations in loading, for example due to a different projectile shape or a different mesh size and/or orientation, might need additional or new calibration efforts. This strong mesh dependency can be shown by rotating the plate of 45° or by using a finer mesh size. Figure 6.19 shows the projectile velocity results for the baseline mesh (solid lines) and for the rotated mesh (dashed lines). As the material direction was defined in the global coordinate system, this does not influence the results and the difference between baseline (called "Failure 2") and the rotated mesh can only be explained by the mesh sensitivity. The simulation of LVG1074 (blue), with the baseline mesh, previously correctly predicted penetration of the projectile with a low exit velocity now predicts a rebound of the projectile when the rotated mesh is used. The pattern of failure also shows differences between the baseline and the rotated mesh (Figure 6.20 and 6.21) with the pattern roughly following the element lines in both cases.

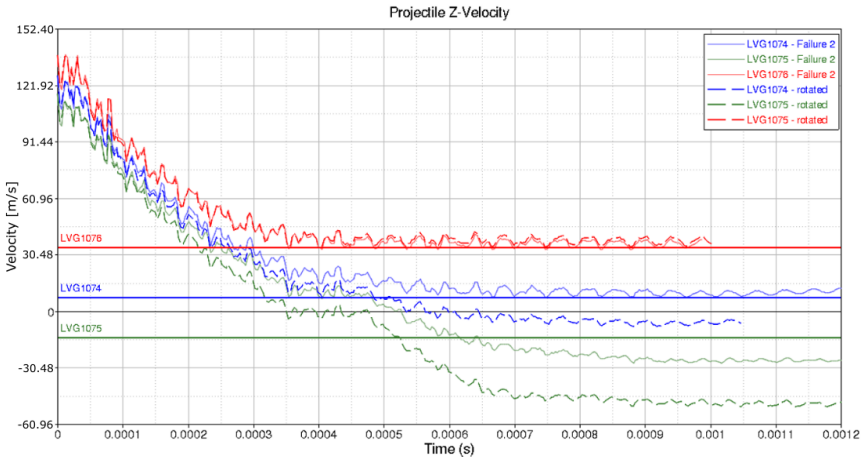

Figure 6.19: Baseline vs Rotated mesh simulation

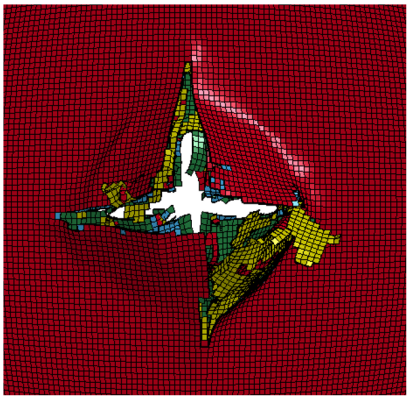

Figure 6.20: Baseline Mesh

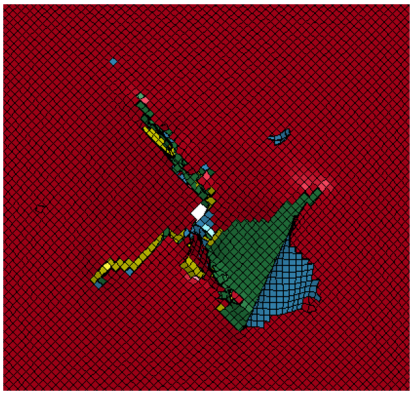

Figure 6.21: Rotated Mesh

In addition to the rotated mesh, the results of the baseline were compared to a finer mesh size of approximately half the element size of the baseline. In this case the projectile velocities change in a different way, with now all three simulations resulting in penetration with high exit velocities as Figure 6.22 shows. The failure pattern of the plate changes as well as Figure 6.20 and 6.21 show.

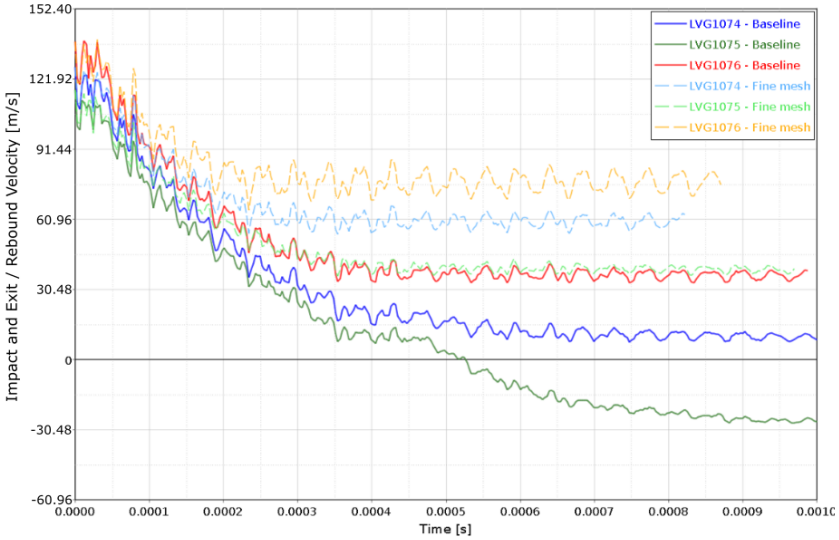

Figure 6.22: Baseline vs Fine mesh

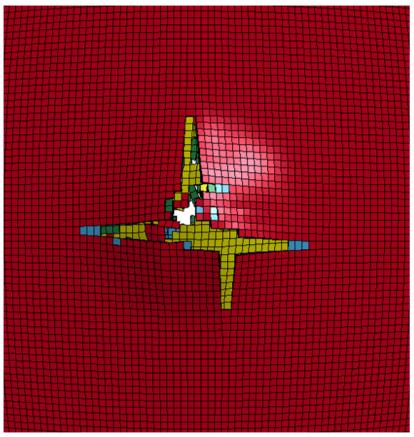

Figure 6.23: Baseline Mesh

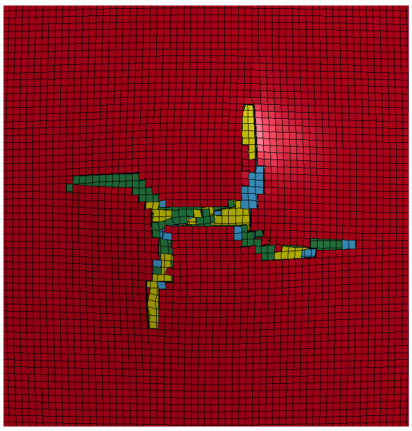

Figure 6.24: Fine Mesh

6.3 Influence of Variation of Elastic and Failure properties in ballistic impacts

6.3.1 Elastic Parameters

Due to the large amount of input parameters to the MAT213 material model, the influence of the elastic material properties in the MAT54 model on ballistic impacts were studied to identify the most important variables for a future stochastic implementation of MAT213. The material properties were scaled up individually by the standard deviation percentage obtained using MAC/GMC (section 4.3.1) and their influence on the simulation results compared qualitatively by looking at the plate displacement in the low velocity impact (LVG1067 – 47.24m/s). In these low velocity impacts, failure did not have an influence on the results. In the higher velocity impact tests on the other hand (LVG1075 – 117.34 m/s, LVG1074 – 127.10 m/s and LVG1076 – 138.37 m/s) failure occurred in the plate, and therefore influenced the obtained results.

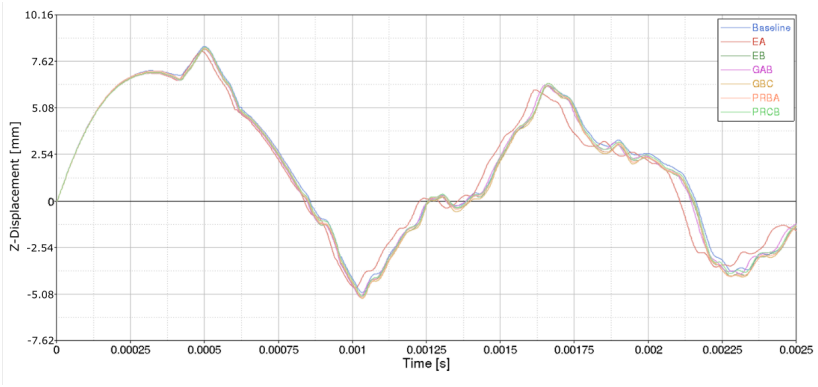

Figure 6.25: LVG1067 with elastic properties scaled individually

In the low velocity impact of LVG1067, the Young's Modulus in fiber direction (EA) was clearly the dominating material parameter as shown in Figure 17. All other material parameters did not influence the plate displacement results significantly. In the higher velocity impacts of LVG1075, LVG1074 and LVG1076, the composite plate was damaged and in the cases of LVG1074 and LVG1076 fully penetrated. Figure 6.26, 6.27 and 6.28 show the resultant projectile displacements for the different scaled elastic properties in the three impact tests. In the contained case (LVG1075) the Shear Modulus 12 (GAB) and the Poisson's ratio 31 (PRCB) influence the results most significantly. In LVG1074, the most important variables are the Shear Moduli in 23 (GBC) and 12 direction (GAB). Similar results are obtained with the highest simulated velocity of LVG1076 with both Shear Moduli having the biggest impact on the result.

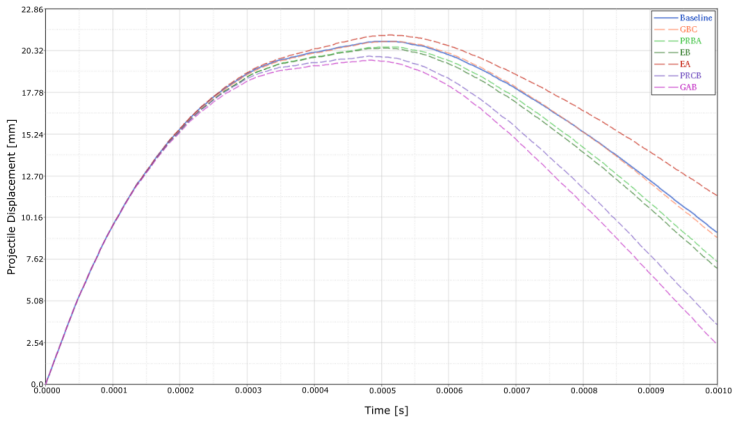

Figure 6.26: LVG1075 Projectile impact direction displacement

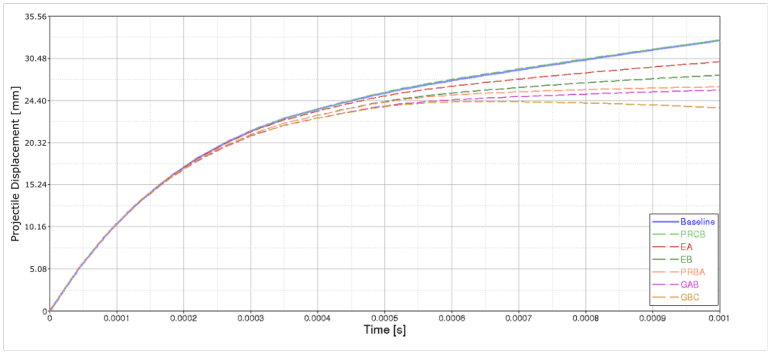

Figure 6.27: LVG1074 Projectile impact direction displacement

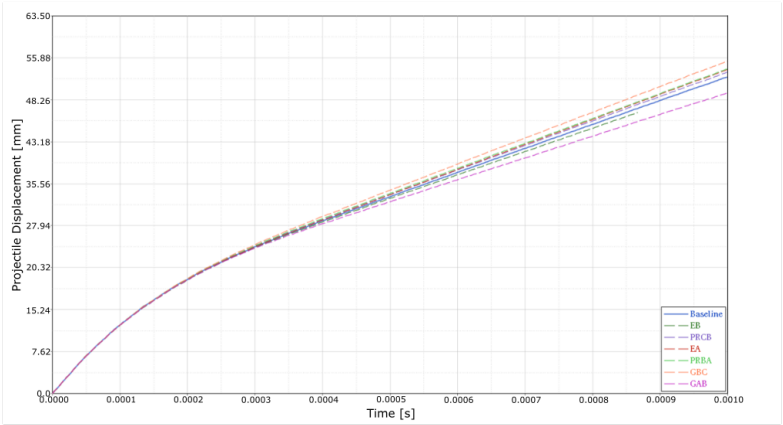

Figure 6.28: LVG1076 Projectile impact direction displacement

In conclusion, in the low velocity impact, where failure did not occur, the

Young's Modulus was the dominating material parameter and in the higher velocity impacts the Shear Moduli.

6.3.2 Failure Parameters in high velocity impacts

The influence of the defined failure parameters of the Erosion card was studied using the three high velocity impacts LVG1075, LVG1074 and LVG1076. The failure parameters were scaled by the absolute difference between mean and maximum / minimum that was obtained using MAC/GMC (section 4.3.2).

For all three ballistic impact velocities the clearly dominating factor was the tensorial shear strain at failure (EPSSH). Figure 6.29, 6.30 ad 6.31 show the projectile velocity over time in the three ballistic impact tests for the scaled failure parameters.

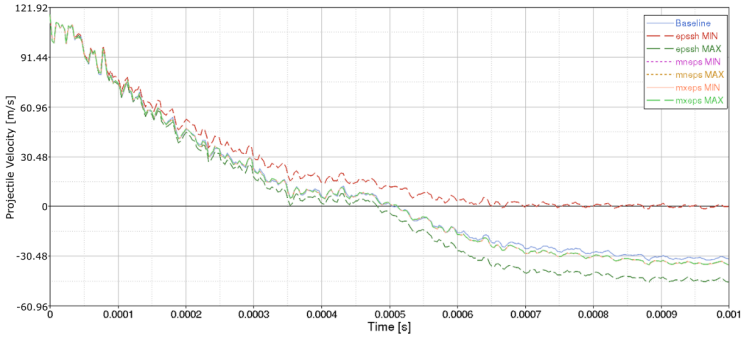

Figure 6.29: LVG1076 Projectile impact direction displacement

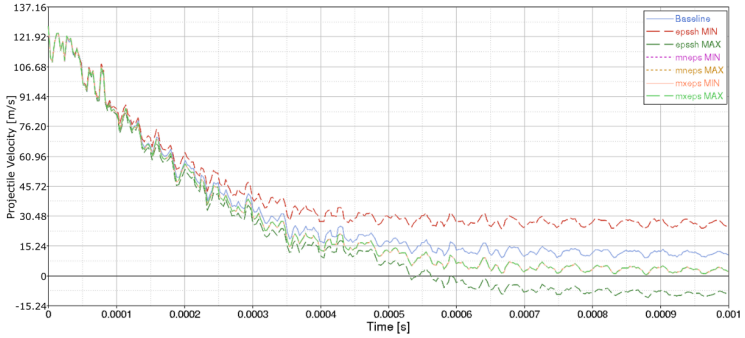

Figure 6.30: LVG1076 Projectile impact direction displacement

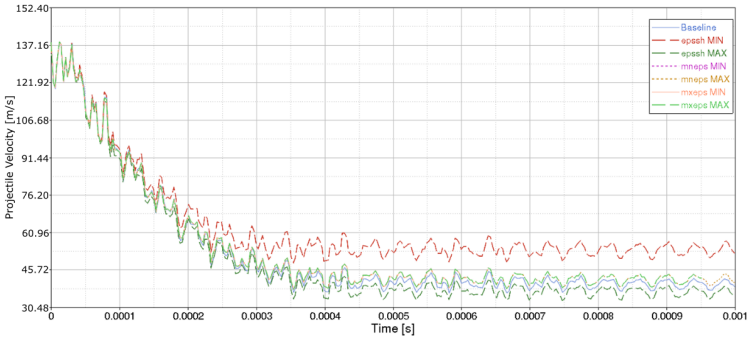

Figure 6.31: LVG1076 Projectile impact direction displacement

6.4 Determining probability of penetration using statistical variations of material parameters

The overall goal of the stochastic analysis is to provide a computational framework to analyze stochastic variations of material parameters and to incorporate their effects into ballistic impact simulations. The stochastic variations of the material parameters that were obtained using the micro mechanics code MAC/GMC were used to create 100 LS-DYNA material cards. Figure 6.32 shows as an example the Young's modulus in fiber direction (EA) for the 100 material cards. These material cards were then randomly assigned to elements of the composite plate with every material card being assigned to the same total number of elements. A representation of this distribution is shown in figure 6.33.

50 ballistic simulations were then setup with velocities being picked randomly in a range in which the 50% probability of penetration was expected due to the previous test and simulation results. The assignment of material IDs to the elements was reshuffled between every simulation. Therefore the impact region could sometimes contain "weaker" materials and sometimes "stronger" materials. Each simulation was run with two different material input sets, once with all material parameters being varied and once with variation of only the most influential parameters as identified in the earlier studies. Table 6.1 shows the binary results of the ballistic impact simulations with 0 representing projectile containment and 1 representing penetration of the plate. Containment was defined as the projectile displacement showing a maximum before the termination time of the simulation, meaning that the projectile rebounded.

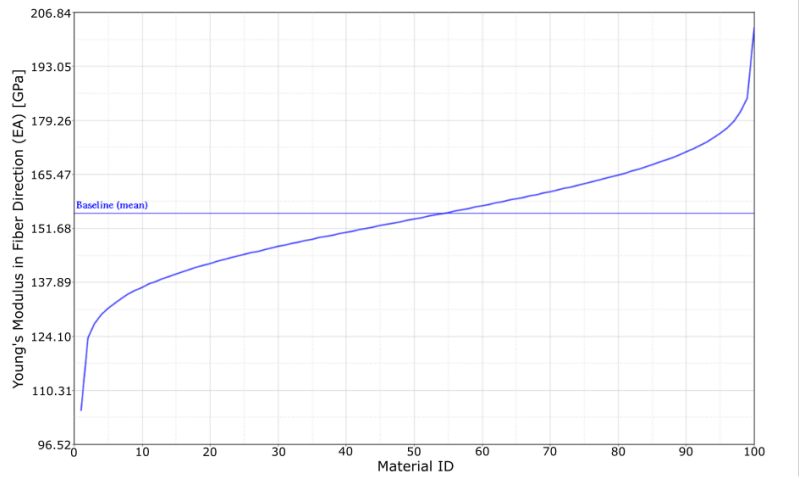

Figure 6.32: EA Distribution - Impact simulation

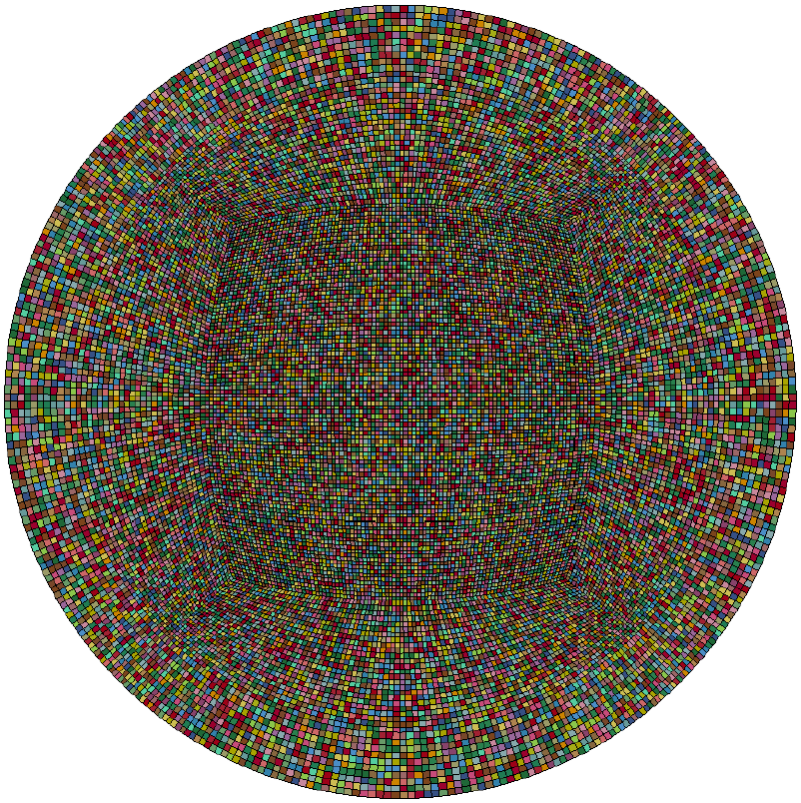

Figure 6.33: EA Distribution - Impact simulation

ID	Velocity [m/s]	All parameters with variation	EA, GAB, GBC, EPSSH with variation
1	117.195	0	0
2	117.398	0	0
3	117.525	0	0
4	117.856	0	0
5	117.881	0	0
6	118.618	0	0
7	119.761	0	0
8	121.539	0	0
9	122.123	0	0
10	122.555	0	0
11	124.612	0	1
12	124.968	0	0
13	125.120	1	1
14	125.145	0	1
15	125.349	0	1
16	126.187	1	0
17	126.238	1	1
18	126.339	1	1
19	126.415	1	0
20	127	1	1
21	127.152	1	1
22	127.152	0	1
23	127.203	1	1
24	127.228	0	1
25	127.279	1	1
26	127.431	1	1
27	127.584	1	1
28	127.838	1	1
29	128.016	1	1
30	128.117	1	1
31	128.117	1	1
32	128.193	1	1
33	128.270	1	1
34	128.346	1	1
35	128.422	1	1
36	128.600	1	1
37	128.701	1	1
38	128.879	1	1

ID	Velocity [m/s]	All parameters with variation	EA, GAB, GBC, EPSSH with variation
39	129.032	1	1
40	129.082	1	1
41	129.362	1	1
42	130.302	1	1
43	131.013	1	1
44	131.038	1	1
45	131.064	1	1
46	131.927	1	1
47	133.019	1	1
48	133.426	1	1
48	133.451	1	1
50	133.908	1	1

Table 6.2: FEM Impact Tests Results

In Figure 6.34 the logistic regression functions, indicating the probabilities of penetration that were computed for the two sets of data, are shown with the raw data points. In green, the two physically tested impact velocities are shown as well. The blue curve shows the regression function for the material input where all parameters were stochastically varied and the red curve where only the most influential material parameters were varied. The "zone of mixed results", or in other words the velocity range from lowest velocity causing penetration to highest velocity in which the projectile was contained for both cases is similar. The velocity at 50% likelihood of penetration with all parameters varied is 124.86 m/s and with the most influential parameters varied 125.75 m/s which is a difference of less than 1%. As the difference between the two analysis is quite low, in future stochastic implementations of MAT213, the focus should lie on the here determined influential parameters.

For a comparison of the determined probability range to the ballistic impact tests conducted at NASA, Figure 26 shows the test impact velocity vs. exit / rebound velocity obtained in the tests in blue. The probability range from 99 probability contained to 99% probability of penetration is shown in yellow. The red marker highlights the 50% probability of penetration velocity. The simulation results suggest that for the LVG1075 impact velocity of 117.34 m/s in 100% of the time the projectile will be contained as it also was in the test. For the impact velocity of the LVG1074 test (127.10 m/s) however, the computed probability of penetration was $\sim$ 90%. In the physical test the projectile penetrated the plate and exited on the back with a relatively low velocity of $\sim$ 7.62

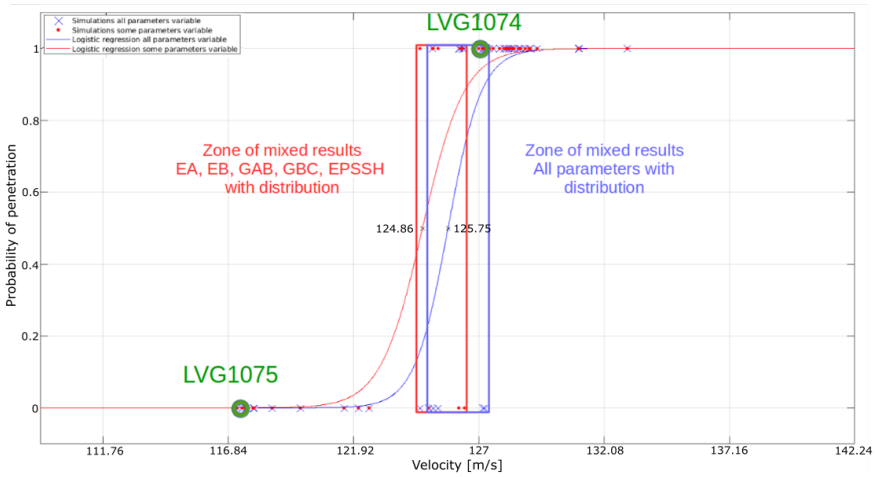

Figure 6.34: Logistic regression functions and zone of mixed results for both sets of simulations

m/s which suggests that in certain circumstances the projectile could have been contained for that velocity. Overall the probabilities of penetration that were obtained in the simulations seem to agree reasonably well with the limited ballistic impact test data that was available in the critical velocity region.

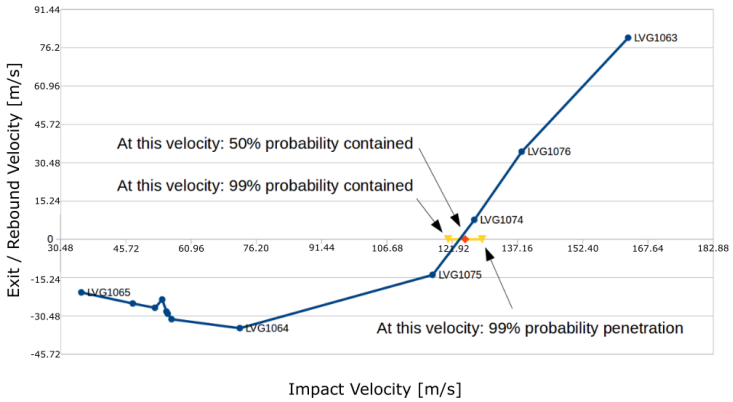

Figure 6.35: Simulation probabilities in comparison to NASA ballistic impact tests

Chapter 7

Conclusions

A computational framework for the determination of probabilities of penetration in ballistic impact tests that takes into account statistical variation of material parameters in composites, was introduced. To obtain physically meaningful stochastic variations of these material parameters, the micro mechanics solver MAC/GMC was used starting from literature data to test the computational framework. These variations of material parameters were incorporated into a ballistic impact simulation utilizing an LS-DYNA MAT54 material card that was validated as part of this study. Several impact velocities with random distributions of LS-DYNA material cards that followed the MAC/GMC material parameter distributions were conducted and logistic regression analysis used to obtain probabilities of penetration. Reasonable agreement between the obtained probabilities of penetration and the limited test results in the critical region was found showing how the variations due to microscale properties distributions. The results of this study will support the implementation of stochastic capabilities into the newly developed Ls-DYNA MAT213 material model supporting the trend of non-deterministic i.e stochastic structural simulations through which more efficient and secure designs can be achieved thanks to the higher level of behaviour predictability.

Bibliography

[1] M. Nariunas A. Baskutis and J. Baskutiene. "The fiber volume fraction influence on mechanical properties of multi-layered carbon tubes". In: *MECHANIKA* 20.6 (2014), pp. 543–549. DOI: http://dx.doi.org/10.5755/j01.mech.20.6.8880.

[2] J. Aboudi. "Micromechanical analysis of thermo-inelastic multiphase short-fiber composites". In: *Composite Engineering* 5.7 (1995), pp. 839–850. DOI: https://doi.org/10.1016/0961-9526(95)93123-D.

[3] Jacob Aboudi. "Micromechanical Analysis of Composites by the Method of Cells". In: *Applied Mechanics Reviews* 42.7 (July 1989), pp. 193–221. ISSN: 0003-6900. DOI: 10.1115/1.3152428. eprint: https://asmedigitalcollection.asme.org/appliedmechanicsreviews/article-pdf/42/7/193/5435686/193_1.pdf. URL: https://doi.org/10.1115/1.3152428.

[4] A. B. Bednarcyk and S. M. Arnold. "MAC/GMC 4.0 User's Manual Volume 3". In: *NASA Technical Memorandum 212077* (2002).

[5] S.D. Rajan et al. C. Hoffarth J. Harrington. "Verification and Validation of a Three-Dimensional Generalized Composite Material Model". In: *13th international LS-DYNA Users Conference* ().

[6] F.C. Campbell. *Structural Coposite Materials*. November 2010. ISBN: 0-61503-037-9.

[7] S. Ghosh. "Micromechanical analysis and multi-scale modeling using the Voronoi cell finite element method." In: *CRC Press* (2011).

[8] S. Ghosh and Y. Liu. "Voronoi cell finite element model based on micropolar theory of thermoelasticity for heterogeneous materials." In: *International Journal for Numerical Methods in Engineering* 38 (1995), pp. 1361–1398. DOI: http://doi.org/10.1002/nme.1620380808.

[9] S. Ghosh and S. Moorthy. "Elastic-plastic analysis of arbitrary heterogeneous materials with the Voronoi Cell finite element method". In: *Computer Methods in Applied Mechanics and Engineering* 121 (1995), pp. 373–409. DOI: http://doi.org/10.1016/0045-7825(94)00687-I.

[10] S. Ghosh and S. N. Mukhopadhyay. “A two-dimensional automatic mesh generator for finite element analysis for random composites.” In: *Computers Structures* 41 (1995), pp. 245–256. DOI: http://doi.org/10.1016/0045-7949(91)90428-O.

[11] J. O. Hallquist. *LS DYNA Keyword User's Manual Volume II Material Models*. 2015.

[12] M. Pandheeradi J. Fish K. Shek and M. S. Shephard. “Computational plasticity for composite structures based on mathematical homogenization: Theory and practice.” In: *Computer Methods in Applied Mechanics and Engineering* 148 (1997), pp. 53–73.

[13] Q. Yu J. Fish and K. Shek. “Computational damage mechanics for composite materials based on mathematical homogenization.” In: *International Journal for Numerical Methods in Engineering* 45 (1987), pp. 1657–1679.

[14] J. P. Johnston. “Stochastic Multiscale Modeling and Statistical Charachterization of Complex Polymer Matrix Composites”. PhD thesis. Arizona State University, August 2016.

[15] G. Nilakantan. “Modeling the Impact of Flexible Textile Composites Through Multiscale and Probabilistic Methods”. PhD thesis. University of Delaware, 2010.

[16] P.M. Mohite P.K. Ilankeeran and S. Kamle. “Axial Tensile Testing of Single Fibres”. In: *Modern Mechanical Engineering* 2.4 (2012), pp. 151–156. DOI: http://dx.doi.org/10.4236/mme.2012.24020.

[17] M. Paley and J. Aboudi. “Micromechanical analysis of composites by the generalized cells model”. In: *Mechanics of Materials* 14 (1992), pp. 127–139. DOI: https://doi.org/10.1016/0167-6636(92)90010-B.

[18] P.J. Bonacuse R.K. Goldberg and S.K. Mital. *Investigation of Effects of Material Architecture on the Elastic Response of a Woven Ceramic Matrix Composite*. January 2012.

[19] A. Sheldon S. Dong K. Carney and L. Graening. “Parametric Optimization of CAE Material Models for Carbon-Fiber-Reinforced Polymer (CFRP) Composites”. In: *presented at the NAFEMS 2017 WC* ().

[20] K. Lee S. Ghosh and S. Moorthy. “Multiple scale analysis of heterogeneous elastic structures using homogenization theory and Voronoi cell finite element method”. In: *International Journal of Solids and Structures* 32 (1995), pp. 27–62. DOI: http://doi.org/10.1016/0020-7683(94)00097-G.

[21] K. Lee S. Ghosh and P. Raghavan. “A multi-level computational model for multi-scale damage analysis in composite and porous materials”. In: *International Journal of Solids and Structures* 38 (2001), pp. 2335–2385. DOI: http://doi.org/10.1016/S0020-7683(00)00167-0.

[22] L. Shen and X.F. Xu. “Multiscale Stochastic Finite Element Method on Random Boundary Value Problems”. In: *The second International Conference on High Performance Computing and Applications, Lecture Notes in Computer Science* (2009).

[23] Donald L. Smith and Dow Marvin B. “Properties of Three Graphite/Toughened Resin Composites”. In: NASA Technical Paper 3102 (September 1991).

[24] R. Sullivan and S. Arnold. “An Annotative Review of Multiscale Modeling and its Application to Scales Inherent in the Field of ICME”. In: (2011).

[25] P. Suquet. “Elements of homogenization for inelastic solid mechanics.” In: *Homogenization Techniques for Composite Media* 272 (1999), pp. 193–278.

[26] B. Wade and P. Feraboli. “Crushing Behavior of Laminated Composite Structural Elements: Experiment and LS-DYNA Simulation”. In: *U.S. Department of Transportation, Federal Aviation Administration* (December 2016).

[27] X. Frank Xu. “Numerical Stochastic Homogenization Method and Multiscale Stochastic Finite Element Method – A Paradigm for Multiscale Computation of Stochastic PDEs”. In: (2010).

[28] Peiyu Yang, Jeremy D. Seidt, and Amos Gilat. *Mechanical Response of T800/F3900 Composite at Various Strain Rates.*

[29] Weidong Yu and Jiangwei Yao. “Tensile Strength and Its Variation of PAN-Based Carbon Fibers. I. Statistical Distribution and Volume Dependence”. In: (2005), pp. –. DOI: DOI10.1002/app.23399.

[30] S. Van der Zwaag. “The Concept of Filament Strenght and the Weibull Modulus”. In: *Journal of Testinf and Evaluation* 17.5 (September 1989), pp. 292–298.